

Charge and heat transport in semiconductor core-shell nanowires with temperature bias

Hadi Rezaie Heris

Thesis of 240 ECTS credits submitted to the Department of Engineering at
Reykjavík University in partial fulfillment of the requirements for the degree of
Doctor of Philosophy

June 15, 2023

Thesis Committee:

Andrei Manolescu, Supervisor
Reykjavik University, Iceland,


Sigurdur I. Erlingsson , Supervisor
Reykjavik University, Iceland,


Snorri Thorgeir Ingvarsson, Advisor
University of Iceland, Iceland,

Mircea Trif, Examiner
International Research Centre MagTop, Polish Academy of Sciences,
Poland,

Charge and heat transport in semiconductor core-shell nanowires

Short title: core-shell nanowires

Copyright © 2023 Hadi Rezaie Heris 

Author ORCID: 0000-0003-2488-5424 

This work is licensed under the Creative Commons Attribution-NonCommercial-NoDerivatives 4.0 International License. You may copy and redistribute the material in any medium or format, provide appropriate credit, link to the license and indicate what changes you made. You may do so in any reasonable manner, but not in any way that suggests the licensor endorses you or your use. You may not use the material for commercial purposes. If you remix, transform or build upon the material, you may not distribute the modified material. The images or other third party material in this thesis are included in the book's Creative Commons license, unless indicated otherwise in a credit line to the material. If material is not included in the book's Creative Commons license and your intended use is not permitted by statutory regulation or exceeds the permitted use, you will need to obtain permission directly from the copyright holder. The use of general descriptive names, registered names, trademarks, service marks, etc. in this publication does not imply, even in the absence of a specific statement that such names are exempt from the relevant protective laws and regulations and therefore free for general use.

Bibliographic information: Hadi Rezaie Heris, 2023, *title*, PhD dissertation, Department of Engineering, Reykjavík University, 118 pp.

ISBN 978-9935-539-12-0 (print version)

ISBN 978-9935-539-13-7 (electronic version)



Printing: Svansprent ehf.

Font: 10pt stix-2

Printed on 90g Sopor paper

To my lovely Family!

Contents

Contents	iv
List of Figures	vi
Preface	xiii
1 Introduction	1
2 Thermoelectric and heat transport at nanoscale	7
2.1 General aspects	7
2.2 Core-shell nanowires as thermoelectric devices	9
2.3 Adjustable factors with effects on the figure of merit	10
2.3.1 Electronic conduction features	10
2.3.2 Phononic thermal conductivity	13
2.3.3 Seebeck coefficient	14
2.3.4 Other factors - Magnetic field and low temperatures	16
3 Geometry effect in nanowires	21
3.1 Geometry effect on electronic charge and heat transport	22
3.2 Geometry effect over phononic thermal conductivity	27
4 Impurities effect on electronic conduction	33
5 Importance of phonon drag in thermopower	41
5.1 Diffusion thermopower	46
5.2 Phonon-drag thermopower	47
6 Summary of papers	53
Paper I	55
Paper II	63

<i>CONTENTS</i>	v
Paper III	72
Paper IV	77
Bibliography	85

List of Figures

1.1	(a) Top view scanning electron microscope (SEM) image of InP core with a hexagonal cross-section (arrows show the crystallographic directions). (b) Top view SEM image of the as-grown InP-InAs core-shell nanowires. (c) 30° tilted view of the InP-InAs core-shell nanowires. (d) Transmission electron microscope (TEM) image of a top segment of an InP-InAs core-shell nanowire. (e) and (f) Fast Fourier transform spectroscopy images taken in the region marked by square 1 and in the region marked by square 2 in (d). (As shown in Ref.[36])	4
2.1	The left figure presents the Seebeck coefficient, electrical conductivity, thermal conductivity, and thermoelectric figure of merit with respect to carrier concentration based on empirical data in ref [57]. The right figure presents thermoelectric figure of merit with respect to temperature for some semiconductor materials. As shown, in ref [58].	11
2.2	Electronic density of states for (a) bulk semiconductor, (b) quantum well, (c) nanowire (or nanotube) (d) quantum dot. As shown, for example, in ref [60]	12
2.3	Electrons thermal conductivity variation in presence of a magnetic field at low temperatures. (Heris et al., CMD2020GEFES)	18
2.4	Phononic thermal conductivity behavior as a function of temperature in low temperatures. (Heris et al., CMD2020GEFES)	19
2.5	Thermoelectric figure of merit in low temperature in presence of a magnetic field. in the calculation of ZT we consider the thermal conductivity of both electrons and phonons. (Heris et al., CMD2020GEFES)	20
3.1	The discretized circular cross-section with external radius of 50 nm and thickness of 20 nm and corresponding energy states	24
3.2	The discretized hexagonal cross-section with external radius of 50 nm and thickness of 20 nm and corresponding energy states	24
3.3	The discretized square cross-section with external radius of 50 nm and thickness of 20 nm and corresponding energy states	25

3.4 The discretized triangle cross-section with external radius of 50 nm and thickness of 20 nm and corresponding energy states 25

3.5 Cross-sectional shapes of solid nanowires. (Heris et al., Supplementary material of Surfaces and Interfaces, 2022) 31

3.6 Cross-sectional shapes of tubular nanowires. (Heris et al., Supplementary material of Surfaces and Interfaces, 2022) 31

4.1 Transmission coefficient as a function of energy for first ten states for tubular nanowires with a triangle cross-section. The external radius is 50 nm and the thickness of the shell is 20 nm for all cases. (a) Tubular nanowire with no impurity (b) Tubular nanowire with 1000 impurity points with a potential of 10 meV (c) Tubular nanowire with 5000 impurity points with a potential of 10 meV (d) Tubular nanowire with 10000 impurity points with a potential of 10 meV. 37

4.2 Density of states as a function of energy for first ten states for tubular nanowires with a triangle cross-section. The external radius is 50 nm and the thickness of the shell is 20 nm for all cases. (a) Tubular nanowire with no impurity (b) Tubular nanowire with 300 impurity points with a potential of 50 meV (c) Tubular nanowire with 300 impurity points with a potential of 100 meV (d) Tubular nanowire with 300 impurity points with a potential of 200 meV. 39

5.1 The diffusion thermopower S_d , phonon drag thermopower S_g , and total thermopower $S_{total} = S_d + S_g$ with respect to temperature. Tubular nanowires with a square cross-sectional area with a thickness of (a) 5 nm shell, (b) 10 nm shell, (c) 15 nm shell and (d) 20 nm shell. 49

5.2 Comparison of S_d and S_g for tubular nanowires with square cross sections and pure nanowires. The lateral size of all nanowires is 20 nm and for nanowires with hollow inside shells, thicknesses is 5,10 and 15 nm. 50

Charge and heat transport in semiconductor core-shell nanowires with temperature bias

Hadi Rezaie Heris

April 17, 2023

Abstract

In this dissertation, we calculate the electronic charge and heat transport generated by a temperature gradient and a chemical potential bias in tubular semiconductor nanowires, in the presence of a magnetic field. We use the Landauer-Büttiker approach to calculate charge current, electronic heat current, Seebeck coefficient, thermal conductivity, and figure of merit. We also study the influence of the cross-section shape and shell thickness on the electronic conduction properties of tubular nanowires. Then, charge and heat transport in tubular nanowires for different polygonal cross-sections and different numbers of impurities with various strengths are studied. Effects of transverse geometry on the thermal conductivity of Si and Ge nanowires are investigated by using molecular dynamics simulations with the LAMMPS software. We consider nanowires with different polygonal cross-sections, tubular (hollow) nanowires, and core/shell nanowires with combinations of Si/Ge and Ge/Si. We also study the diffusion and phonon drag thermopower in Si nanowires through numerical calculations with tight-binding models and quantum transport.

Keywords / Efnisord: Thermoelectrics, core-shell nanowires, tubular nanowires, charge transport, heat transport, thermal conductivity, Seebeck coefficient, phonon drag

Acknowledgments

Completing this Ph.D. thesis has been a remarkable journey, and I am immensely grateful to the many individuals in this wonderful country who have played a significant role in making this achievement possible. First, I express my gratitude to my supervisor, Dr. Andrei Manolescu whose guidance, expertise, and patience have been invaluable throughout this research endeavor. I am indebted to the members of my thesis committee, Dr. Sigurdur I. Erlingsson and Dr. Snorri Ingvarsson, for their insightful feedback, and expert evaluation. I would like to extend my thanks to my colleagues and fellow researchers who have supported and helped me throughout this project with their camaraderie and encouragement which made this experience both instructive and enjoyable. I am especially thankful to Ania Sitek, Movaffaq Kateb, and Kristjan Klausen. I would also like to express my sincere appreciation to my family and friends both in Iran and Iceland for their unwavering love, and encouragement, and for their continuous support and belief in my abilities which have been a constant source of motivation. Finally, my deepest and warmest appreciation to my beloved wife Elham for all her sacrifices and for being my partner in life and in academia. I would like to acknowledge the financial support provided by Rannis Nos. 195943-051 and 229078-051.

Preface

This dissertation is original work by the author, Hadi Rezaie Heris. A major portion of the thesis is based on four refereed journal papers (three published and one accepted for publication) elaborated during the course of Ph.D. study, and one manuscript in the final phase, on phonon drag, to be submitted for publication soon after the thesis defense. The published papers appear as per their submitted version at the end of the thesis. The overall list of journal papers throughout this study is listed in below.

Published ISI Journal papers:

- Heris, Hadi Rezaie, Movaffaq Kateb, Sigurdur I. Erlingsson, and Andrei Manolescu. "Thermoelectric properties of tubular nanowires in the presence of a transverse magnetic field." *Nanotechnology* 31, no. 42 (2020): 424006.
- Heris, Hadi Rezaie, Movaffaq Kateb, Sigurdur I. Erlingsson, and Andrei Manolescu. "Effects of transverse geometry on the thermal conductivity of Si and Ge nanowires." *Surfaces and Interfaces* 30 (2022): 101834.
- Heris, H. R., K. O. Klausen, Anna Sitek, S. I. Erlingsson, and A. Manolescu. "Charge and heat currents in prismatic tubular nanowires." In *2022 International Semiconductor Conference (CAS)*, pp. 177-180. IEEE, 2022.

ISI journal paper accepted for publication

- Heris, Hadi Rezaie, Kristjan Ottar Klausen, Anna Sitek, Sigurdur Ingi Erlingson, and Andrei Manolescu. "Effect of Impurities on Charge and Heat Transport in Tubular Nanowires." Accepted by Nanotechnology Journal, arXiv:2302.02164 (2023)."

Chapter 1

Introduction

Nanomaterials are at the intersection of nanoscience and nanotechnologies, connecting these two areas and enabling the development of new technologies and materials. Nanomaterials are defined as materials with at least one dimension below a hundred nanometers. Quantum dots, nanowires and thin films have three, two, and one dimensions constrained to this order. Due to their small size, nanomaterials exhibit unique properties that are different from those of their bulk counterparts. This is because of the closeness of all their constituting atoms to material boundaries and high surface area to volume ratio which causes quantum mechanical effects to become significant in this size regime. Among these nanostructures, nanowires have attracted considerable attention due to their potential applications in several fields of technology such as nanoelectronics [1]–[4], quantum information processing [5], [6], thermoelectrics and energy conversion devices [7]–[11], optics and photoluminescence [12]–[14], integrated circuits [15], [16], and sensors [17], [18]. The growing interest in nanowires arises mainly from their unique electrochemical and mechanical properties, highly anisotropic geometry, large surface-to-volume ratio, and carrier and

phonon confinement [17], [19]–[22]. The ability to fabricate nanowire heterostructures, enables energy band engineering in both axial [23], [24] and radial [25]–[28] directions. The design of radial, or core–shell, nanowire heterostructures based on III-V semiconductors enables the control of charge and heat transfer through the specific geometry and shell thickness [29]–[31]. The cross-section of such nanowires is typically polygonal, most often with a hexagonal cross-section and the charge density peaks at the shell corners [32]–[34]. Although other prismatic geometries such as square and triangle have also been fabricated [35], [36]. Also, semiconductor core-shell nanowires with insulating (undoped) core and conductive (doped) shell provide a tubular conductor with conduction electrons captured inside the shell [37]. Experimentally it is also possible to remove the core and obtain hollow nanowires with vacuum inside [38]. Understanding and investigating electronic conductance features and variations as a function of transverse geometry and shell thickness, and the transported heat through the core are key to the design of such nanoscale heterostructures.

Core-shell nanowires can be grown using various methods such as photolithography [39], etching [40], electro-chemical deposition [41], chemical vapor deposition [42], [43], and metal-organic vapor phase epitaxy (MOVPE) [36]. Due to excellent control over nanowire crystal structures and morphology, MOVPE is one of the most frequently used methods for growing core-shell nanowires. Within the MOVPE process, two mechanisms for growing nanowires are utilized: metal particle-assisted vapor-liquid-solid (VLS) growth and selective area epitaxy (SAE) growth [44]. The following description outlines an experimental approach to producing InP-InAs core-shell nanowires with a triangular cross-section as an example. In the case of InP-InAs core-shell nanowires growth process start with a thick layer of SiN_x via plasma-

enhanced chemical vapor deposition on an InP single crystal wafer. Once a thin photoresist material, and a 200-nanometer-thick resist layer of CSAR 62 are applied using spin coating, circular holes then can be patterned into the layers through electron beam lithography (EBL). Reactive-ion etching (RIE) can be used to etch the SiN_x layer, with the EBL patterned double resist layer serving as the etch mask. A solvent based on 1-methyl-2-pyrrolidinone will remove the resist layers at a temperature of 90°C , following this, the growth substrate needs to be cleaned by rinsing it with deionized water and isopropyl alcohol (IPA) and by subjecting it to oxygen plasma ashing. The preparation of the growth substrate is completed, when the patterned SiN_x mask is polished in diluted hydrofluoric acid (diluted with water at a ratio of 1:100) for a duration of 30 seconds. Using the SAE method, nanowires can grow within the mask opening areas in a horizontal flow MOVPE reactor, while pressure is 100 mBar, and total gas flow rate is 6 liters per minute. Source gases for the process are trimethylindium (TMIn), phosphine, and arsine. Initially, the substrate undergoes annealing at 750°C for a duration of 10 minutes under phosphine flow. The InP nanowire cores will grow at a temperature of 710°C for a duration of 10 minutes, using a molar fraction of 1.2×10^{-5} for TMIn and 2.5×10^{-2} for phosphine. Next, by disconnecting the supply of the group III precursor the temperature will reduce to 460°C , and at this temperature, the supply of phosphine must be halted, and arsine is introduced. Afterward, TMIn reintroduction into the reactor facilitates the growth of InAs shells for a period of 5 minutes. The molar fractions for TMIn and arsine must be set at 6.7×10^{-6} and 8.4×10^{-4} , respectively. To avoid decomposition of the InAs surfaces, the sample must be cooled within the reactor under arsine flow. Observe the ultimate outcome of the procedures that lead to the formation of InP-InAs core-shell nanowires in Fig.1.1.

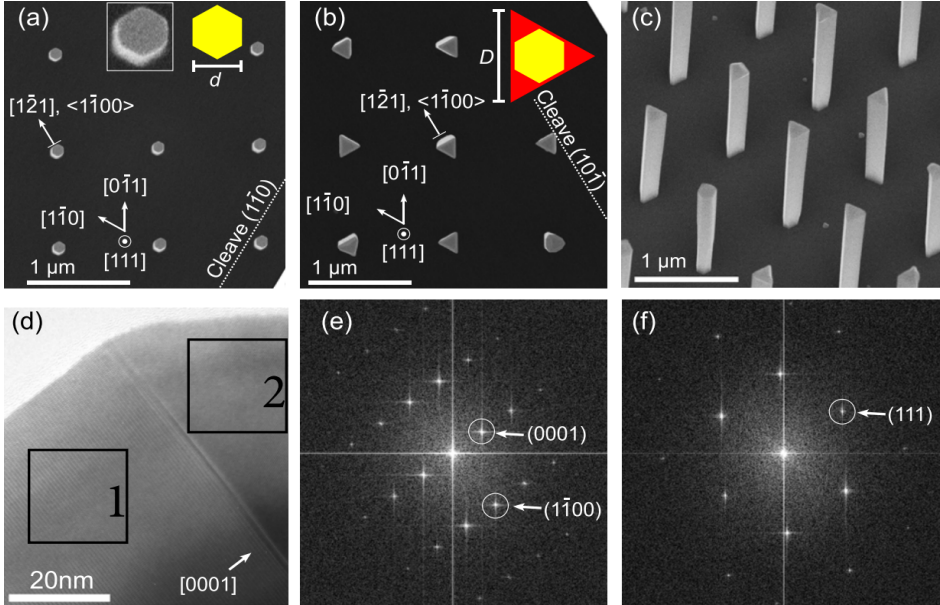


Figure 1.1: (a) Top view scanning electron microscope (SEM) image of InP core with a hexagonal cross-section (arrows show the crystallographic directions). (b) Top view SEM image of the as-grown InP-InAs core-shell nanowires. (c) 30° tilted view of the InP-InAs core-shell nanowires. (d) Transmission electron microscope (TEM) image of a top segment of an InP-InAs core-shell nanowire. (e) and (f) Fast Fourier transform spectroscopy images taken in the region marked by square 1 and in the region marked by square 2 in (d). (As shown in Ref.[36])

In this dissertation, we focus on exploring the different physical properties of III-V semiconductors core-shell nanowires. We mainly studied cross-section effect on different physical properties in these nanowires. We have investigated the electronic charge and heat transport in prismatic tubular nanowires. The perpendicular magnetic field effect over the transmission of electrons, Seebeck coefficient, electronic thermal conductivity and figure of merit have been studied. Impurities effect on heat and charge transport by electrons in different cross-sections of nanowires investigated, while for impurities with consider different number and different strength.

For understanding phononic heat transport in core-shell nanowires we studied the effect of transverse geometry on the thermal conductivity of Si and Ge nanowires, in these simulations we use molecular dynamics for simulation of heat transfer in tubular nanowire and Si-Ge and Ge-Si core-shell nanowires. Also, diffusion and phonon drag as two components of thermopower have been studied in pure and tubular nanowires.

Chapter 2

Thermoelectric and heat transport at nanoscale

2.1 General aspects

Thermoelectricity is the process of converting heat into electricity and vice versa which was discovered by Thomas Johann Seebeck in the nineteenth century [45]. The Seebeck effect, the Peltier effect, and the Thompson effect are the three distinct phenomena that constitute thermoelectricity. The Seebeck effect is a phenomenon in which a temperature difference between two dissimilar electrical conductors or semi-conductors produces a voltage difference between the two substances. The Peltier effect refers to the thermoelectric phenomenon of the transfer of heat energy that occurs between two materials when an electric current passes through. Thompson effect describes the heating or cooling of a current-carrying conductor with a temperature gradient. Thermoelectric materials have attracted a lot of attention to applications in waste heat recovery for power generation and in refrigeration [46]. The

main goal in this field is enhancing the efficiency of energy conversion, which requires higher Seebeck coefficient and electrical conductivity and low thermal conductivity. However, optimizing these parameters is a challenging task because most of these quantities are coupled. For instance, in bulk materials, the Seebeck coefficient depends on the carrier density but is inversely correlated with the electrical conductivity. While electrical and thermal conductivities are interrelated according to Wiedemann-Franz law [47].

The best option to find the optimum conditions for thermoelectric conversion is figure of merit ZT . Dimensionless figure of merit is defined as

$$ZT = \frac{S^2 \sigma T}{\kappa}, \quad (2.1)$$

where S is Seebeck coefficient, σ is electrical conductivity, κ is thermal conductivity and T is temperature. The thermal conductivity term itself consists of two terms ($\kappa = \kappa_e + \kappa_{ph}$), electronic thermal conductivity and phononic thermal conductivity.

The Seebeck effect (also known as thermopower) describes the conversion of heat into electricity and the creation of a voltage difference across a material when its ends are exposed to dissimilar temperatures. The voltage difference (ΔV) produced in the presence of a small temperature difference ($\Delta T \approx 0.5$ K) under open an open-circuit condition (i.e. electric current in system is zero) defines thermopower of the system as ($S = -\Delta V / \Delta T$). The reason for this effect can be explained by temperature driven random motion of charge carriers, which are electrons in metals and n-type semiconductors and holes in p-type semiconductors. The carriers on the hotter side have larger kinetic energy than those at the colder side, which yields a net transport to the cold side. The accumulated carriers generate a voltage that can be positive

or negative, depending on the type of carriers. So, metals and n-type semiconductors exhibit a negative Seebeck coefficient, whereas p-type semiconductors show a positive Seebeck coefficient.

2.2 Core-shell nanowires as thermoelectric devices

Some theoretical studies [48] suggested that the use of nanoscale structures in thermoelectric materials could lead to an improvement in ZT , which prompted additional exploration of this field. This is mainly due to quantum-mechanical effects which increase the power factor ($S^2\sigma$) with respect to bulk materials. There are plenty of experimental and theoretical works which studied the effect of low dimensions on nanowires and other nanostructures and also their thermoelectric applications [49]–[53].

Compared to thin films with only one confined dimension, nanowires have two limited dimensions, which enable better utilization of size-related phenomena. Furthermore, nanowires have one unrestricted dimension-unlike quantum dots that have none- which makes them capable of withstanding thermal gradients due to their elongated structures. Due to these reasons, nanowires are excellent candidates for the improvement of thermoelectric transport properties among different nanostructures. Due to their nanometric diameter and also their micrometric length, nanowires that are intended to exploit the thermoelectric effect shows a series of geometric effects related to low dimensionality. Especially, core-shell nanowires with different cross-sectional areas present interesting physical properties for system.

2.3 Adjustable factors with effects on the figure of merit

Carrier concentration has a significant influence over transport properties and it is interrelated in a manner that figure of merit ZT is maximized for semiconductors. According to Eq.(2.1), the best thermoelectric materials have high S and high σ and low κ . Insulator electrical conductivity is lower than semiconductors and in the case of metals Seebeck coefficient is lower than semiconductors, also metal show higher thermal conductivity values (See Fig.2.1). Furthermore, with semiconductors, one can control carrier concentration by doping and manipulate transport properties by impurities. For these reasons, semiconductors are intended to be used in thermoelectric applications and not insulators or metals. Different semiconductors provide a different figure of merit behavior with respect to temperature. By considering desired temperature regime, one can choose the best semiconductor material for the thermoelectric application (See Fig.2.1). For instance, in bismuth telluride alloys (Bi-Te), it is possible to lower thermal conductivity without affecting the Seebeck coefficient, also it is easy to control carrier concentration. Conventional thermoelectric materials such as Bi_2Te_3 , SiGe and PbTe present ZT values near 1, which yields 5%-15% efficiencies in thermoelectric generators [54]. Also, the role of band structure for bismuth and bismuth antimonide nanowires arrays has been studied experimentally [55], [56].

2.3.1 Electronic conduction features

In contrast to metals, in doped semiconductors, thermal conductivity does not change significantly with changing carrier concentration. So, for reaching a maximum figure of merit an optimal carrier concentration (n) shall maximize the thermoelectric

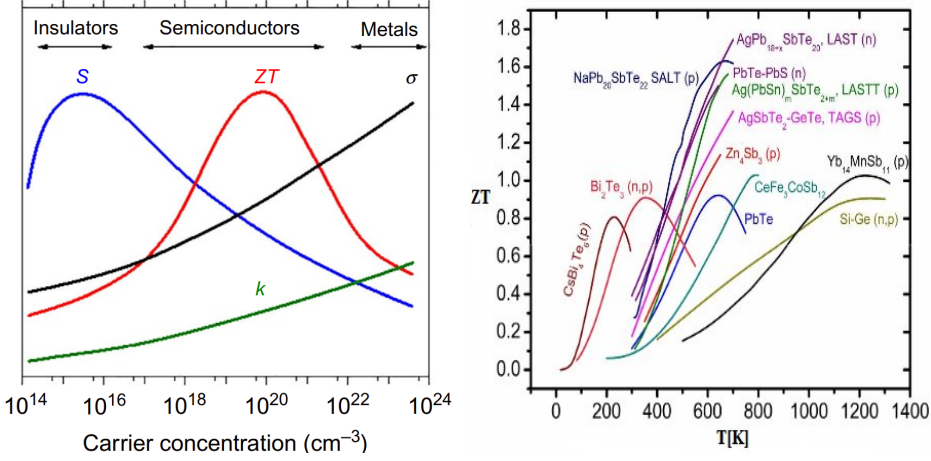


Figure 2.1: The left figure presents the Seebeck coefficient, electrical conductivity, thermal conductivity, and thermoelectric figure of merit with respect to carrier concentration based on empirical data in ref [57]. The right figure presents thermoelectric figure of merit with respect to temperature for some semiconductor materials. As shown, in ref [58].

power factor ($S^2\sigma$). The optimal power factor value can be enhanced by using the quantum confinement effect. Electrical conductivity can be defined as $\sigma = ne\mu$, where n is carrier concentration, e is the charge of carriers (+ for p-type and - for n-type), and μ is carrier mobility. If we consider μ constant, for reaching the maximum value of the power factor we need to maximize S^2n . The Seebeck coefficient S can be defined based on the derivation using the Boltzmann transport equation with relaxation time approximation. So S^2n can be defined as [54]

$$S^2n = \frac{n}{(e.T)^2} \left(\frac{\langle \tau.E \rangle}{\langle \tau \rangle} - E_F \right)^2, \quad (2.2)$$

where E_F is Fermi Level, $\langle E \rangle$ is the average energy of electrons and τ is the average time that an electron can travel before scattering. If we consider τ constant with energy, $\langle \tau E \rangle / \langle \tau \rangle = \langle E \rangle$, then the power factor increase with the difference be-

tween the average energy of electrons and the Fermi level energy. Electrons fulfilling available energy levels in doped semiconductors define both of these energies. Low-dimensionality effects over the fraction of filled levels in a determined range of energy can be calculated by the density of states and the Fermi distribution function [59]. From quantum mechanics calculations, one can derive the shape and properties of the density of states functions. The density of states is continuous for nanowires (as long as at least one of the dimensions is still large), and the density of states magnitude increases with decreasing diameter of nanowires [49], [50].

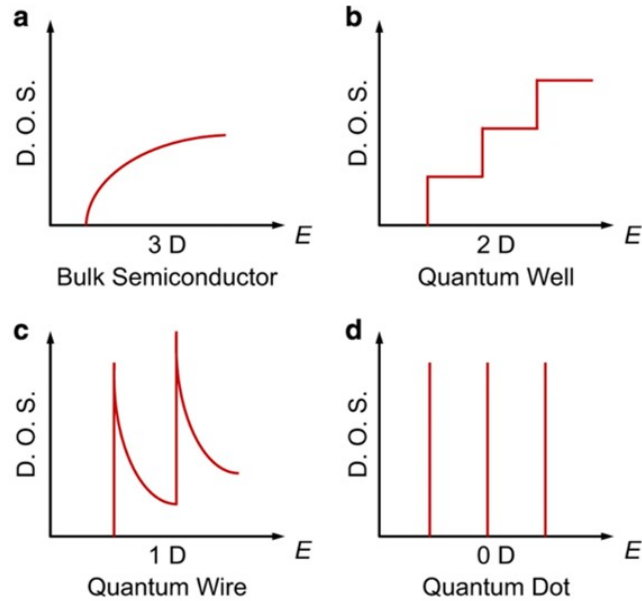


Figure 2.2: Electronic density of states for (a) bulk semiconductor, (b) quantum well, (c) nanowire (or nanotube) (d) quantum dot. As shown, for example, in ref [60]

2.3.2 Phononic thermal conductivity

To enhance the figure of merit, an alternative method is to reduce the thermal conductivity of the semiconductor material. In the system, heat is transported by electrons and phonons, so total thermal conductivity is composed of a lattice (atomic vibrations) component and an electronic contribution. Although in semiconductors, one can assume ($\kappa_e \ll \kappa_{ph}$). Because according to Wiedemann-Franz law, electrical thermal conductivity is proportional to electrical current. Using a low-dimension approach will not provide high Seebeck and electrical conductivity in comparison to electrical thermal conductivity, due to the fact that electrons necessarily transport heat and charge at the same time. For these reasons, efficient thermoelectrics requires low phononic thermal conductivity κ_{ph} . There are several phenomena that can lead to a reduction in the magnitude of κ_{ph} such as phonon boundary scattering, phonon scattering in edges of prismatic transverse cross-section, scattering due to lattice imperfection or presence of impurities, and scattering produced by other particles or quasiparticles [61]. The phonon lifetime is commonly given by Matthiessen rule, expressing the total inverse lifetime as the sum of the inverse lifetimes corresponding to each scattering mechanism. The phonon mean free path can be decreased if we limit our dimensions to small ranges (which are different from one material to another). Also with prismatic cross-sectional tubular nanowires phonons mainly saturate to edges and a limited mean free path provides small thermal conductivity, while in core-shell nanowires core phonons frequency is different from shell phonons which leads to phonon-phonon scatter. We will discuss about these subjects in detail in Chapter 5.

2.3.3 Seebeck coefficient

Thermal fluctuations diffuse charge carriers constantly inside a conductive material and carriers with higher energy levels move more than those with lower energy levels. In the absence of any voltage or temperature differences, the diffusion of carriers is perfectly balanced, resulting in zero current on average. A net current can be generated either by a voltage difference (Ohm's law), or a temperature difference. Charge carrier provides a thermoelectric effect in the presence of temperature gradient and uniform voltage (uniform chemical potential). So on the hotter side of the material, there is greater diversity in the energy levels of the charge carriers as compared to the colder side and charge carriers with high energy levels migrate away from the hotter region, resulting in entropy generation as they drift towards the colder end of the device.

The Seebeck coefficient (also known as thermopower) S is the voltage difference (ΔV) produced in the presence of a small temperature difference (ΔT) between two points of a conductor under an open circuit condition (electric current in system is zero). It is defined by ratio $-\Delta V/\Delta T$ for the materials with negative mobile charges, and $\Delta V/\Delta T$ for positive mobile charges materials. Fundamentally, a voltage difference applied to a system signifies a variation in the thermodynamic chemical potential of charge carriers. The direction of the current, when a voltage difference is present (in constant temperatures), is governed by the universal thermodynamic mechanism wherein particles flow from regions of high chemical potential to those of low chemical potential. According to the Mott formula Seebeck coefficient for metals and semiconductors is described differently [62]. Due to the fact that in semimetals and metals, transport only occurs near the Fermi level ($E \approx \mu \pm k_B T$); while in semiconductors, transport occurs far away from the Fermi level ($E_c - \mu \gg k_B T$).

The phonon drag is another contributor to thermopower, additional to diffusion thermopower (diffusion of carriers from the hot to the cold region). Phonon drag thermopower originates from the momentum that is transferred to carriers via their coupling to non-equilibrium acoustic phonons in the presence of temperature gradient. This contribution happens in the temperature region where phonon-electron scattering is predominant, which is $T \approx \theta_D/5$ (θ_D is Debye temperature) [63].

The overall thermopower consists of two contributors: diffusion thermopower S_d and phonon drag thermopower S_g ,

$$S = S_d + S_g . \quad (2.3)$$

The diffusion thermopower originates from diffusion of the carriers from the hot to the cold side, while the phonon drag thermopower results from the transfer of momentum from non-equilibrium acoustic phonons to carriers in the presence of a temperature gradient.

From a fundamental point of view, studying the Seebeck coefficient provides important information about charge carriers' behavior and the electron-scattering mechanisms in a system (we will discuss in detail in Chapters 3 and 4), and even electron-phonon (e-ph) scattering (we will discuss in detail in Chapter 5). Also, the efficiency of thermoelectric energy conversion can be significantly enhanced in nanoscale systems by quantum confinement effects on thermoelectric transport properties.

2.3.4 Other factors - Magnetic field and low temperatures

The thermoelectric properties of nanowires can be altered by certain effects occurring within them. Also, the behavior of charge carriers in nanowires can be affected by several factors, such as scattering due to the nanowire's cross-sectional geometry, scattering caused by roughness or surface defects, impurities, two-surface interface, and interaction with phonons. For instance, a study suggests that the presence of surface states at the Si/SiO₂ interface may be playing a role in enhancing the electrical conductivity of n-type silicon nanowires [64]. The presence of abnormally coordinated atoms in grain boundaries results in a thin charged layer, which may act as an energy filter for charge carriers. Those with low energies are likely to be backscattered and unable to pass through the barrier, while high-energy carriers can surpass it [65].

The Fourier law describes thermal transport very well for bulk materials while it is no longer valid if one of the dimensions is smaller than the mean-free path of phonons. In such a small system, the thermal current is dependent to the temperature difference (ΔT) between hot and cold reservoirs and it is not proportional to the temperature gradient dT/dx . Also thermal conductance is quantized in multiples of the universal value

$$\kappa_0 = \frac{\pi^2 k_B^2 T}{3h} \equiv g_0 T, \quad (2.4)$$

where $g_0 = 9.4 \times 10^{-13} \text{ W/K}^2$ [66]–[68]. κ_0 is the upper limit of the thermal conductance that a single acoustic phonon mode can carry. This fundamental upper limit can be regarded as a quantum of thermal conductance, which originates from quantum mechanics. The thermal conductance quantum κ_0 contain the thermal energy

($k_B T$) and electrical conductance contains electrical charge (e), so the quantization of thermal conductance is very similar to the quantization of electrical conductance $G_0 = e^2/h$.

In low-temperature (below 20 K) regimes optical phonons are not excited yet, and in 1D systems there are four acoustic modes (one longitudinal, one twisting, and two transverse) that carriers thermal conductivity beside electrons [69]. In high temperatures the main part of thermal transport is by phonons, while in very low temperatures electrons contribution to the total thermal transport will increase more and more ($\kappa_e \gg \kappa_{ph}$) [70], [71]. Also, it has been shown that the presence of a magnetic field leads to significant changes in thermoelectric properties [72]–[75], the thermal conductivity of carrier [76], [77], and Seebeck coefficient [78], [79]. The fact that in low temperatures most of the heat transport is carried by electrons and by implementing a magnetic field one can change the electronic properties in the system was the motivation to us to study more this temperature regime. So first, we calculate transported heat associated with electrons in a tubular nanowire with 30 nm radius in the presence of an external magnetic field perpendicular to its axis. We use Landauer-Buttiker approach to calculate the transport quantities below 21 K in the presence of a magnetic field up to 3 T. The result of these calculations has been presented in Fig.2.3.

The thermal conductivity of tubular nanowires decreases with the increasing magnitude of the magnetic field, This reduction for the case of $B = 3$ T is $\approx 35\%$ in comparison with the case with no magnetic field. Next, we calculate heat transport due to phonons in molecular dynamics (MD). All the parameters for this simulation are the same as in the previous case. There were eight simulations with MD with the same parameters but different temperature gradients for each case. Fig.2.4 shows the

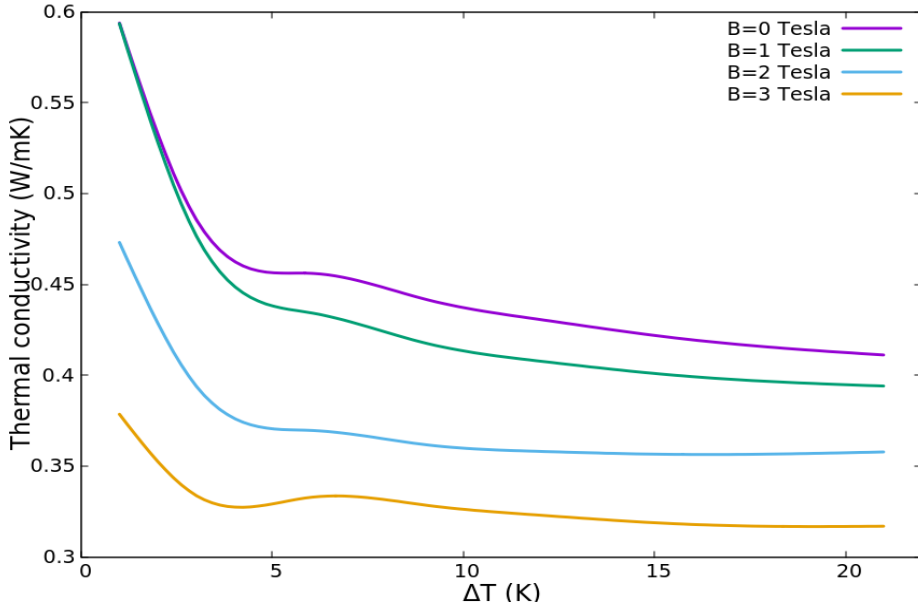


Figure 2.3: Electrons thermal conductivity variation in presence of a magnetic field at low temperatures. (Heris et al., CMD2020GEFES)

results of these simulations and a parabolic fitting to these data.

Roughly speaking average electronic heat transport is fourfold of phononic heat transport (Compare Fig.2.3 and Fig.2.4). Despite the fact that a strong magnetic field reduces the electron's heat transport, still electronic thermal conductivity values stay much higher than phonon ones.

In the last phase to understand both the magnetic field effect on electronic heat transport and phonons behavior in low temperatures, we calculate the thermoelectric figure of merit by using them. In Eq.(2.1) we consider transported heat as a sum of transported heat by both electrons and phonons ($\kappa = \kappa_e + \kappa_{ph}$), and Seebeck coefficient obtained from the system with zero electric current (open-circuit condition). Substituting all of these parameters in Eq.(2.1) presents a magnetic field effect on the

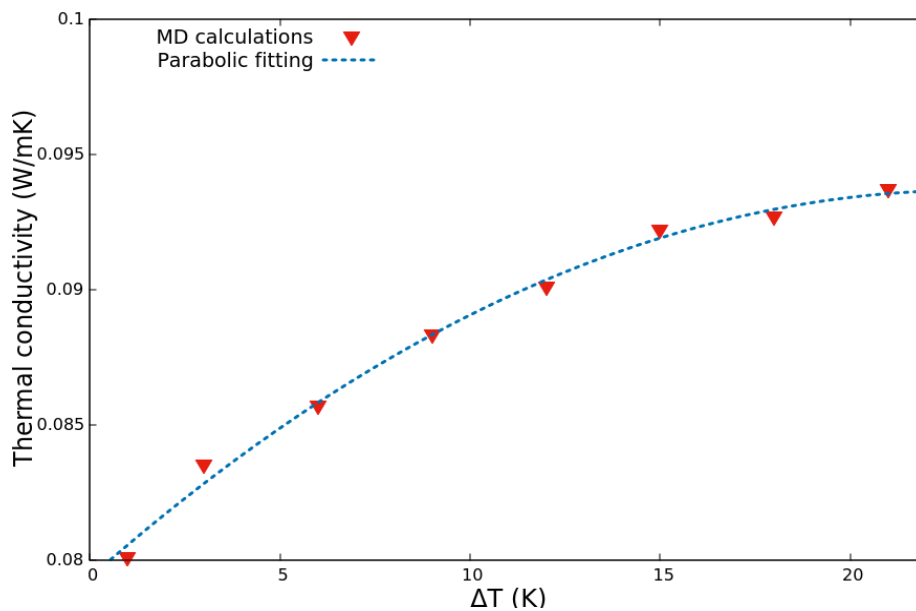


Figure 2.4: Phononic thermal conductivity behavior as a function of temperature in low temperatures. (Heris et al., CMD2020GEFES)

figure of merit in low temperatures (See Fig.2.5).

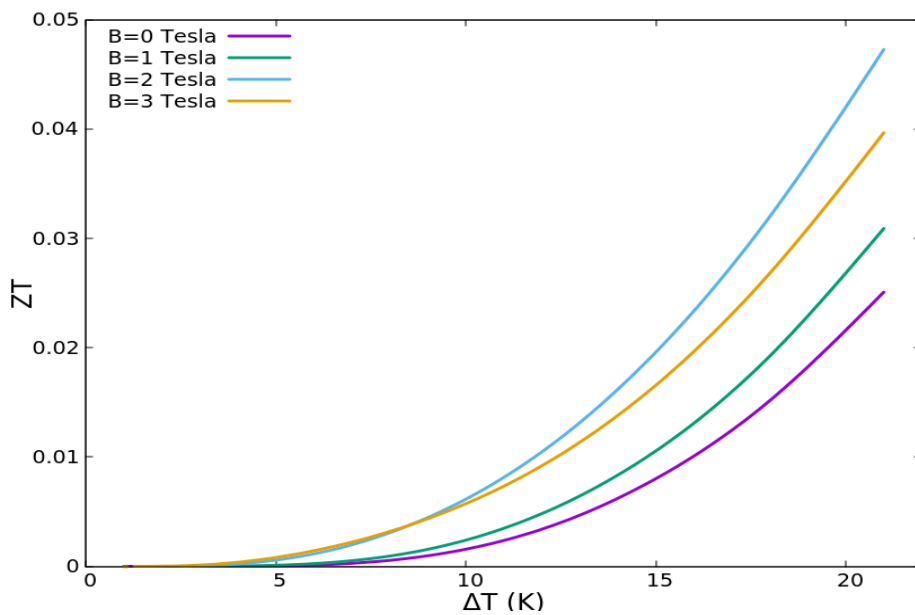


Figure 2.5: Thermoelectric figure of merit in low temperature in presence of a magnetic field. in the calculation of ZT we consider the thermal conductivity of both electrons and phonons. (Heris et al., CMD2020GEFES)

Chapter 3

Geometry effect in nanowires

Nanowires with a prismatic transversal cross-sectional area have been demonstrated to have excellent electronic [80]–[82], optical [83], photovoltaics [84], solar cell [85] and thermal [30], [86]–[88] and thermoelectrics properties [10]. For many of these applications having knowledge about the thermal conductivity and electrical conductivity of nanowires is crucial. For instance, low thermal conductivity and high electrical conductivity are essential for a high figure of merit in thermoelectrics [89]–[91], while in order to dissipate heat from nanochips, nanoelectronic devices require high thermal conductivity and heat sinks [92], [93]. Semiconductor core-shell nanowires that have a prismatic transverse cross-sectional area have some advantages over other nanowires. First, there is an option of choosing and combining different materials in core-shell nanowires which provide diverse physical properties. Second, charge carriers' conduction properties can be engineered through the transverse cross-section of the shell, while heat can be suppressed in the transverse cross-section of the core due to finite size confinement.

Studying electrical conduction features and phononic heat transfer simultane-

ously both with respect to transverse cross-section is a very complex task. Due to this reason, first we study charge and heat current in prismatic tubular nanowires and after that, we study thermal conductivity in prismatic tubular nanowires and core-shell nanowires.

3.1 Geometry effect on electronic charge and heat transport

In most cases in core-shell nanowires, electronic charge and heat transport in shells. Tubular nanowires can be considered as semiconductor core-shell nanowires with an insulating core and conductive shell, which conduction only takes place in the shell. It is also possible to obtain hollow in the center of nanowires, by etching core part [38]. Nanowires with a core-shell structure made from III-V semiconductors typically have a polygonal shape and are mostly prismatic in nature. The typical prismatic geometry is hexagonal, although other cross-section shapes such as square and triangular have been fabricated [94]–[99].

To study the transversal cross-section effect on the electronic conduction of tubular nanowires, we consider models with cylindrical, hexagonal, square, and triangular geometries. we assume an external radius of 50 nm for the polygonal shell which refers to the radius of the circle that encloses the complete cross-sectional area. Initial side thickness will be 20 nm (then for understanding the thickness effect we model shells with thicknesses of 5, 10 and 15 nm), electrons conduction features will be computed in the presence of a temperature gradient and chemical potential bias. In polygonal cross-sectional shells, the energy of the lowest states is concentrated at the corners, creating a significant energy gap between these corner states and the subsequent group of states localized on the sides of the polygon [100], [101]. The size of this energy gap grows as the shell thickness and the number of corners decreases

[33], [100].

The Hamiltonian of the system consists of two parts, the transverse and the longitudinal term. The transverse Hamiltonian operates on a lattice of points that spans the cross-sectional area of the shell. After defining a radial lattice that provides a circular disk, we integrate the desired polygonal shell onto this lattice and remove any lattice points outside the shell from the Hamiltonian [33], [102]. The cross-sectional shape of prismatic shells is determined by the number of radial and angular sites, which ranges are from 10 to 15 and 40 to 54 respectively. The exact number of sites depends on the polygonal shape and the thickness of the shell. The transverse geometry of our nanowire models and corresponding energy values for the first ten states has been presented in figures 3.1-3.4. Charge current I_c and heat current I_Q is calculated by using Landauer-Buttiker approach

$$I_c = \frac{e}{h} \int \Gamma(E)[f_L(E) - f_R(E)]dE , \quad (3.1)$$

$$I_Q = \frac{1}{h} \int \Gamma(E)[E - \mu][f_L(E) - f_R(E)]dE , \quad (3.2)$$

where Γ is the transmission function, μ is average chemical potential and

$$f_{L,R}(E) = \frac{1}{1 + e^{(E - \mu_{L,R})/k_B T_{L,R}}} , \quad (3.3)$$

is the Fermi function for the left (L) or right (R) reservoirs with the chemical potential $\mu_{L,R}$ and temperature $T_{L,R}$.

Increasing the chemical potential leads to a corresponding increase in electrical current for all shapes. Additionally, polygonal geometries yield higher current values compared to circular geometry. While the energy states differ for each cross-sectional

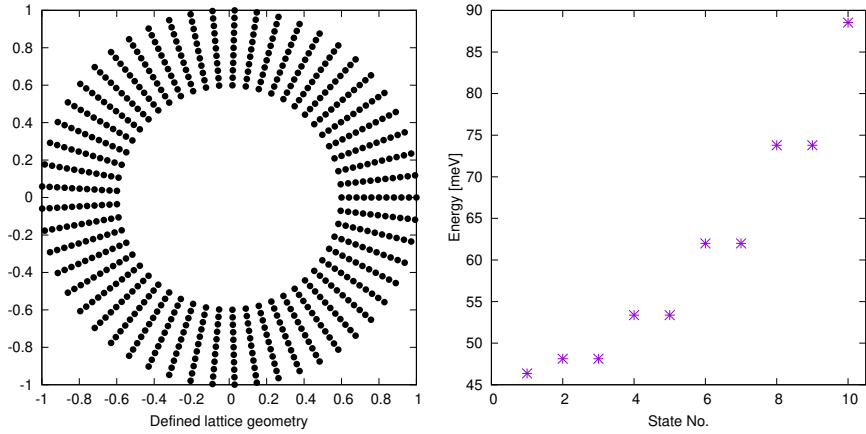


Figure 3.1: The discretized circular cross-section with external radius of 50 nm and thickness of 20 nm and corresponding energy states

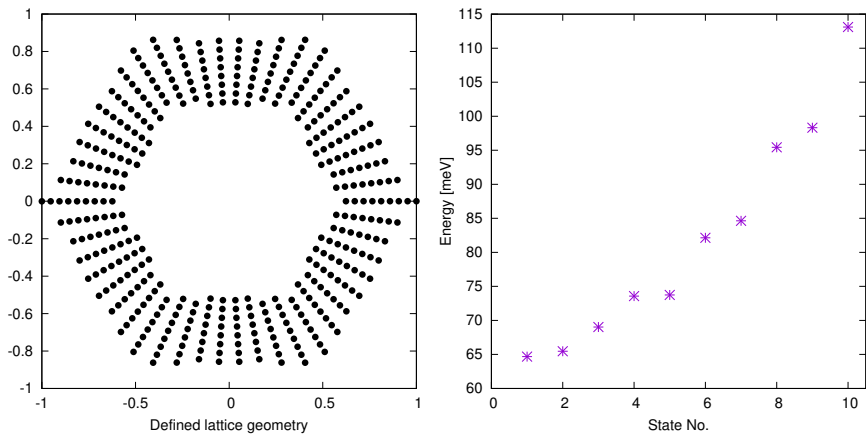


Figure 3.2: The discretized hexagonal cross-section with external radius of 50 nm and thickness of 20 nm and corresponding energy states

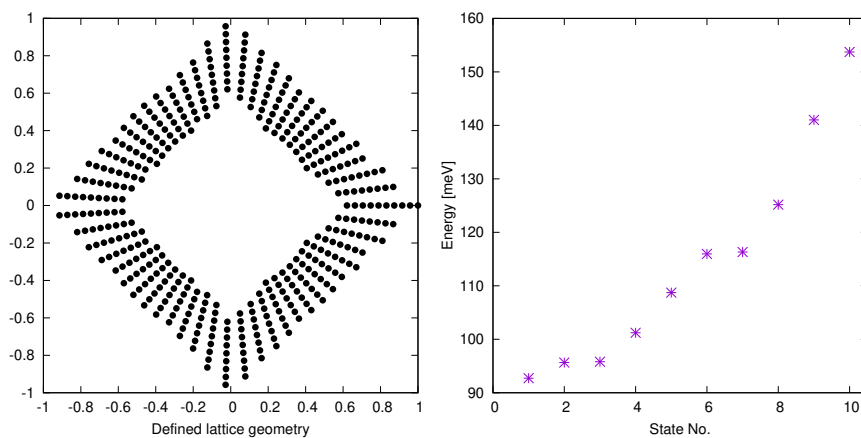


Figure 3.3: The discretized square cross-section with external radius of 50 nm and thickness of 20 nm and corresponding energy states

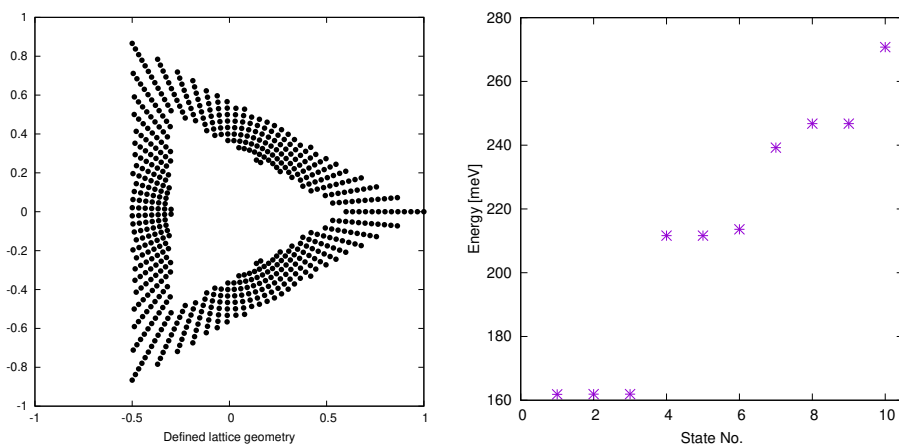


Figure 3.4: The discretized triangle cross-section with external radius of 50 nm and thickness of 20 nm and corresponding energy states

shape, the charge current values for all cases can be explained by the transmission function and the energy window associated with the chemical potentials. An increase in chemical potentials causes an increase in the number of energy states that participate in the transmission process, resulting in a higher flow of charge current. In all shapes of the cross-section, the electrical current becomes saturated at high values of chemical potential; while, an increase in chemical potential results in a peak for heat current followed by a sharp decline. Another result from our calculation shows that at low temperatures, polygonal shapes with fewer corners exhibit lower charge current. However, as the temperature is increased, this trend is reversed and polygonal shapes with fewer corners show higher charge current. Tubular nanowire with triangular cross-section have the highest transported heat current and circular shape have the lowest values. Also for further investigating about shell's thickness effects over electronic charge and heat transport, we studied triangle shells with thicknesses of 5, 10, 15 and 20 nm (external radius is fixed at 50 nm) in presence of temperature gradient and chemical potential bias. The relationship between the aspect ratio of the polygonal cross-section (i.e., the ratio of thickness to diameter). Specifically, in the case of a triangle, the difference in energy levels between states localized at corners and those localized on sides increases significantly as the thickness of the shells decreases [101]. An increase in chemical potential causes a greater number of states to take part in transmission, leading to an increase in electric current, irrespective of the thickness of the sample. The extent of this increase varies with the thickness of the sample, and while there is a step-like behavior for the 5 nm shell, it gradually transitions into an almost linear function. When the shell thickness is relatively small compared to the nanowire diameter, the corner localization has a more significant impact on electron distribution, consequently, in thinner shells, the energy gap

between corner and side states is higher. Due to this reason, it was expected to have a step-like behavior in thinner shells, which gradually disappears as the shell thickness increases. Thermoelectric current increases with increasing shell thickness and it has an almost linear relationship with the temperature bias. By considering all obtained results we can note that the charge and heat conductivity are highly dependent on the geometry and vary considerably with changes in the chemical potential and temperature biases. Also, in the presence of a temperature gradient, shells with a triangular cross-section result in greater charge and heat currents. A decrease in shell thickness results in a significant change in the charge and heat currents. For further and detailed information about electronic conduction variation with temperature gradient and chemical potential bias in tubular nanowires with different cross sections and thicknesses, we encourage readers to study [29].

3.2 Geometry effect over phononic thermal conductivity

The thermal conductivity of nanowires is significantly distinct from that of bulk materials because of their small size and large surface-to-volume ratio [103]–[105]. This can be attributed to phonon scattering resulting from finite size confinement, increased scattering caused by boundary conditions, or phonon transport quantization. In silicon nanowires with a diameter less than 20 nm, the phonon dispersion is altered because of phonon confinement, leading to a notable reduction in phonon group velocities [106], [107]. According to experimentalists, the thermal conductivity of individual single crystalline Si nanowires is two orders of magnitude lower than the bulk value [108]. The transverse cross-section of nanowires plays an important role in determining the surface-to-volume ratio, and several computational [87], [109]–[111] and experimental [112]–[114] studies establish a correlation between the

heat transport properties of nanowires and their particular geometry. Engineering the geometry of nanowires is one of the methods used to scatter phonons in nanostructured materials [115]. Especially, with core-shell nanowires, one can control electron and phonon scattering mechanisms and also provide different channels for heat and charge transfer [25], [87], [116]–[119].

We choose molecular dynamics (MD) for the study of phonon behavior, due to the fact that the time scale and spatial resolution employed in MD simulations fit well for observing atomic vibrations. There are several studies to calculate the thermal conductivity of nanowires with MD using different approaches such as equilibrium molecular dynamics (EMD) [120]–[123], non-equilibrium molecular dynamics (NEMD) [124]–[126], and reverse non-equilibrium molecular dynamics (rNEMD) [127]–[130]. Each approach has been using a different algorithm to solve the problem, but we choose rNEMD due to the fact that in studying the thermal conductivity of nanowires it has some obvious advantages over other methods. Some of these advantages are building desired temperature gradient [124], less computation cost for the auto-correlation function to be convergent, the linear temperature profile in the neighborhood of the hot and cold segments [126], and small fluctuations in temperature and heat flux [131]. We use the Müller-Plathe [131] method in (rNEMD) approach to compute the thermal conductivity of tubular and core-shell nanowires with different geometries. In this method, the density of heat flux Q is characterized as the quantity of energy transferred across a surface of a specific area perpendicular to the direction of flux within a defined period of time. The thermal conductivity can be obtained by Fourier law

$$Q = -\kappa \nabla T, \quad (3.4)$$

where ∇T is the temperature gradient determined from atomic velocities. if we consider the z axis as the direction of temperature propagation, then we can define thermal conductivity as

$$\kappa = - \lim_{\partial T / \partial z \rightarrow 0} \lim_{t \rightarrow \infty} \frac{\langle Q_z \rangle}{\langle \partial T / \partial z \rangle}, \quad (3.5)$$

where t is the simulation time, and it is longer than the relaxation time after setting the initial conditions. We employ silicon and germanium possessing a diamond structure as model systems in our simulations. Electrons' heat conduction is very small compared to the phonons in the intrinsic (undoped) Si, so in our atomistic model, we ignore electron transport. We use the large scale atomic/molecular massively parallel simulator (LAMMPS) from Sandia National Laboratory [132] to solve Newton's equation of motion in MD simulation. The Si nanowires were inserted into an orthogonal simulation box that accommodates their length, and it is several times larger than the diameter in the transverse directions (See Fig.3.5 and Fig.3.6). Fixed boundary conditions are implemented in the transverse directions (x and y), and periodic boundary conditions are applied along the nanowire axis (z direction). The [111] lattice direction was used to orient the nanowire axis that gives (111) planes at the nanowire cross-section. Previous studies [122], [133]–[135] show that κ is dependent on the nanowire length in the simulation, so to understand the length effect we considered different nanowire lengths (10–120 nm). Our results show that for pure silicon nanowires, the thermal conductivity increases rapidly at lengths below 100 nm, but at higher lengths varies more slowly and reaches a constant value. Also, there is a huge increase in the thermal conductivity magnitudes when length increases. For instance, at 100 K the thermal conductivity for the 120 nm length nanowire is almost eight times higher than for the one with 10 nm length. These

results are in agreement with findings from previous (MD) studies [86], [136]. For understanding the effect of the nanowire cross-section on the thermal conductivity, we fix the length of nanowires and look at the influence of the cross-sectional area with respect to temperature. We simulate nanowires with the circular transversal cross-section with radii of 1, 1.4, 2.1, 2.8, and 5.5 nm. Generally, in all temperature regimes nanowires with higher cross-sectional areas provide higher thermal conductivity. Some studies have reported similar results for nanowires with square and circular shapes [87], [137], [138]. Building a vacuum inside nanowires (tubular nanowires) leads to a reduction in thermal conductivity values regardless of geometry shapes, and further expanding this hollow inside nanowires results in more and more reduction in thermal conductivity. Among different geometries, tubular triangle shapes exhibit more reduction in thermal conductivity magnitude. It is difficult to calculate the thermal conductivity of core-shell nanowires, due to different phonon scattering mechanisms. Some of these complexities are phonon scattering due to different geometries, phonon-phonon interference at the interface between the core and the shell, and different phonon group velocities and stress (arise from different materials) along the common interface. Due to these complexities, we perform several simulations for Si/Ge and Ge/Si core-shell nanowires with different cross-section shapes, full report and extra information can be found at [30].

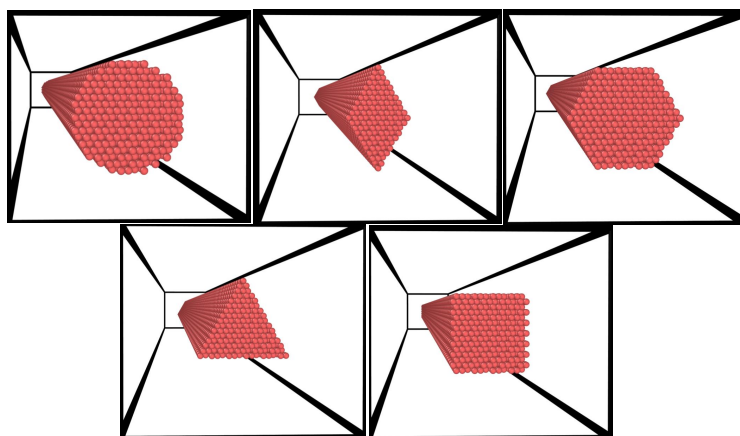


Figure 3.5: Cross-sectional shapes of solid nanowires. (Heris et al., Supplementary material of Surfaces and Interfaces, 2022)

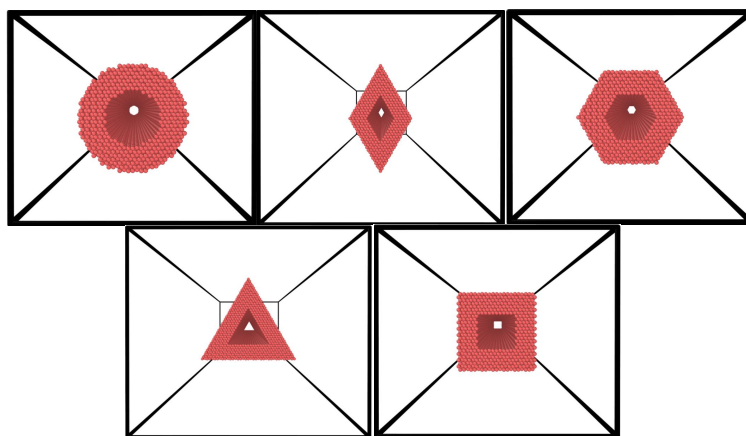


Figure 3.6: Cross-sectional shapes of tubular nanowires. (Heris et al., Supplementary material of Surfaces and Interfaces, 2022)

Chapter 4

Impurities effect on electronic conduction

Main changes in electronic charge and heat transport in nanowires originate from four fundamental factors: Cross-section geometry, surface roughness, impurities, and phonons. The effect of nanowires' cross-section geometry on both electronic and phononic conduction features has been fully discussed in the previous chapter. Here we neglect the phonon effect on electronic conduction properties (electron-phonon interaction) because electronic properties will be discussed in thin shells, but for the case of nanowires with large cross-sectional areas in the next chapter, we will cover electron-phonon interaction in detail. The surface roughness effect on thermal conductivity can be calculated by knowing relaxation times for the scattering of phonons [139] and its effect on the charge current can be estimated for different materials [140]. Therefore, from the aforementioned four fundamental factors impurities' effect still remains and requests more investigation which we are going to cover in this chapter.

It is essential to understand both charge and heat current behavior in nanoscale studies, and we try to provide a comprehensive view of impurities' effect on the electronic conduction of tubular nanowires. The presence of impurities in tubular nanowires has a notable impact on their conduction characteristics, and its effect is different for each geometry with respect to chemical potential bias or temperature gradient. Also, the numbers of impurities or their intensities lead to distinct behavior in each geometry. Nowadays it is feasible to fabricate tubular nanowires with the desired cross-section and different doping variations, so it is important to study the direct relation between different cross-sections and transport properties of core-shell nanowires in presence of impurities. Nanowires with different cross-section areas are built as it is described in chapter 3.1 and we calculate the charge and heat current using the Landauer-Buttiker approach with Eq.(3.1) and Eq.(3.2). we study the conduction under the temperature gradient and a chemical potential bias separately to see each one's effect clearly. The chemical potential bias is present at the two ends of the nanowire, and during each calculation step, we modify the values of the left and right reservoirs simultaneously ($\Delta\mu = \mu_L - \mu_R = 3 \text{ meV}$). The corner and side states are energetically separated by an interval that depends on the geometry and on the aspect ratio of the polygonal, the energy gap between states is high in the first 10 modes. So irrespective of variations in geometries or impurities, we use the first 10 transverse modes in our numerical computation. Distinct energy spectra emerge for each cross-sectional area, resulting in the appearance of different chemical potential windows. So, there are maximum and minimum values of the chemical potentials for each specific geometry. The electronic conduction is calculated between the ground state and the highest states for each geometry. (Temperature is fixed $T_L = T_R = 200 \text{ K}$.)

In the case of a temperature gradient, in the first step, we set $T_L = 36$ K and $T_R = 1$ K and we increase the temperature of both sides simultaneously. This process was repeated 10 times and the left temperature values varies between 36 – 420 K. While temperature gradient is always fixed $\Delta T = T_L - T_R = 35$ K and chemical potentials of each geometry is $\mu_L = \mu_R = (\mu_{max} + \mu_{min})/2$.

To compare impurities' effect on different geometries, we consider tubular nanowires with no impurity and same shape tubular nanowires with 10000 impurities each one with a potential of 10 meV. It is obvious that implementing disorder leads to a reduction in charge and heat current values with respect to both temperature gradient and chemical potential bias but the amount of this reduction is different from one geometry to another. The utmost reduction of the charge current is related to the nanowires with a circular cross-section with respect to chemical potential bias while the highest reduction in the case of heat transport is related to the nanowire with a triangle cross-section with respect to the temperature gradient. The charge current of any geometry is determined by the transmission function and the energy window associated with the chemical potential. So whether it is pure wires, and or those with impurities, a higher chemical potential allows a larger number of states to participate in the transmission and achieve high charge current. Roughly speaking implementing impurities leads to a reduction in charge current values 15% (average of the triangle)-43% (average of circular) with respect to chemical potential bias and 8% (average of the triangle)-31% (average of circular) with respect to the temperature gradient.

The heat current reduction due to impurities are different for each geometry, although this variation is small. On average the circular cross-section shows 30%, and the triangular cross-section 15% reduction of the heat current values in the presence

of impurities. Reference [141] provides more detailed information about the electronic charge and heat current variation as a function of chemical potential bias or temperature gradient for different cross-sectional tubular nanowires.

In the next step, we focus on the number of the impurity's effects on electronic conduction. For checking the number of impurities effect in tubular nanowires with a triangle cross-section we start with pure nanowires and then add 100-1000-5000 and 10000 points of impurities with the potential of 10 meV. As you can see from Fig.4.1(a), the Energy as a function of transmission coefficient provide step-like behavior for pure nanowire. By adding 1000 impurities, these steps show disturbance in their values and they lose their sharpness Fig.4.1(b). By adding more points of impurities step like behavior for energy versus transmission vanishes gradually and it inclines to linear trend.

The charge and heat current values of nanowires with 100 impurities point is very close to pure nanowires and nanowire with 1000 impurities show a small deviation from pure one. By increasing the number of impurities to 5000 and 10000 points the charge and heat current decreases more and more with respect to both temperature gradient and chemical potential bias in comparison to pure nanowires values. A small number of impurities will not play a noticeable role in the reduction of conduction. A small number of impurities will not play a noticeable role in the reduction of conduction but a further increase in the number of impurities leads to 15%-25% reduction in the charge current of triangular shells.

To understand the impurities intensity effect over the conduction feature, in the same manner, we choose triangle shells with 20 nm thickness. We start with measuring the charge and heat current of pure tubular nanowires with no impurity. Then we add 300 points of impurities with the potential of 50-100 and 200 meV. The elec-

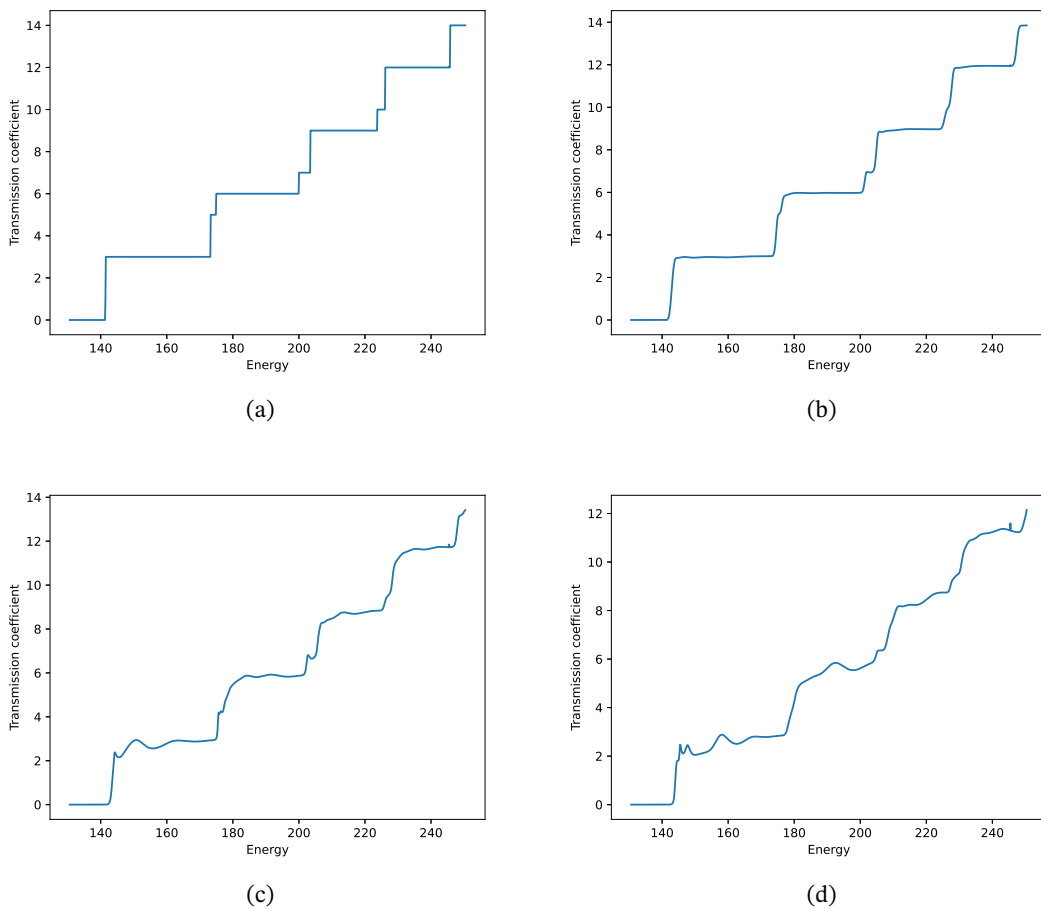


Figure 4.1: Transmission coefficient as a function of energy for first ten states for tubular nanowires with a triangle cross-section. The external radius is 50 nm and the thickness of the shell is 20 nm for all cases. (a) Tubular nanowire with no impurity (b) Tubular nanowire with 1000 impurity points with a potential of 10 meV (c) Tubular nanowire with 5000 impurity points with a potential of 10 meV (d) Tubular nanowire with 10000 impurity points with a potential of 10 meV.

tronic density of states for nanowires has been presented in Fig.4.2. Fig.4.2 (a), displays the density of states for tubular nanowires in the absence of impurities. It ex-

hibits the anticipated shapes of the density of states, as depicted in Fig.2.2. By implementing impurities with stronger potential in the system, perturbation increases and consequently the magnitude of the density of states decreases. In contrast to the trend that we see in the number of impurities effect, in calculating the intensity effect of impurities we observe fast deviation of electronic conduction values from the pure nanowires. In low-temperature regimes and small chemical potentials, the charge current values of nanowires with highly intense impurities are close to pure nanowires but gradually this gap increases. The reduction of the currents in triangle shells becomes 50% and for hexagonal shells in some cases 85%. In presence of intense impurities, triangular shells suppress electrical current less than heat current. Also, intense impurities in hexagonal shells lead to a significant reduction of 75 - 85% (on average) in conduction properties, when the chemical potential and temperature is varied.

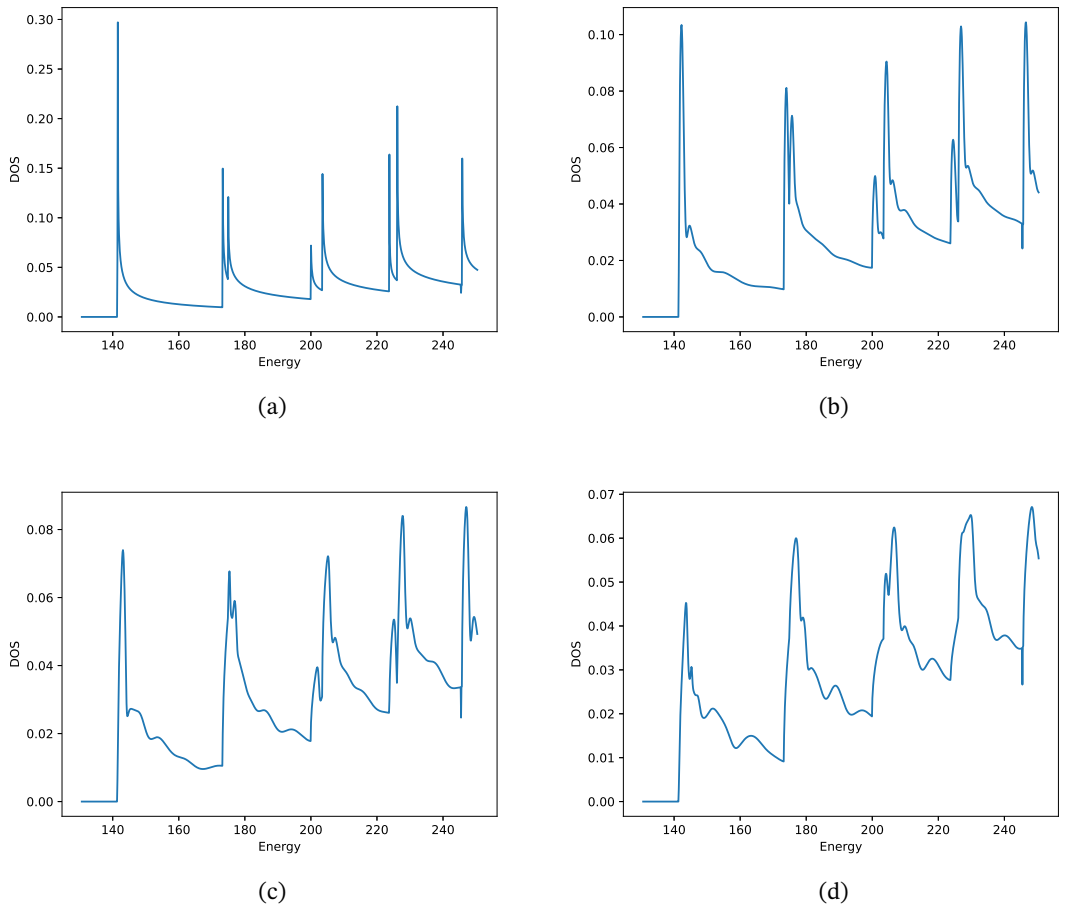


Figure 4.2: Density of states as a function of energy for first ten states for tubular nanowires with a triangle cross-section. The external radius is 50 nm and the thickness of the shell is 20 nm for all cases. (a) Tubular nanowire with no impurity (b) Tubular nanowire with 300 impurity points with a potential of 50 meV (c) Tubular nanowire with 300 impurity points with a potential of 100 meV (d) Tubular nanowire with 300 impurity points with a potential of 200 meV.

Chapter 5

Importance of phonon drag in thermopower

The efficiency of thermoelectric energy conversion can be significantly increased in the low-dimensional system, And it is essential to study electron and phonon coupling phenomena on the nanoscale to understand the thermoelectric transport properties. Thermopower is the most well-studied parameter in the field of thermoelectrics, and it provides important information about electronic band structures, electron scattering, and electron-phonon scattering mechanisms.

As it is discussed in the previous chapters the thermopower consists of two terms according to Eq.(2.3). In this chapter, we discuss diffusion thermopower and phonon drag thermopower in nanowires. Diffusion thermopower S_d is referred to the diffusion of carriers from the hot to the cold side. Also, there is another phenomenon which is related to electron-phonon interaction in the system. During electron-phonon interaction, phonons cause an increase in the effective mass of charge carriers which is known as phonon drag. So, the thermopower associated with phonon drag orig-

inates from the transfer of momentum to carriers through acoustic phonons in the presence of a temperature gradient. In this chapter, we start with the Boltzmann equation to describe electron transport in equilibrium and non-equilibrium conditions, then we introduce a collision term due to electron-phonon scattering. The phonon distribution will be determined by the steady-state Boltzmann equation for phonons by considering relaxation time approximation. We introduce a new term that accounts for the phonon drag effect and then calculate diffusion and phonon drag thermopower in nanowires. In the last phase, we present some of our results which are obtained from numerical calculations on a tight-binding model (By using Kwant) for both terms of thermopower in the system.

To explain electron transport phenomena (heat and electric current), it is useful to introduce a distribution function. The distribution function $f_k(r, t)$, describes the probability of finding an electron with a particular spin orientation in the vicinity of position r and time t , in the state with wave vector k . By considering steady-state situations, time can be neglected and densities of electric and heat currents can be expressed like

$$J = -\frac{g_s g_v |e|}{A} \sum_k f_k v_k, \quad (5.1)$$

$$Q = \frac{g_s g_v}{A} \sum_k f_k (E_k - E_F) v_k, \quad (5.2)$$

where g_s and g_v are the spin and valley degeneracies, E_F is the Fermi energy and $v_k = (1/\hbar)\nabla_k E_k$ is the electrons group velocity. The electron distribution is characterized by the Fermi-Dirac function when there are no external fields or thermal gradient present, and the system is in equilibrium,

$$f_k^0 \equiv f^0(E_k) = 1/(\exp[E_k - E_F/k_B T] + 1). \quad (5.3)$$

In the presence of a thermal gradient ∇T and a static field E in the plane, the perturbed electron distribution function can be determined by the steady-state Boltzmann equation,

$$v_k \cdot \nabla_r f_k - (|e|\hbar)E \cdot \nabla_k f_k = (\partial f_k / \partial t)_{collision}. \quad (5.4)$$

The first and second terms on the left side of Eq.(5.4) are showing the change in distribution function due to the electron diffusion in presence of a thermal gradient and due to electrons acceleration by an external field, respectively. The right-hand side in Eq.(5.4) refers to the collision term and consists of both electron elastic and inelastic scatterings as

$$(\partial f_k / \partial t)_{collision} = -(f_k - f_k^0) / \tau_{es}(E_k) + (\partial f_k / \partial t)_{e-ph}^a + (\partial f_k / \partial t)_{e-ph}^e, \quad (5.5)$$

where the first term refers to the elastic electron scattering (i.e. by ionized impurities, interface roughness, alloy disorder). Relaxation time approximation is used in the elastic scattering. $(\partial f_k / \partial t)_{e-ph}^a$ is electron scattering by phonons-absorption process and $(\partial f_k / \partial t)_{e-ph}^e$ is electron scattering by phonons-emission process. At low temperatures the population of optical phonons is negligible, so acoustic phonons role is important in electron scatterings. By considering the sum of longitudinal and two transverse acoustic modes, the collision term due to e-ph coupling is [142]

$$(\partial f_k / \partial t)_{ep}^{a-e} = \sum_{k'} \sum_{q,s} [f_{k'}(1 - f_k)P_{q,s}^{a-e}(k', k) - f_k(1 - f_{k'})P_{q,s}^{a-e}(k', k)], \quad (5.6)$$

where $P_{q,s}^{a-e}(k', k)$ is the intrinsic rate of electron transition from a state k to the state k' by absorbing-emitting one acoustic phonon with wave vector q in mode s . The 3D phonon wave vector is expressed as $q = (q_{\parallel}, q_z)$, where q_{\parallel} is parallel to the electron layer (xy -plane). Cantrell and Butcher [142] derived the transition rates using Fermi's golden rule. And this transition rate must satisfy the below condition

$$f_k^0(1 - f_{k'})P_{q,s}^{a(0)}(k, k') = f_{k'}^0(1 - f_k)P_{q,s}^{e(0)}(k', k). \quad (5.7)$$

Phonon distribution in equilibrium $N_{q,s}^0$ is described by the Bose-Einstein function

$$N_{q,s}^0 = 1 / [\exp(\hbar\omega_{q,s}/k_B T) - 1], \quad (5.8)$$

and with exert of relaxation time approximation, phonon distribution $N_{q,s}$ can be determined by steady state Boltzmann equation

$$v_p(q, s) \cdot \nabla_r N_{q,s} + [(N_{q,s} - N_{q,s}^0) / \tau_p(q, s)] = (\partial N_{q,s} / \partial t)_{pe}, \quad (5.9)$$

where $v_p(q, s) = \nabla_q \omega_{q,s}$ is the phonon group velocity. The second term on left hand-side of Eq.(5.9) presents phonon collision with boundaries and lattice imperfection by relaxation time $\tau_p(q, s)$. And right-hand term in Eq.(5.9) refers to the rate of change in phonon distribution due to scattering with electrons

$$(\partial N_{q,s}/\partial t)_{pe} = g_s g_v \sum_{k,k'} [f_{k'}(1-f_k)P_{q,s}^e(k',k) - f_k(1-f_{k'})P_{q,s}^a(k',k)]. \quad (5.10)$$

The coupling between the electron and phonon Boltzmann equations arises from the simultaneous presence of f_k and $N_{q,s}$ in the collision terms described by Eq. (5.6) and (5.10). The electron and phonon distribution functions can be linearized like $f_k = f_k^0 + f_k^1$ and $N_{q,s} = N_{q,s}^0 + N_{q,s}^1$, under the assumption that the thermal gradient and electric field are sufficiently weak. Note that f_k^1 is associated to ∇T and E and $N_{q,s}^1$ to ∇T . By substituting these expressions into Eq.(5.4) and (5.9) and with some algebra [142], [143], the linearized electron Boltzmann equation is

$$\frac{df_k^0}{dE_k} v_k \cdot \left(\frac{E_k - E_F}{T} \nabla T + |e|E \right) + U(k) = \frac{f_k^1}{\tau_{es}(E_k)}, \quad (5.11)$$

where the first and second terms from left-hand side are related to drift electrons with temperature gradient and external field, respectively. And the new term $U(k)$ is responsible for the phonon-drag contribution

$$U(k) = \frac{1}{k_B T^2} \sum_{k'} \sum_{q,s} \hbar \omega_{q,s} \tau_p(q,s) (\Gamma_{k',k} - \Gamma_{k,k'}) v_p(q,s) \nabla T, \quad (5.12)$$

where

$$\Gamma_{k',k} = f_k^0 (1 - f_{k'}^0) P_{q,s}^{a0}(k, k'), \quad (5.13)$$

is the average rate of absorption of phonons of wave vector q and mode s which cause electron transmission from a state k to k' when both electrons and phonon are in thermal equilibrium.

5.1 Diffusion thermopower

For calculating diffusive thermopower, we neglect phonon drag contribution to the non-equilibrium electron distribution function and we set $U(k) = 0$ in eq.(5.11). Then, by substitution of f_k^1 in Eq.(5.10) and comparing with macroscopic transport equations $J = \sigma E + L \nabla T$ [144], we yield following expressions for electrical conductivity σ and the thermoelectric coefficient L

$$\sigma = - \int \sigma(E_k) (df_k^0/dE_k) dE_k, \quad (5.14)$$

$$L_d = - \frac{1}{|e|T} \int \sigma(E_k) (df_k^0/dE_k) (E_k - E_f) dE_k. \quad (5.15)$$

At low temperatures, where normally S_d dominates, electron momentum relaxation time is mainly limited by elastic scattering. Now, the diffusion thermopower can be obtained by expanding $\sigma(E_k)$ linearly about E_F [145] and from the ratio $S_d = -L_d/\sigma$,

$$S_d = - \frac{\pi^2 k_B^2}{3|e|} T \frac{d \ln[\sigma(E_k)]}{dE_k} \Big|_{E_k=E_F}. \quad (5.16)$$

With some assumptions for energy and electron relaxation time (which is unique for each material) [146], [147], diffusion thermopower can be written as [148]

$$S_d = -(p + 1) \frac{\pi^2 k_B^2}{3|e|E_F} T, \quad (5.17)$$

where parameter $p = (d \ln \tau_{es}/d \ln E_k)_{E_F}$ determines the energy dependence of the transport lifetime and is of the order of unity. p sign depends on the scattering mechanism that limits the electron mobility. The parameter p determines both the magnitude and the sign of diffusion thermopower [149], [150]. According to Eq.(5.17)

when $p < -1$ it changes S_d sign, which means a reversal of the total thermopower is expected. In contrast, the sign of phonon drag thermopower S_g is determined only by the type of carriers (negative for electrons and positive for holes). For holes the minus sign in Eq.(5.16) and (5.17) will be omitted.

5.2 Phonon-drag thermopower

The phonon-drag contribution to the perturbed electron distribution function is a measure of the momentum transfer between electrons and phonons in a material, and it can have important effects on the transport properties. For calculating phonon drag thermopower, we return to the linearized Boltzmann Eq.(5.11) and write the phonon-drag contribution to the perturbed electron distribution function as $f_k^{1g} = \tau_{es}(E_k)U(k)$. The phonon-drag contribution to the thermoelectric current $J_g = L_g \nabla T$ can be evaluated by substituting f_k^{1g} in Eq.(5.1). Similarly to diffusion thermopower, phonon drag thermopower can be obtained from the ratio $S_g = -L_g/\sigma$ [142],

$$S_g = \frac{g_s g_v |e|}{2\sigma A k_B T^2} \sum_k \sum_{k'} \sum_{q,s} \hbar \omega_{q,s} \tau_p(q,s) v_p(q,s) \cdot [\tau_{es}(E_k) v_k - \tau_{es}(E_{k'}) v_{k'}] \Gamma_{k',k}, \quad (5.18)$$

where $v_p(q,s) = \nabla_q \omega_{q,s}$ ($\omega_{q,s} = v_s q$) is the phonon group velocity, and $\tau_p(q,s) = l_p/v_s$ is phonon relaxation time. l_p is limited by the dimension of the sample and defines the boundary scattering regime, this parameter is also temperature dependent and play important role in determining phonon drag thermopower. With some approximations (energy dependence of the momentum relaxation time and slow variation of τ_{es} the energy scale of $\hbar \omega_{q,s}$) [142], the phonon mean-free path has been assumed to be the same for the three acoustic branches [151]. These approximations

lead to simple dependencies of phonon drag thermopower on the temperature and the sheet density

$$S_g \propto \frac{T^n}{n_s^{3/2}}, \quad (5.19)$$

where, $n = 4$ when electrons are coupled to phonons via piezoelectric interaction [152], [153], or $n = 6$ electrons are coupled to phonons via a deformation potential [154].

In our models, all nanowires have a fixed length of 100 nm. We choose a square shape for their transversal cross-section. In the case of tubular nanowires, the hollow volume along the center of the nanowire has also a square shape. First, we consider a full nanowire (no hollow volume) with 20 nm side thickness in x and y directions to calculate diffusion thermopower, assuming there is no phononic heat transfer through the nanowire. Then, by considering acoustic phonon modes in the z direction, we implement the electron-phonon coupling term in the energy conservation equation and we calculate phonon drag thermopower. Note that, by implementing a temperature gradient in the system we provide a non-equilibrium electron and phonon distribution function in all directions. But due to the fact that our main temperature bias is defined between leads, in the z direction, and also the length in this direction is longer than the nanowire thickness, the main part of phonon drag phenomena occurs along the z direction and it is negligible in the x and y directions.

Fig. 5.1 represents the diffusion, the phonon drag, and the total thermopower values in different tubular nanowires with square cross sections. As you can see from all the figure diffusion thermopower has the main role in building up the total thermopower; and total thermopower behavior with respect to temperature is very similar to the diffusion case. Tubular nanowires with small side thickness show

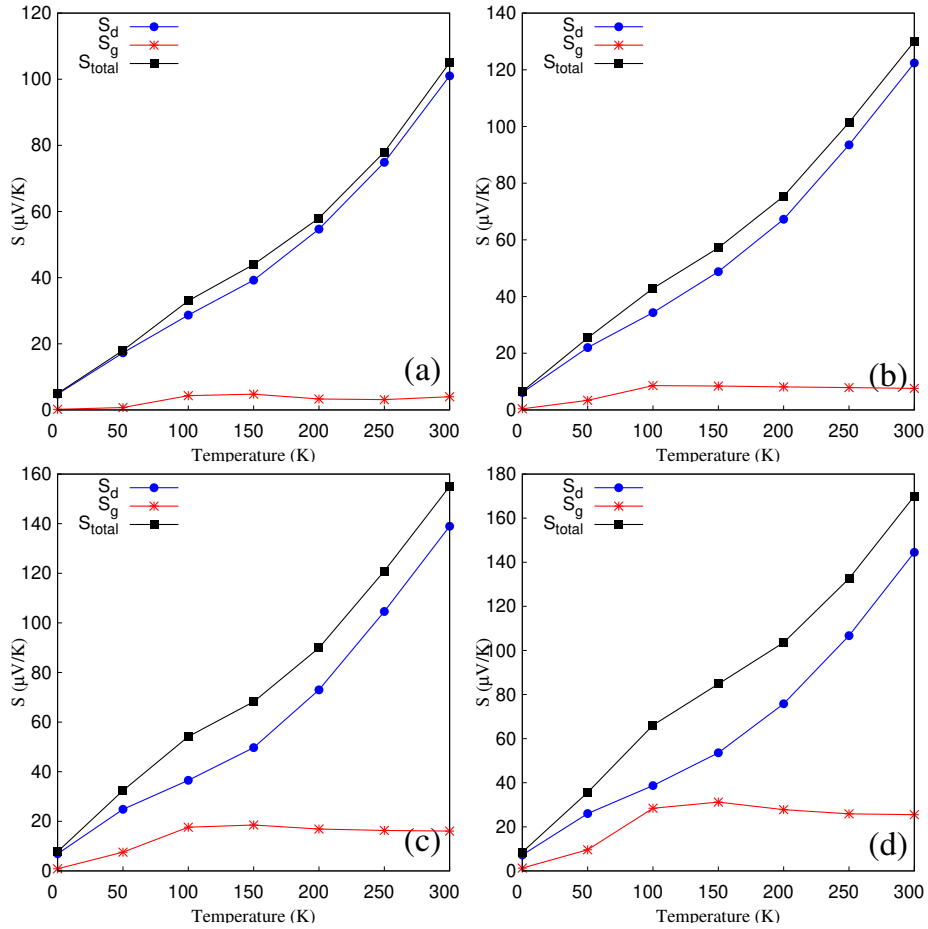


Figure 5.1: The diffusion thermopower S_d , phonon drag thermopower S_g , and total thermopower $S_{total} = S_d + S_g$ with respect to temperature. Tubular nanowires with a square cross-sectional area with a thickness of (a) 5 nm shell, (b) 10 nm shell, (c) 15 nm shell and (d) 20 nm shell.

low values of phonon drag in comparison to pure nanowires (compare S_g values in Fig.5.1 (a) and (d)). In tubular nanowires with decreasing hollow size in the center, phonon drag thermopower magnitudes increase and in some temperature regimes (100-200 K) it is close to diffusion thermopower. This can be explained by the fact

that in thinner tubular nanowires phonons scattering increases, due to the boundary and geometry scattering. A small mean free path for phonons leads to small electron-phonon interaction and consequently small phonon drag thermopower. Increasing temperature leads to high transmission function and energy associated with the chemical potential, so it is expected to see total thermopower values increase in higher temperatures. Fig.5.2 presents diffusion and phonon drag thermopowers behavior with respect to temperature separately.

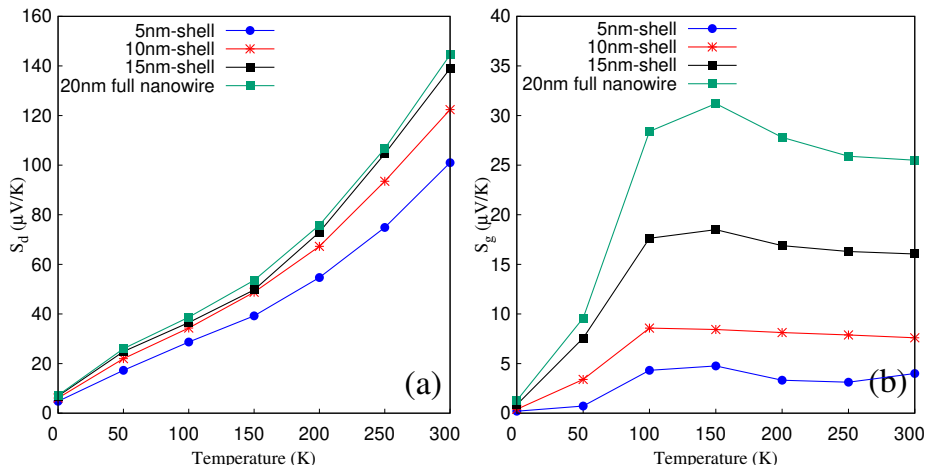


Figure 5.2: Comparison of S_d and S_g for tubular nanowires with square cross sections and pure nanowires. The lateral size of all nanowires is 20 nm and for nanowires with hollow inside shells, thicknesses is 5, 10 and 15 nm.

Full nanowire shows a high amount of phonon drag thermopower in comparison to tubular nanowires. By decreasing the thickness of nanowires phonons tend to scatter more and consequently provide small phononic mean free. As result, for thinner tubular nanowires we see small phonon drag thermopower. In full nanowires, phonon drag contribution to the total thermopower is close to the values of diffusion thermopower, but with decreasing thickness of nanowire, this share of phonon

drag decreases. Also, we consider carrier concentration effect on phonon drag thermopower by changing energy level above Fermi level. Electron-phonon coupling term will play a much more important role in scattering mechanisms by increasing the number of electrons. As a consequence, phonon drag phenomena lead to an additional increase of the total thermopower.

Chapter 6

Summary of papers

Papers I and III discuss the electronic charge and heat transport in tubular nanowires in different conditions. Paper II discusses phononic heat transport in core-shell nanowires and paper IV discusses impurities effect on nanowires.

- **Paper I: Thermoelectric properties of tubular nanowires in the presence of a transverse magnetic field**

We calculate the electronic charge and heat transport generated by temperature gradient and chemical potential bias in tubular semiconductor nanowires, in presence of a magnetic field. We use the Landauer-Büttiker approach to calculate charge current, electronic heat current, Seebeck coefficient, thermal conductivity and figure of merit.

- **Paper II: Effects of transverse geometry on the thermal conductivity of Si and Ge nanowires**

We use molecular dynamics simulations with the LAMMPS software to explore the effects of geometry on the thermal conductivity of silicon and germanium

nanowires. So, we consider nanowires with different polygonal cross-sections, tubular (hollow) nanowires, and core/shell nanowires with combinations of Si/Ge and Ge/Si.

- **Paper III: Charge and heat currents in prismatic tubular nanowires**

In this paper, we study the influence of the cross-section shape and shell thickness on the electronic conduction properties of tubular nanowires. We use the Landauer-Büttiker approach to calculate the charge and electric heat currents generated by a temperature gradient or a chemical potential bias.

- **Paper IV: Effect of Impurities on Charge and Heat Transport in Tubular Nanowires**

We study impurities effect on charge and heat transport in tubular semiconductor nanowires with different cross-sectional areas. The Landauer-Büttiker approach is used to calculate the transport quantities originating from a temperature gradient and a chemical potential difference. Different numbers of impurities with various intensities have been studied in each polygonal cross-section.

Paper I

Thermoelectric properties of tubular nanowires in the presence of a transverse magnetic field

Hadi Rezaie Heris, Movaffaq Kateb, Sigurdur I Erlingsson and Andrei Manolescu

School of Science and Engineering, Reykjavik University, Menntavegur 1, IS-102 Reykjavik, Iceland

Received: 28 February 2020

Accepted: 25 June 2020

Published: 28 July 2020

Thermoelectric properties of tubular nanowires in the presence of a transverse magnetic field

Hadi Rezaie Heris , Movaffaq Kateb, Sigurdur I Erlingsson and Andrei Manolescu 

School of Science and Engineering, Reykjavik University, Menntavegur 1, IS-102 Reykjavik, Iceland

E-mail: hadi19@ru.is and manoles@ru.is

Received 28 February 2020, revised 8 June 2020

Accepted for publication 25 June 2020

Published 28 July 2020



Abstract

We calculate the charge and heat current associated with electrons, generated by a temperature gradient and chemical potential difference between two ends of a tubular nanowire of 30 nm radius in the presence of an external magnetic field perpendicular to its axis. We consider a nanowire based on a semiconductor material, and use the Landauer-Büttiker approach to calculate the transport quantities. We obtain the variation of the Seebeck coefficient (S), thermal conductivity (κ), and the figure of merit (ZT), with respect to the temperature up to 20 K, and with the magnetic field up to 3 T. In particular we show that the Seebeck coefficient can change sign in this domain of parameters. In addition κ and ZT have oscillations when the magnetic field increases. These oscillations are determined by the energy spectrum of the electrons.

Keywords: thermoelectrics, nanowires, Seebeck coefficient, figure of merit ZT , thermal conductivity

(Some figures may appear in colour only in the online journal)

1. Introduction

Thermoelectric materials have attracted considerable attention due to their potential applications in electronics [1–4], as energy conversion devices [5–9], or as components of complex instruments used in medical science [10]. Thermoelectric devices display interesting properties such as being very reliable because they do not contain any moving part, being of very small size, and most importantly, capable of energy harvesting from waste heat of environment, that makes them very attractive for industry [5, 11, 12]. Semiconductor nanowires are promising candidates for thermoelectric applications, along with their rich and complex electrical, optical, and photovoltaic properties [13–16]. Nanowires have played an important role in this research direction due to their ability to provide efficient thermoelectric elements with low thermal conductivity and high figure of merit (ZT) [17–19].

In particular, core-shell nanowires based on III-V semiconductors enable the control of charge, and possibly heat transfer through the specific geometry and shell thickness. With a

doped shell and undoped core one can obtain a tubular conductor [20] with conduction electrons captured inside the shell. Most often such nanowires have a hexagonal cross section and the charge density peaks at the shell corners [21–25]. A nanowire made of a single material, for example InAs, may also become a tubular conductor if the conduction electrons are pushed towards the nanowire walls due to a favorable band bending at the surface [26]. Assuming a tubular distribution of the electrons in the nanowire, an journal localization mechanism, that we focus on in this paper, is produced by a magnetic field perpendicular to the nanowire axis, and in that case the electron density within the shell increases in the direction perpendicular to the field, where the so called snaking states are formed [27–30].

In a recent paper where two of the present authors were involved, it has been predicted theoretically that a temperature gradient can lead to reversal of thermoelectric current in tubular nanowires in the presence of transverse magnetic field, at low temperatures [31], meaning that the electrons can either flow from the hot to the cold lead, or vice versa. This prediction

indicates the importance of the magnetic field effect on the thermoelectric properties of a tubular conductor, but it still awaits an experimental validation.

In the present paper we want to address, still theoretically, the efficiency of a thermoelectric element based on a tubular conductor in a perpendicular magnetic field. Efficient thermoelectric devices are supposed to produce a considerable electric current, but at the same time to limit the heat flow [32, 33]. These characteristics are incorporated in the dimensionless figure of merit ZT , which is defined as

$$ZT = \frac{S^2 \sigma T}{\kappa}, \quad (1)$$

where S is the Seebeck coefficient, σ is the electrical conductivity, κ the thermal conductivity, and T the temperature. Hence, there are several parameters that need to be optimized to reach maximum value of ZT . In our physical system we know that the thermoelectric current is a nontrivial function of the magnetic field and temperature [31], and the first step of the present paper will be to obtain the Seebeck coefficient. After that, we will look at the thermal conductivity and finally at ZT .

The thermal conductivity reported for crystalline nanowires is more than two orders of magnitude lower than the bulk values [34]. Also, the phonon scattering at the nanowire surface substantially reduces their thermal conductivity and increases the thermoelectric power factor ($S^2 \sigma$) [35]. The diversity of fabrication methods for introducing dopants or impurities into the lattice is an journal reason that makes the semiconductor nanowires important for their thermoelectric characteristics [36–40]. The thermal transport in nanoscale systems, whose dimension is much smaller than the mean free path of electrons, cannot be explained by a simple law due to the presence of quantum-mechanical features and strong non-linear behavior [41]. At intermediate temperatures where ballistic and diffusive phonons coexist, the thermal conductance decreases non-linearly with the length. And especially at low frequency, where the acoustic phonons give the major contribution to the thermal conductance [42]. But at low temperatures charge carriers have an important role in thermal transport quantized in multiples of the universal value $\pi^2 k_B^2 T / 3 h$, also electrical conductance is quantized in multiples of universal value $G_0 = e^2 / h$ which can be understood within Landauer's formula [43, 44].

It has been shown that a magnetic field produces large changes in the thermoelectric properties, including the reduction of thermal conductivity of charge carriers [45]. This has been demonstrated experimentally for $\text{Bi}_{88}\text{Sb}_{12}$ at 78–295 K and magnetic fields up to 1.7 T. The magnetic field has been also studied for $\text{GaAs-Ga}_{1-x}\text{Al}_x\text{As}$ heterojunction up to 20 T [46]. The results showed an oscillatory behavior of thermopower (S) with the applied magnetic field. The magnetic field has been also studied for Bi nanowires array at 50–300 K which showed there is an optimum magnetic field for power factor [47].

The material of the paper is structured in these steps: In section 2 we present the model and the energy spectra of

our system, the tubular conductor in perpendicular magnetic field. Then, in section 3 we discuss and show the results for the Seebeck coefficient, for the thermal conductivity, and for the figure of merit. Finally, the conclusions are collected in section 4.

2. Model and methods

In this paper, we consider electronic transport in a tubular, cylindrical nanowire, in the presence of a longitudinal temperature difference and a uniform magnetic field transverse to the axis of the cylinder. The conduction takes place only in a narrow shell at the surface and not through the bulk [26].

The Hamiltonian of the system can be written as

$$H = \frac{(-i\hbar\nabla + e\mathbf{A})^2}{2m_{\text{eff}}} - g_{\text{eff}}\mu_B s B \quad (2)$$

where B is the magnetic field in the x direction, i.e. perpendicular to the nanowire length which is oriented along the z axis, and $\mathbf{A} = (0, 0, By)$ is the corresponding vector potential. Also, e is the electron charge, $m_{\text{eff}} = 0.023m_0$ and $g_{\text{eff}} = -14.9$ are the effective electron mass and bulk g -factor of InAs, μ_B is the Bohr's magneton and $s = \pm 1$ is the spin label. We chose the effective mass and g -factor as for InAs because this is a relatively common material used for core-shell nanowires. We assume that electrons propagate along the nanowire without interacting with journal electrons.

System parameters are $R = 30$ nm, $B = 0 - 3$ T and also by considering material parameter for InAs, we can calculate the heat current and electrical current driven by the temperature bias and chemical potential difference between the two ends of the nanowire, where we assume external leads are contacted. We calculate the charge current I_c and heat current I_Q through the nanowire using the Landauer approach:

$$I_c = \frac{e}{h} \int \mathcal{T}(E) [f_R(E) - f_L(E)] dE, \quad (3)$$

$$I_Q = \frac{1}{h} \int \mathcal{T}(E) [E - \mu] [f_R(E) - f_L(E)] dE, \quad (4)$$

where \mathcal{T} is the transmission function, and

$$f_{L,R}(E) = \frac{1}{1 + e^{(E - \mu_{L,R}) / kT_{L,R}}}$$

is the Fermi function for the left (L) or right (R) reservoir with chemical potential $\mu_{L,R}$ and temperature $T_{L,R}$. We consider a temperature bias $\Delta T = T_R - T_L > 0$, with T_L always fixed at 0.5 K, and a chemical potential bias $\Delta\mu = \mu_R - \mu_L$, with $\mu_L = \mu - \Delta\mu/2$ and $\mu_R = \mu + \Delta\mu/2$, where μ is fixed at 4.2 meV and $\Delta\mu$ is varied between 0 – 0.4 meV.

Ballistic transport of electrons in nanowires leads to a transmission \mathcal{T} , as a function of energy, with a step behavior. Nanowires showing such step-like behaviour have been measured, and in the presence of a low, but achievable impurity

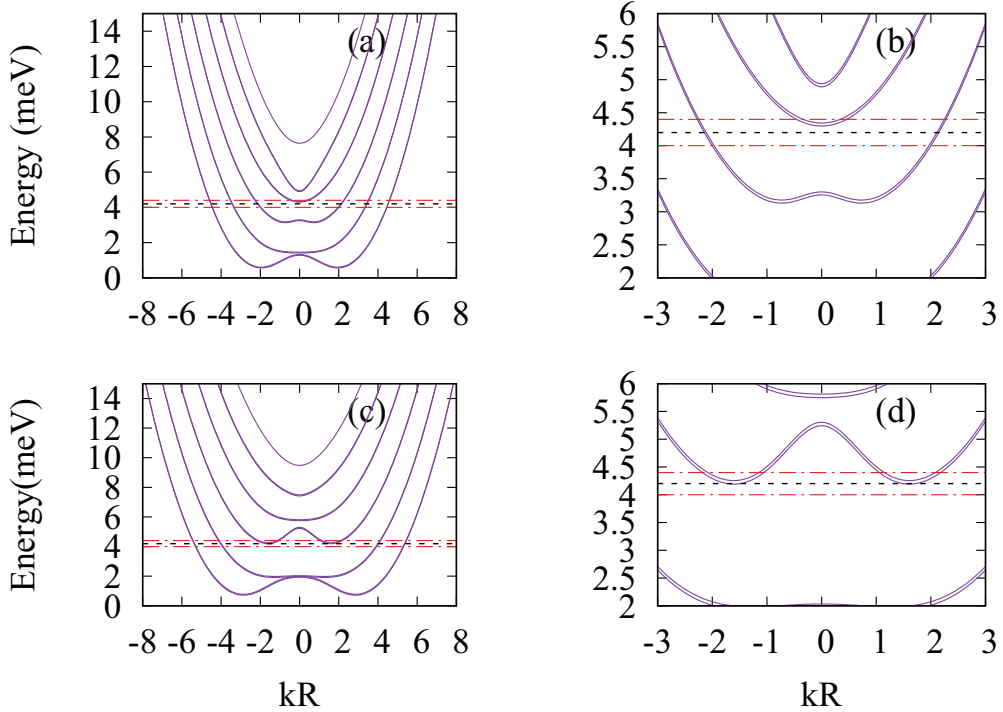


Figure 1. Energy spectra for a cylinder of infinite length and radius $R = 30$ nm in presence of transverse magnetic field $B = 1.8$ T (a) and (b), and $B = 2.5$ T (c) and (d). The black horizontal dotted lines indicate the chemical potential $\mu = 4.2$ meV and red horizontal dotted lines indicate the chemical potential $\mu = 4.0$ meV & $\mu = 4.4$ meV, respectively. (b) and (d) are the magnified image of (a) and (c) around the μ .

density the steps are still visible [48]. Based on this experimental fact we assume ballistic transport in our system. The transmission function in the presence of impurities can be obtained with the recursive Green's function method [31, 49]. For nanowires with inhomogeneities, such as impurities, a non-uniform diameter, surface changes, or stacking faults, the conductance becomes a series of transmission resonances due to quantum dot like states [35]. In that case transport calculations based on elastic scattering have been performed up to 24 K, so we can neglect inelastic collisions in our temperature range [31, 35, 37].

The eigenstates of the Hamiltonian (2) are calculated by numerical diagonalization in a basis set corresponding to plane waves $\exp(ikz)$, with k the wave vector in the longitudinal direction, and angular momentum eigenfunction $\exp(im\varphi)$, with $m = 0, \pm 1, \pm 2, \dots$, in the transversal plane (x, y) where the electrons are confined on a circle of radius R [27]. The resulting energy spectra for magnetic fields $B = 1.8$ T and 2.5 T are shown in figure 1. These spectra have an interesting feature: they may not always monotonic functions of k when it has a fixed sign. Meaning that the transport channels, i.e. the number of states with a fixed energy, which in general increases with increasing the energy, in this case may also decrease. Consequently, the thermoelectric current may change sign [31].

In the transport calculations we will consider that only electrons that are close to μ in energy contribute to the heat transport. The chemical potentials are chosen such that μ is close to a subband bottom. In figures 1(b) and (d) we show this energy interval for two values of the magnetic field.

3. Results and discussion

3.1. Seebeck coefficient

The Seebeck coefficient or the thermopower, S , is defined by the ratio $-\Delta V/\Delta T$, where the voltage difference ΔV is produced in presence of a small temperature difference ΔT between two points of a conductor, under an open circuit condition. Usually the thermopower consists of two additive contributions: diffusion S^d , and phonon drag S^s . The first one originates from the diffusion of carriers (electrons or holes) and second one comes from the momentum that is transferred to carriers via their coupling to non-equilibrium acoustic phonons in the presence of a temperature gradient [50–52]. For the total thermopower $S = S^d + S^s$ there is a very good agreement between theory and experiments at temperature below 21 K for example in bulk silicon [53]. However, at this low temperatures, where normally S^d dominates, we can neglect the phonon

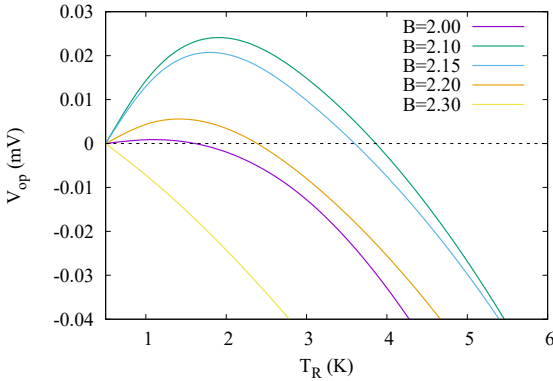


Figure 2. Open circuit voltage as function of right lead temperature in indicated values of magnetic field.

drag contribution to the non-equilibrium electron distribution function, and consider elastic scattering as the main mechanism that limits the electrons' momentum relaxation time.

The Seebeck coefficient is important for two reasons. First, this coefficient provides fundamental information about the electronic energy structure and the electron scattering mechanism in a system. Second, there is some evidence suggesting that thermoelectric energy conversion can be more efficient in low-dimensional systems [54]. For example, for a semiconductor, a large magnitude of Seebeck coefficient requires only one type of carrier, because mixed n-type and p-type conduction will send both carriers through contacts, leading to a reduced Seebeck voltage. The relation between the carrier concentration and Seebeck coefficient, for bulk states, is given by:

$$S = \frac{8\pi^2 k_B^2}{3eh^2} m^* T \left(\frac{\pi}{3n} \right)^{2/3}, \quad (5)$$

where n is the carrier concentration and m^* is the effective mass of carriers. Although a low carrier concentration of insulators and semiconductors result in large Seebeck coefficient, it also leads to a low electrical conductivity, $1/\rho = \sigma = ne\mu_c$, where the electrical conductivity and electrical resistivity are related to n through the carrier mobility μ_c [5, 55, 56]. There is also anjournal conflict with the effective mass of the charge carriers, in a manner that large effective mass provide high thermopower but low electrical conductivity.

In the present work we consider ballistic transport such that the electronic energy spectra have the main role in the behavior of the thermopower. We assume that the scattering due to impurities have negligible effects, and that is a reasonable approximation in a sufficiently clean system [37, 40]. Using the transmission functions for the calculated energy spectra we determine the voltage in an open circuit condition, V_{op} , from the chemical potential bias necessary to bring to zero the electric current in the system [equation (3)]. That means we evaluate $\Delta\mu = \mu_R - \mu_L = eV_{op}$ as a function of the temperature of the right lead, for different values of magnetic field.

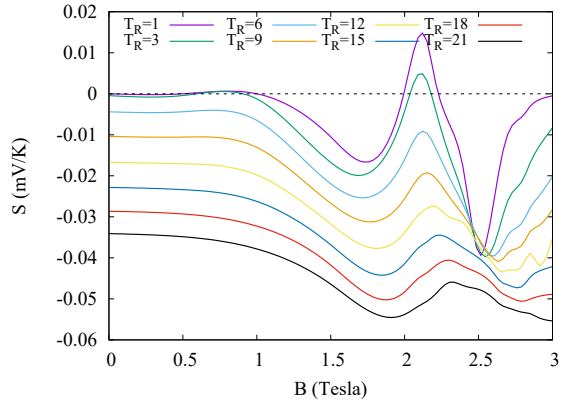


Figure 3. Seebeck coefficient with magnetic field for different values of T_R where $\mu = 4.2$ meV and $T_L = T_R - 0.1$ K (i.e. $T_L \approx T_R$).

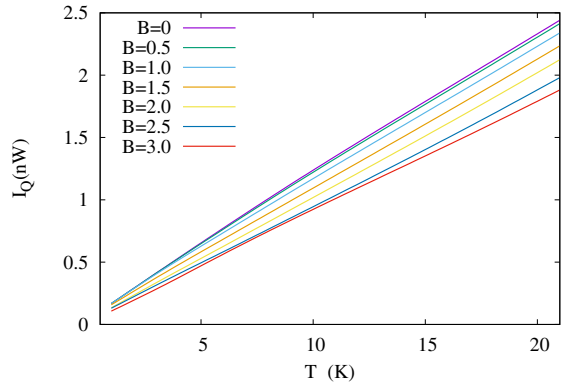


Figure 4. Heat current as function of the temperature of the right contact T_R for the indicated magnetic field values and the chemical potential $\mu = 4.2$ meV.

As one can see in figure 2 the open circuit voltage has a non-linear dependence on the temperature bias, for magnetic fields between 2.0 – 2.3 T. More remarkably is though the change of sign as a function of the temperature, which occurs because of the nonmonotonic variation of the transmission function with respect to the energy [31].

We obtain numerically the Seebeck coefficient, $S = V_{op}/\Delta T$, as the linear coefficient of V_{op} as function of the temperature gradient, $S = V_{op}/\Delta T$, by performing the procedure described above with a small temperature bias, $\Delta T = T_R - T_L = 0.1$ K. This time both T_R and T_L are varied. We calculate the Seebeck coefficient at the specific μ situated close to a subband minimum, where the insensitivity of S^g to the energy dependence of electron relaxation time has a direct impact on the phonon-drag contribution to the magnet-journalmpower tensor, that results in S^d becomes dominating over S^g .

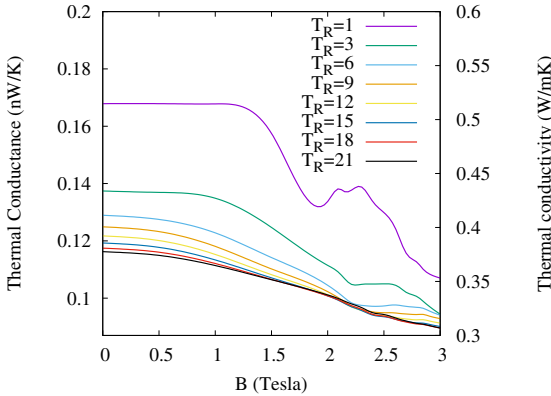


Figure 5. Thermal conductivity and thermal conductance of the tubular nanowire vs. magnetic field for several indicated temperatures of the right lead. The nanowire length is $L = 100$ nm and radius $R = 30$ nm.

Figure 3 shows the variation of S with the magnetic field at different temperatures $T_R \approx T_L$. It can be clearly seen that S starts with nearly a constant value, and then continues with an oscillatory behavior, with increasing magnetic field, for all T_R studied here. The amplitude of oscillation becomes smaller at higher T_R . An oscillatory behavior with respect to magnetic field has been obtained earlier in the 2D electron gas, in the fractional quantum Hall regime, but without a sign change [46]. Oscillations of the thermopower vs. the chemical potential with sign changes were predicted a long time ago for quantum dots [57], and confirmed experimentally [58], but as a consequence of isolated resonances. Besides, at low fields, i.e. in the constant regime of S , it has been shown that the increase of the temperature gradient increases S , and that is in agreement with our results. Indeed, at low temperatures (1–6 K) and magnetic field above 2 T our oscillations and the sign change of the thermopower are expected from the similar behavior of the thermoelectric current and open circuit voltage discussed above. And at higher temperatures the oscillations become smoothened and without a sign change.

3.2. Thermal conductivity

One of the fundamental factors for high efficient thermoelectric conversion is the thermal conductivity, which needs to be minimized. There are many possibilities to reduce the thermal conductance of a nanosystem [34]. Our next step is to evaluate the heat transported by the electrons of our system, which accompany the transport of electric charge. We calculate the heat current as function of the temperature of the right lead, for different values of the magnetic field, using equation (4), and $\Delta\mu = 0$. We can see in figure 4 that with increasing the magnetic field strength, the heat current decreases, but not dramatically. Also, the heat current is more influenced by the magnetic field at high temperatures, for example at 20 K compared to 0.5 K. The reason of this behavior is the distribution of

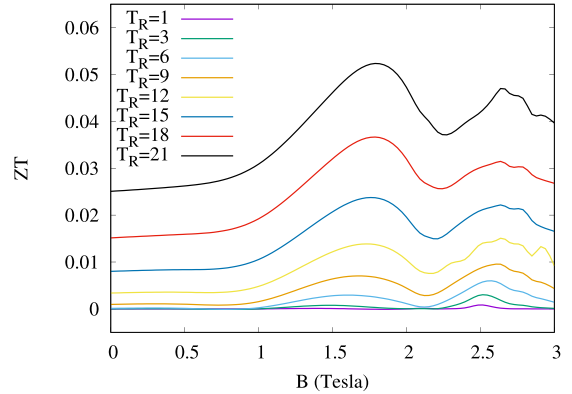


Figure 6. ZT as function of magnetic field where $\mu = 4.2$ meV.

carriers over the energy states such that more electrons are localized due to the closed cyclotron motion imposed by the field, and fewer of them are available for transport. Note also that the heat current does not change sign, as the charge current does, that is in agreement with the second law of thermodynamics.

The thermal conductance, $\bar{\kappa} = dI_Q/dT_R$, and thermal conductivity, $\kappa = L/(\pi R^2)\bar{\kappa}$, as functions of the magnetic field, for different temperatures of the right lead, are shown in figure 5. Here we use the whole cross sectional area of the cylinder, although the transport of both heat and charge occurs through the shell defined by the outer surface. The full cross sectional area is however relevant if the core is also included in the heat transport with phonons, which are neglected at our low temperatures.

The figure clearly indicates two regions with (i) constant κ and $\bar{\kappa}$ at low fields and (ii) a non-linear reduction at higher applied magnetic field. We can see almost the same trend for κ (or $\bar{\kappa}$) for different temperatures, but that is more evident at lower T_R . It is obvious that the increase of the magnetic field leads to a reduction of the thermal conductance and thermal conductivity, but the amount of these changes are different for each temperature. The reduction of the contributions of charge carriers (electrons or holes) to the thermal conductivity has been observed in experimental studies for both bulk and nanowire arrays [45, 47].

3.3. Figure of merit

Next, in order to find the optimum conditions for thermoelectric conversion, we need to calculate ZT using equation (1). High electrical conductivity and low thermal conductivity is required to maximize or optimize ZT , that is achievable by considering lattice thermal conductance and materials characteristics [59–61]. In ZT formula the cross sectional area of the full cylinder (πR^2) used in the thermal conductivity is going to be compensated by the area used in electrical conductivity. Electrical conductivity calculated from $\sigma = dI_c/dV$, where for each specific temperature and magnetic field several values of I_c and $V = (\mu_R - \mu_L)/e$ were calculated separately and got

differentiated. Figure 6 represents ZT as function of magnetic field for different temperatures of the right contact.

Again, the figure shows two regions, of constant and oscillating ZT , respectively. It is also clear that increasing the temperature shifts ZT to higher values, in both regions, non-linearly. Also, at low temperatures, the figure of merit shows limited changes with increasing magnetic field, but for temperatures more than 9 K we have some obvious variation of ZT values. There are two peaks for ZT in the figure, which is a specific result of magnetic field presence. At all temperatures studied here, the peaks are located at about $B = 1.8$ T and 2.5 T with a slight shift to higher field at higher temperature. Thus, regardless of the temperature difference, there is an optimum magnetic field that leads to maximum ZT . In addition, although we are referring to low temperatures, doubling the value of ZT just by applying to the system an external magnetic field is interesting tuning possibility.

With increasing the temperature above 20 K, one would expect an increase of ZT simply because of the temperature factor in the definition, Equation (1). But, of course, the phononic contribution to the heat transport increases with temperature, and the phonon drag and lattice vibrations will end up by dominating over the diffusive heat transport due to electrons. However, experimental values for the thermal conductivity κ in nanowires with diameters between 20–100 nm shows a saturation behavior for temperatures above 100 K to values like 10–40 W mK⁻¹ [34]. Therefore, for such a temperature we can expect the figure of merit of our system to become roughly ten times bigger than the values shown in figure 6.

4. Conclusions

In this paper we have calculated the most important thermoelectric parameters, such as heat and electric current, the open circuit voltage V_{oc} , Seebeck coefficient S , thermal conductivity κ , and figure of merit ZT , produced by electrons confined within a tubular nanowire due to a temperature bias, in presence of transverse magnetic field. To this end, heat current and electrical current variations are obtained in the temperature range between (0–20 K). Increasing the magnetic field leads to reduction in thermal conductivity, which is more pronounced at lower temperatures. The energy spectrum of electrons is a nonmonotonic function of the wave vector along the nanowire, and so is the transmission function with respect to the energy. Consequently V_{oc} can change sign when the temperature gradient or the magnetic field increase. Both S and ZT have a constant to oscillatory transition with increasing the magnetic field. For example for a cylinder radius of 30 nm, ZT presents two peaks at about 1.8 and 2.5 T which are independent of the temperature.

These feature allow a substantial tuning of the thermoelectric response of the nanowire with changing the temperature or with applying an external magnetic field. To the best of our knowledge, although several groups have performed thermoelectric measurements of nanowires at low temperatures [9, 19, 25, 34–36], experimental investigations

of tubular conductors based on core–shell geometry in a transverse magnetic field have not been reported yet. Therefore it is our hope that our theoretical results will stimulate such an experimental work.

Acknowledgment

This work was supported by the Icelandic Research Fund, Grant 195943-051.

ORCID iDs

Hadi Rezaie Heris  <https://orcid.org/0000-0003-2488-5424>
 Andrei Manolescu  <https://orcid.org/0000-0002-0713-4664>

References

- [1] Paulsson M and Datta S 2003 *Phys. Rev. B* **67** 241403
- [2] Weber J, Potje-Kamloth K, Haase F, Detemple P, Völklein F and Doll T 2006 *Sensors Actuators A* **132** 325–30
- [3] Suarez F, Nozariasbmarz A, Vashaee D and Öztürk M C 2016 *Energy Environ. Sci.* **9** 2099–113
- [4] Suarez F, Parekh D P, Ladd C, Vashaee D, Dickey M D and Öztürk M C 2017 *Appl. Energy* **202** 736–45
- [5] Snyder G J and Toberer E S 2011 Complex thermoelectric materials *Materials for Sustainable Energy: A Collection of Peer-Reviewed Research and Review Articles from Nature Publishing Group* (Singapore: World Scientific) pp 101–10
- [6] Wood C 1988 *Rep. Prog. Phys.* **51** 459
- [7] Fergus J W 2012 *J. Eur. Ceram. Soc.* **32** 525–40
- [8] Nolas G, Morelli D and Tritt T M 1999 *Ann. Rev. Mater. Sci.* **29** 89–116
- [9] Prete D et al 2019 *Nano Lett.* **19** 3033–9
- [10] Cosman E R 1990 Thermometric cardiac tissue ablation electrode with ultra-sensitive temperature detection US Patent 4,966,597
- [11] Dudzinski L, Hamley J, McCallum P, Sandifer C, Sutliff T J and Zakrajsek J F 2014 Nasa's radioisotope power systems program status *12th Int. Energy Conversion Conf.* 3462
- [12] Vining C B 2009 *Nat. Mater.* **8** 83–5
- [13] Zhao X, Wei C, Yang L and Chou M 2004 *Phys. Rev. Lett.* **92** 236805
- [14] Kateb M, Ahmadi V and Mohseni M 2013 *Sol. Energy Mater. Sol. Cells* **112** 57–64
- [15] Kateb M, Safarian S, Kolahdoust M, Fathipour M and Ahmadi V 2016 *Sol. Energy Mater. Sol. Cells* **145** 200–5
- [16] Tian B, Kempa T J and Lieber C M 2009 *Chem. Soc. Rev.* **38** 16–24
- [17] Rossella F, Pennelli G and Roddaro S 2018 Measurement of the thermoelectric properties of individual nanostructures *Semiconductors and Semimetals* vol 98 (Amsterdam: Elsevier) 409–44
- [18] Hong M, Lyu W, Wang Y, Zou J and Chen Z G 2020 *J. American Chem. Soc.* **142** 2672–81
- [19] Díez G G, Gordillo J M S, Pujadó M P, Salleras M, Fonseca L, Morata A and Rubio A T 2020 *Nano Energy* **67** 104191
- [20] Gül O, Demarina N, Blömers C, Rieger T, Lüth H, Lepsa M I, Grützmacher D and Schäpers T 2014 *Phys. Rev. B* **89** 045417
- [21] Ferrari G, Goldoni G, Bertoni A, Cuoghi G and Molinari E 2009 *Nano Lett.* **9** 1631–5
- [22] Sitek A, Thorgilsson G, Gudmundsson V and Manolescu A 2016 *Nanotechnology* **27** 225202

- [23] Sitek A, Serra L, Gudmundsson V and Manolescu A 2015 *Phys. Rev. B* **91** 235429
- [24] Torres M U, Sitek A, Erlingsson S I, Thorgilsson G, Gudmundsson V and Manolescu A 2018 *Phys. Rev. B* **98** 085419
- [25] Fust S et al 2020 *Adv. Mater.* **32** 1905458
- [26] Heedt S, Manolescu A, Nemnes G, Prost W, Schubert J, Grutzmacher D and Schapers T 2016 *Nano Lett.* **16** 4569–75
- [27] Manolescu A, Rosdahl T, Erlingsson S I, Serra L and Gudmundsson V 2013 *European Phys. J. B* **86** 445
- [28] Rosdahl T O, Manolescu A and Gudmundsson V 2015 *Nano Lett.* **15** 254–8
- [29] Manolescu A, Nemnes G A, Sitek A, Rosdahl T O, Erlingsson S I and Gudmundsson V 2016 *Phys. Rev. B* **93** 205445
- [30] Chang C H and Ortix C 2016 *Int. J. Mod. Phys.* **30** 1630016
- [31] Erlingsson S I, Manolescu A, Nemnes G A, Bardarson J H and Sanchez D 2017 *Phys. Rev. Lett.* **119** 036804
- [32] Boukai A I, Bunimovich Y, Tahir-Kheli J, Yu J K, Goddard III W A and Heath J R 2008 *Nature* **451** 168–71
- [33] Mingo N 2004 *Appl. Phys. Lett.* **84** 2652–4
- [34] Li D, Wu Y, Kim P, Shi L, Yang P and Majumdar A 2003 *Appl. Phys. Lett.* **83** 2934–6
- [35] Wu P M, Gooth J, Zianni X, Svensson S F, Glusckke J G, Dick K A, Thelander C, Nielsch K and Linke H 2013 *Nano Lett.* **13** 4080–6
- [36] Pennelli G, Elyamny S and Dimaggio E 2018 *Nanotechnology* **29** 505402
- [37] Erlingsson S I, Bardarson J H and Manolescu A 2018 *Beilstein J. Nanotechnol.* **9** 1156–61
- [38] Domínguez-Adame F, Martín-González M, Sánchez D and Cantarero A 2019 *Phys. E Low-dimensional Syst. Nanostruct.* **113** 213–25
- [39] Vuttivorakulchai K, Luisier M and Schenk A 2018 *J. Appl. Phys.* **124** 205101
- [40] Thorgilsson G, Erlingsson S I and Manolescu A 2017 *J. Phys. Conf. Series* **906** 012021
- [41] Cahill D G, Ford W K, Goodson K E, Mahan G D, Majumdar A, Maris H J, Merlin R and Phillpot S R 2003 *J. Appl. Phys.* **93** 793–818
- [42] Yadav H K, Gupta V, Sreenivas K, Singh S, Sundarakannan B and Katiyar R 2006 *Phys. Rev. Lett.* **97** 085502
- [43] Yamamoto T, Watanabe S and Watanabe K 2004 *Phys. Rev. Lett.* **92** 075502
- [44] Yamamoto T and Watanabe K 2006 *Phys. Rev. Lett.* **96** 255503
- [45] Wolfe R and Smith G 1962 *Appl. Phys. Lett.* **1** 5–7
- [46] Fletcher R, Maan J, Ploog K and Weimann G 1986 *Phys. Rev. B* **33** 7122
- [47] Hasegawa Y, Ishikawa Y, Morita H, Komine T, Shirai H and Nakamura H 2005 *J. Appl. Phys.* **97** 083907
- [48] Kammhuber J et al et al 2016 *Nano Lett.* **16** 3482–6
- [49] Ferry D and Goodnick S M 1999 *Transport in Nanostructures* (Cambridge: Cambridge university press) vol 6
- [50] Tsaousidou M 2010 *Front. Nanosci. Nanotechnol.* **2** 477
- [51] Fletcher R, Pudalov V, Feng Y, Tsaousidou M and Butcher P 1997 *Phys. Rev. B* **56** 12422
- [52] Fletcher R, Harris J, Foxon C, Tsaousidou M and Butcher P 1994 *Phys. Rev. B* **50** 14991
- [53] Behnen E 1990 *J. Appl. Phys.* **67** 287–92
- [54] Tsaousidou M 2010 *Front. Nanosci. Nanotechnol.* **2** 477
- [55] Hicks L and Dresselhaus M S 1993 *Phys. Rev. B* **47** 16631
- [56] Rowe D M 2018 *CRC Handbook of Thermoelectrics* (Boca Raton, FL: CRC Press)
- [57] Beenakker C W J and Staring A A M 1992 *Phys. Rev. B* **46** 9667
- [58] Svensson S, Persson A, Hoffmann E, Nakpathomkun N, Nilsson H, Xu H, Samuelson L and Linke H 2012 *New J. Phys.* **14** 033041
- [59] Dresselhaus M S, Chen G, Tang M Y, Yang R, Lee H, Wang D, Ren Z, Fleurial J P and Gogna P 2007 *Adv. Mater.* **19** 1043–53
- [60] Chen G, Dresselhaus M, Dresselhaus G, Fleurial J P and Caillat T 2003 *Int. Mater. Rev.* **48** 45–66
- [61] Rosi F 1968 *Solid State Electron* **11** 833–68

Paper II

Effects of transverse geometry on the thermal conductivity of Si and Ge nanowires

Hadi Rezaie Heris, Movaffaq Kateb, Sigurdur I Erlingsson and Andrei Manolescu

Department of Engineering, School of Technology, Reykjavik University, Menntavegur 1, Reykjavik IS-102, Iceland

Received: 17 November 2021

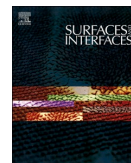
Accepted: 23 February 2022

Published: 25 February 2022



Contents lists available at ScienceDirect

Surfaces and Interfaces

journal homepage: www.sciencedirect.com/journal/surfaces-and-interfaces

Effects of transverse geometry on the thermal conductivity of Si and Ge nanowires

Hadi Rezaie Heris^{*}, Movaffaq Kateb, Sigurdur I. Erlingsson, Andrei Manolescu

Department of Engineering, School of Technology, Reykjavik University, Menntavegur 1, Reykjavik IS-102, Iceland

ARTICLE INFO

Keywords:

Thermal conductivity
Nanowires
Heat transfer
Molecular dynamics
Müller-Plathe

ABSTRACT

We explore the effects of geometry on the thermal conductivity (κ) of silicon and germanium nanowires, with lengths between 10–120 nm and diameters up to 5–6 nm. To this end we perform molecular dynamics simulations with the LAMMPS software, using Tersoff interatomic potentials. We consider nanowires with polygonal cross section and we discuss the effect of the transverse geometry on the thermal conductivity. We also consider tubular (hollow) nanowires and core/shell combinations of Si/Ge and Ge/Si, and we compare the heat transport of the core/shell structure with that of the separated core and shell components.

1. Introduction

Semiconductor nanowires have a great potential in several fields of modern technology, such as nanoelectronics [1–4], lasers [5], solar cell [6], or thermoelectrics [7]. For many of these applications understanding the thermal conductivity of nanowires is essential. Nano-electronic devices demand a high thermal conductivity and heat sinks to dissipate heat from nano chips [8], while a low thermal conductivity is important for achieving a high thermoelectric figure of merit [9,10].

Due to the small size and large surface to volume ratio the thermal conductivity of nanowires is substantially different from that of the bulk material. That can be explained by the limited phonon scattering due to finite size confinement, by the increased scattering imposed by the boundary conditions, or by the quantization of phonon transport. For example, in nanowires of diameter smaller than 20 nm, the phonon dispersion is modified due to phonon confinement, causing a significant decrease of the phonon group velocities [11,12]. Experimentally, it has been reported that the thermal conductivity of individual single crystalline Si nanowires is more than two orders of magnitude lower than the bulk value [13]. The geometry plays an important role in determining the surface to volume ratio of nanowires. Several computational [14–16] and experimental [17] studies show a relation between heat transport properties of nanowires and specific cross-sectional shapes.

Barriers or geometric shapes can be engineered in nanostructured materials to modify the scattering of phonons. In particular core/shell nanowires have attracted great interest for several properties, including electron and phonon scattering, and heat and charge current through

different channels [18–21]. core/shell nanowires provide more degrees of freedom for tuning their properties compared to the uniform nanowires. core/shell nanowires can also have high carrier mobility [22] and very low phonon thermal conductance due to the enhancement of surface scattering [16], which are essential attributes for reaching higher thermoelectric efficiency. Previous studies addressed the effects of surface construction and geometry on nanowires' intrinsic electrical conductivity [23], thermal conductivity [24], mechanical [25] and thermoelectric properties [26]. The growth of semiconductor nanowires with specific cross-section is a current research focus in fabrication of nanowires, since many of their properties depend on the geometry [27, 28], such as hexagonal [29–31], square [32,33] and triangular [28,31, 34] cross-section.

Great effort has been made to study heat transport through core/shell nanowires. These studies show that a deposition of a thin shell [35], the interface roughness [36] and depression and localization of long-wavelength phonon modes reduce the thermal conductivity of nanowires [37]. Also the drastic reduction of thermal conductivity can be achieved through cross-section modulation [14,16]. The finite size effects related to the length of the nanowire have been obtained for silicon nanowires with square cross-section and lengths between 6–54 nm [38] and for Si/Ge core/shell nanowire with the same square geometry [19].

Among the variety of theoretical approaches molecular dynamics (MD) has received considerable attention for the study of phonon behaviour. This is mainly due to the fact time-scale and spatial resolution in MD simulation perfectly fits for observation of atomic vibrations.

^{*} Corresponding author.

E-mail addresses: hadi19@ru.is (H.R. Heris), manoles@ru.is (A. Manolescu).

Since the pioneering work of Green and Kubo [39,40], several algorithms for calculating κ within the MD framework have been developed. In the Green-Kubo approach ensemble average of the instantaneous heat flux auto-correlation is related to κ through fluctuation-dissipation theorem. Note that Green-Kubo algorithm does not require a temperature gradient and thus it is referred to as equilibrium molecular dynamics (EMD) [41]. The method has been already applied to nanowires of various polygonal cross-sections and infinite length [42–45]. The lack of temperature gradient initiated a debate whether EMD method is proper for one-dimensional solids or should be modified (cf. Ref. [46] and refs. therein). However, the major problem with EMD was its computation cost, namely for the auto-correlation function to be convergent. This motivated the non-equilibrium molecular dynamics (NEMD) approach based on imposing a temperature gradient and utilizing Fourier's law to calculate κ . Since then several studies have been devoted to understanding the origin of difference in κ determined by EMD and NEMD approaches (cf. Refs. [46–48]). The temperature gradient in NEMD is achieved by thermostating hot and a cold segments at different temperatures or adding and removing an equal amount of heat to these segments. Thus, it is generally believed that NEMD approach mimics better the experimental condition. However, the NEMD approach often presents a non-linear temperature profile in the neighborhood of the hot and cold segments. Whether or not the non-linear portions must be included in determining κ is still an ongoing debate [48]. Besides, the NEMD approach gives large fluctuations temperature/heat flux unless e.g. imposing a large temperature gradient to have the heat flux distinguishable from the noise [49]. Then the large heat flux requires a longer simulation to be converged. Müller-Plathe [49] introduced the reverse-NEMD (rNEMD) approach in which the heat flux is imposed by exchanging kinetic energy between the hot and cold segments, and produces a temperature gradient. This way the heat flux is already known from the amount of exchanged energies. Besides, the rNEMD method conserves the energy and thus overcomes the dependency on a specific ensemble.

In the present paper we calculate with MD simulations the heat conductivity of silicon nanowires with different shapes of the cross-section, hollow nanowires, and Si/Ge core/shell nanowires of triangular shape. We use the rNEMD method to investigate the thermal conductivity in tubular and core/shell nanowires with different geometries of the cross-section: cylindrical, hexagonal, square, diamond, and triangular. We begin with a theoretical background of rNEMD in Section 2. Then, Section 3 describes our model and method to calculate the heat flux and thermal conductivity. In Section 4 we discuss the thermal conductivity variation with the nanowires length and cross-sectional geometry, and also the thermal conductivity variation from solid nanowires to tubular ones with different geometries. We also compare the thermal conductivity of Si/Ge and Ge/Si core/shell nanowires with triangular cross-section. Finally, the conclusions are reported in Section 5.

2. Theoretical background on the reverse non-equilibrium molecular dynamics (rNEMD) approach

We use the rNEMD method by Müller-Plathe to compute the heat flux and thermal conductivity of our models of nanowires [49]. In this approach the heat flux density Q is defined as the amount of energy transferred in a given time through a surface of a given area which is perpendicular to the flux direction. The thermal conductivity κ is calculated by Fourier's law:

$$Q = -\kappa \nabla T \quad (1)$$

where ∇T is the gradient of the temperature T determined from atomic velocities. If we take z direction as the direction of the temperature gradient along the nanowire, we can define the thermal conductivity as

$$\kappa = - \lim_{\partial z \rightarrow 0} \lim_{t \rightarrow \infty} \frac{\langle Q_z \rangle}{\partial T / \partial z} \quad (2)$$

where t is the simulation time, in practice longer than the relaxation time of the atomic structure after the initial conditions. In order to make sure the determined κ exactly belongs to the nanowire axis, the Müller-Plathe algorithm requires extra considerations.

The nanowire must be divided into n segments along its axis, n being an odd integer, and each segment having the same thickness, volume, and number of atoms. The temperature in the segment S_k , $k = 1, 2, \dots, n$, is given by

$$\frac{3}{2} N_k k_B T_k = \frac{1}{2} \sum_{i \in S_k}^{N_k} m_i v_i^2 \quad (3)$$

where the sum extends over the N_k atoms contained in S_k , with masses m_i , velocity vectors v_i , k_B being Boltzmann's constant. For the case of periodic boundary conditions, the hot segment is almost located in the middle of the nanowire, corresponding to $S_{(n/2)+1}$, and the cold segment is created at the first S_1 . Note that due to the periodic boundary condition the heat flows from the hot segment to both ends of the wire. The temperature gradient is produced by exchanging the v_i of the most energetic atoms situated in the S_1 with the least energetic atom situated in the $S_{(n+1)/2}$. Considering how often the exchange process is performed and how many atoms are included in each exchange step, one can control ΔT between hot and cold segments. This allows producing a linear ΔT between the hot and cold segments [49], in contrast to other NEMD methods. The heat flux per unit area and time is calculated as

$$Q_z = \frac{1}{2A} \frac{dE}{dt} \quad (4)$$

where A is cross-sectional area of the wire, counted twice because of the heat flow in both directions, from the central hot segment to the lateral cold segments. Assuming the validity of a linear response (Fourier's law), the thermal conductivity is calculated by combining Eqs. (1) and (4).

To check the spatial distribution of the heat flux within the nanowire cross-section we utilized atomistic values along the nanowire axis. The per-atom heat current (\mathbf{q}) is given by

$$\mathbf{q}_i = \frac{1}{\Omega} \frac{d}{dt} \mathbf{r}_i E_i, \quad (5)$$

where Ω is atomic volume, E_i is the total (potential and kinetic) energy of particle i and \mathbf{r}_i is its position vector. Although there exist a temperature gradient ΔT , at the atomistic level we do not need a temperature gradient because $\frac{d}{dt} E_i$ considers variation of per-atom kinetic energy through time. With \mathbf{q}_i being the microscopic or atomistic or per-atom value, macroscopic equivalent can be obtained by $Q_z = \sum_i q_i^z$. For a pair potential Eq. (5) can be expressed as

$$\mathbf{q}_i = \frac{1}{\Omega} \left[E_i \mathbf{v}_i + \frac{1}{2} \sum_j (\mathbf{F}_{ij} \cdot \mathbf{v}_i) \mathbf{r}_{ij} \right], \quad (6)$$

where \mathbf{v}_i is the velocity vector of the particle and \mathbf{F}_{ij} and \mathbf{r}_{ij} are force and separation vector, respectively, between particle i and its neighbor(s) j . Note that Eq. (5) includes \mathbf{r}_i that is meant for liquids i.e. when energy can be transferred by movements of atoms. The second term in the right hand side of Eq. (6) is the virial contribution to the heat flux and thus one may rewrite Eq. (6) as

$$\mathbf{q}_i = \frac{1}{\Omega} [E_i \mathbf{v}_i + \boldsymbol{\sigma}_i \mathbf{v}_i], \quad (7)$$

where $\boldsymbol{\sigma}_i$ is per-atom stress tensor of atom i . Now one can decouple \mathbf{q}_i into different directions e.g. assuming the z being parallel to the nano-

wire axis and direction of interest

$$\mathbf{q}_i^j = \frac{1}{\Omega} [E_i \mathbf{v}_i^j + \boldsymbol{\sigma}_i^x v_z + \boldsymbol{\sigma}_i^y v_x^j + \boldsymbol{\sigma}_i^z v_y^j], \quad (8)$$

with superscript being the directions. We refer the interested readers to Ref. [50] for discussion on the stress correction when manybody potentials such as Tersoff is used.

3. The atomistic model

We use silicon and germanium with diamond structure as a model systems in our simulations. An atomistic model which ignores electron transport can be realistic for silicon since electrons in the intrinsic (undoped) Si contribute very little to the heat conduction compared to the phonons. This can be achieved by MD simulation and solving Newton's equation of motion. To this end we utilized the large scale atomic/molecular massively parallel simulator (LAMMPS) from Sandia National Laboratory [51].

The Si nanowires were placed within a orthogonal simulation box that fits the length of nanowires, but it is several times larger than its diameter in the transverse directions, as shown in Figures S1 and S2 of the supplementary materials. We apply fixed boundary conditions in transverse directions (x and y), and periodic boundary conditions along the nanowire axis (z direction). A question that might arise here is if our nanowires can be considered as having infinite length. As pointed out previously [45], and as will be discussed in the results, κ is dependent on the actual nanowire length included in the simulation. However, the nanowire length utilized here does not correspond to the real sample size in experiment. This means that periodic boundary condition can reduce the finite size effect, but due to the phonons it can not be completely removed. For this reason we considered different nanowire lengths (10–120 nm) and discuss the issue further in the results.

The nanowire axis was aligned along the [111] lattice direction that gives (111) planes at the nanowire cross-section. In order to understand the trade-off between the effect of surface area and cross-section area we compared uniform and hollow nanowires with equal cross-sections. The cavity, or hole, in the hollow nanowires is built with a central empty channel inside the material and again, we compare different geometries by keeping the transverse area constant. In order to generate the core-shell nanowires we replaced core atoms with a different materials and the entire core-shell was relaxed to reach equilibrium interatomic distances. This gives an interface similar to that of hetero epitaxial system.

An important requirement for MD simulation of solid materials is the availability of accurate interatomic potentials [52]. Several MD simulations studies on thermal conductivity show strong dependence of these results on the empirical interatomic potential used [53,54]. Such potentials have mostly been developed for technologically important materials, such as silicon and germanium. Among them, the Tersoff potential [55] and its variants are most commonly used [45,46]. It is a many-body potential that allows the description of covalently bonded materials, capturing the quantum mechanical nature of the bonding, and explicitly incorporating the dependence of the bond order on local environment. We compared Tersoff potential with the popular Stillinger-Weber potential and a more recent EDIP potential as well as DFT in determining relevant thermodynamic properties such as heat capacity. The results are presented in the supplementary materials. We utilized Tersoff [56] potential for Si–Si, Ge–Ge and Si–Ge interactions.

We proceed with a two step relaxation process. First, the nanowire is relaxed using the isothermal-isobaric ensemble (NPT) at the desired equilibrium temperature T_{eq} in order to allow the atoms to expand until nearly zero stress is achieved along the nanowire axis, within 50 ps. We utilized Nose-Hoover thermostat to achieve desired temperature during the relaxation. In the second step, the energy exchange between the hot and cold regions is performed, in order to develop a stationary temperature profile along the nanowire axis, for another 50 ps using the

microcanonical ensemble (NVE). Note that NVE allows the average temperature over all segments to remain constant and equal to T_{eq} . We applied different settings for the exchange to produce the temperature differences being in the range of 10–60 K between the central and the side segments. We used the velocity Verlet algorithm for time integration [57,58] using a time step of 0.5 fs, and ΔT and consequently κ were determined when averaged data points were converged. We used 10^3 samples to calculate each of the averaged ΔT points.

In Fig. 1 we show the cumulative energy transferred along the cylindrical nanowire axis for temperatures between 50 - 300 K. We can see that heat transfer increases linearly with respect to the number of time steps, and that is different for each temperature. This is an indication of the fact that steady state temperature profile is reached and thus we can use Fourier's formula for calculating the thermal conductivity. Note that below 50 K the heat flux carried by electrons is comparable with the contribution of phonons, so studies at lower temperature have to consider and both electrons and the upper limit of the thermal conductance for phonons. This fundamental upper limit (a quantum of thermal conductance) is the maximum value of thermal conductance that an acoustic phonon mode can take [59,60]. Also at higher temperatures numerical approaches of Holland's model (extended Callaways model) can describe thermal conductivity of silicon and germanium up to 1000 K easily [61].

4. Results and discussion

4.1. Length dependence of the thermal conductivity

There are several reports on the dependency of thermal conductivity to the length of nanowire within MD framework [62,63]. The Fourier's law describes thermal transport in bulk materials, but it is not valid for nanowires with lengths less than phonon mean-free path. For shorter nanowires ($L \ll \lambda$), it has been shown experimentally that the thermal conductivity does not have a constant value [64]. The thermal conductivity variation of these nanowires is strongly related to the temperature regime. At low temperature where the optical phonons are not excited and thermal current is carried ballistically by acoustic phonons, thermal conductivity can be described by Landauer formulation for phonons [65,66]. Meanwhile for temperature regime higher than 20 K thermal conductivity is not proportional to the system length and increase non-linearly with the length due to contribution of both ballistic and diffusive phonons [63,65].

The thermal conductivity of a pure silicon nanowire increases rapidly with nanowire length below 100 nm. This behavior is in agreement with previous MD studies [38,67]. The thermal conductivity varies more slowly at higher lengths and reaches a constant value at lengths over 1000 nm. This slow variation of the thermal conductivity implies that the nanowire is in the diffusive phonon transport regime.

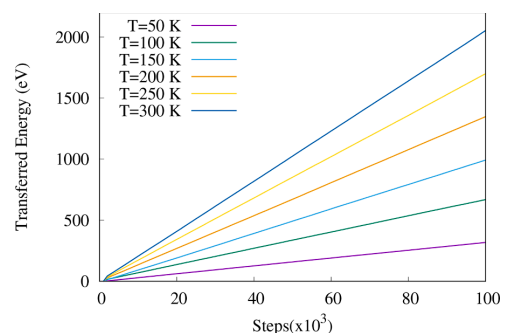


Fig. 1. Cumulative energy transferred from the hot to the cold segments of the nanowire with elapsed time. Each simulation step corresponds to 0.5 fs.

The variation of the thermal conductivity with the length of the nanowire could be understood by considering a linear variation of the reciprocal of the thermal conductivity with respect to the reciprocal of the nanowire length, or a power law behavior of the thermal conductivity with respect to the length.

Considering the temperature regime and nanowires of different lengths, we describe our results with a power law relation. The thermal conductivity increases with respect to the length of the nanowire according to L^α , where α varies between 0.30-0.48 for $L < 30$ nm, and reaches a constant value of 0.56 for $30 \text{ nm} < L < 150$ nm. The variation of κ with the nanowire length can be understood as the limitation imposed to contribution of long wavelength phonons. As the nanowire length increases a wider spectrum of phonons contribute to the calculated heat flux. We study nanowires with different lengths along z direction to see how the thermal conductivity behave when the length is comparable to the phonon mean free path.

Our calculated thermal conductivity is displayed in Fig. 2, for nanowires with length L from 10 to 120 nm, having cylindrical shape. We can see a huge increase of the thermal conductivity by increasing the nanowire length. For instance at 100 K, the thermal conductivity κ for the 120 nm length nanowire is almost eight times higher than for the one with 10 nm length.

4.2. Effect of the nanowire cross-section on the thermal conductivity

If we fix the length of nanowires and look at the influence of the cross-sectional area on thermal conductivity with respect to temperature, we can see an increase of the thermal conductivity with increasing the area. Although these variations are not same for each temperature, the trend is observable. Specifically at 300 K the thermal conductivity magnitude increase more than two times by increasing radius of cylindrical nanowires from 1 nm to 5.5 nm, as shown in Fig. 3.

The dependence of the thermal conductivity and thermoelectric properties of silicon nanowires on the cross-sectional shape and surface modification had been studied before [23,24,26]. In our present study we consider the effect of different geometries. We fix some parameters such as length, cross-sectional area, and the number of atoms in a cross section, for all shapes, and we only change shape of the nanowire cross section, from circle to triangle, diamond, hexagon and square. The results are shown in Fig. 4(a). The thermal conductivity of silicon nanowires is about a factor of two lower than for bulk silicon [13]. Inelastic surface scattering and finite size phonon effects contribute to the low thermal conductivity of nanowires, which is consistent with prior results [26,68]. Nanowires with square and circle cross-sectional area show very close values of thermal conductivity, the values for the circular case being slightly larger for all temperatures. In some studies similar results for square and circle shaped nanowires had been reported [16,68,69]. In

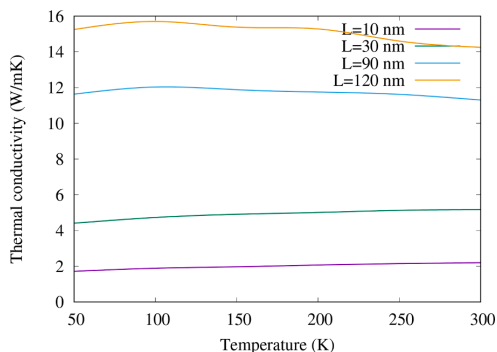


Fig. 2. Variation of thermal conductivity for a cylindrical nanowire of 5.5 nm diameter with length increase.

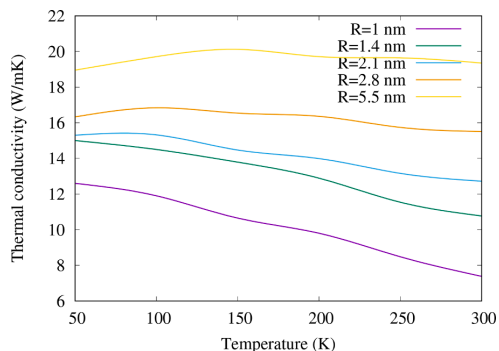


Fig. 3. Thermal conductivity of cylindrical nanowire with different diameters, indicated in legend, at a constant length of 120 nm.

our study the nanowires with triangular cross-section area (with a fixed area of 24 nm^2) have the highest thermal conductivity of all shapes. Below that, the next values correspond to diamond and hexagon.

The largest conductivity for triangular nanowires seems to be related to the largest flat surfaces present in this geometry. Or, the presence of many edges, or corners of the cross section, reduce the conductivity. In other words, the thermal conductivity increases with increasing the surface-to-volume ratio, or perimeter-to-area ratio of the cross section, because our nanowires have all the same length. Since the cross sectional area A of all shapes is also the same, the smallest ratio corresponds to the cylinder ($3.5/\sqrt{A}$), followed by the hexagon ($3.7/\sqrt{A}$), square ($4/\sqrt{A}$), diamond ($4.3/\sqrt{A}$), and triangle ($4.6/\sqrt{A}$). Our thermal conductivities obey this order, except for the square case. Our interpretation of this exception is related to the unit cell of the material (diamond), which does not accommodate well in the square cross section of a nanowire with its length in the [111] direction. In Figure S1 of the supplementary materials one can see a zigzag distribution of the surface atoms in the square case. The corner-to-corner distance for the square nanowire is thus smaller than for atoms with a better alignment, like in the other geometries, and the effective surface-to-volume ratio for the square geometry is actually smaller than expected. To understand better this situation, we tried to change step-wise the corner angles of the diamond shape in order to observe the evolution of the thermal conductivity to the results for the square shape. However, for many shapes in between diamond and square the relaxed structures had irregular surfaces and the results for the thermal conductivity were not stable. We believe this is an additional indication of the geometrical mismatch between the nanowire geometry and the unit cell, at least at this small scale considered in our work.

4.3. Hollow nanowires

We are modeling tubular nanowires by omitting atoms from the nanowire center, and see a huge decrease of the thermal conductivity values for all shapes. That is predictable due to the increase of the surface to volume ratio. The consequence is phonon confinement and enhanced phonon scattering, leading to lowering of the thermal conductivity in the tubular nanowires in comparison with uniform nanowires. In the next phase by considering the same cross-sectional area, number of atoms, and nanowire length, this time we increase the empty space inside the nanowire material. Explicitly the thermal conductivity decreases with increasing the nanowire radius, as shown in Fig. 5 for the circular and triangular cases. All the other shapes show same behavior. The larger radii (both internal and external) leads to lower thermal conductivity. The reduction for the triangular cross section can be more than 50%, which is the largest effect for all studied shapes.

Next, in Fig. 6 we show a snapshot of the average of the heat flux

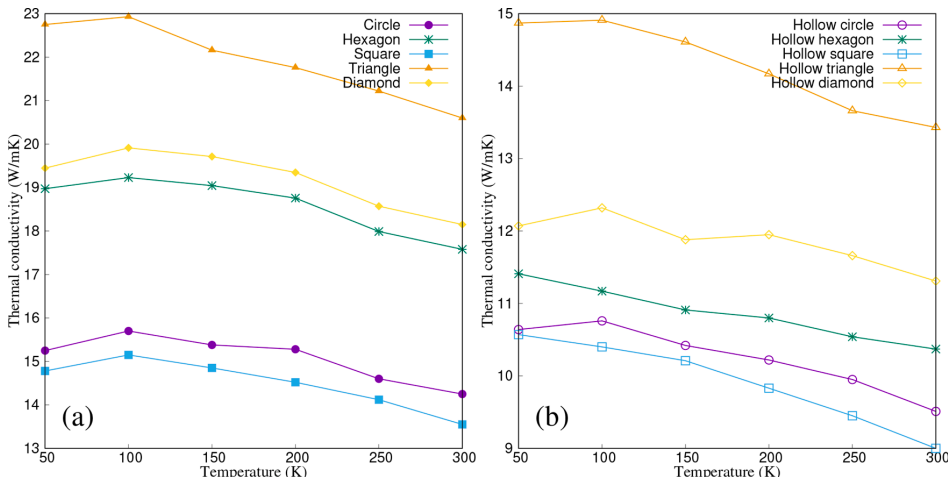


Fig. 4. Thermal conductivity variation with temperature for different geometries. (a) solid nanowires with length of 120 nm and surface area of 24 nm² (b) Tubular nanowires with length of 120 nm and surface area of 24 nm².

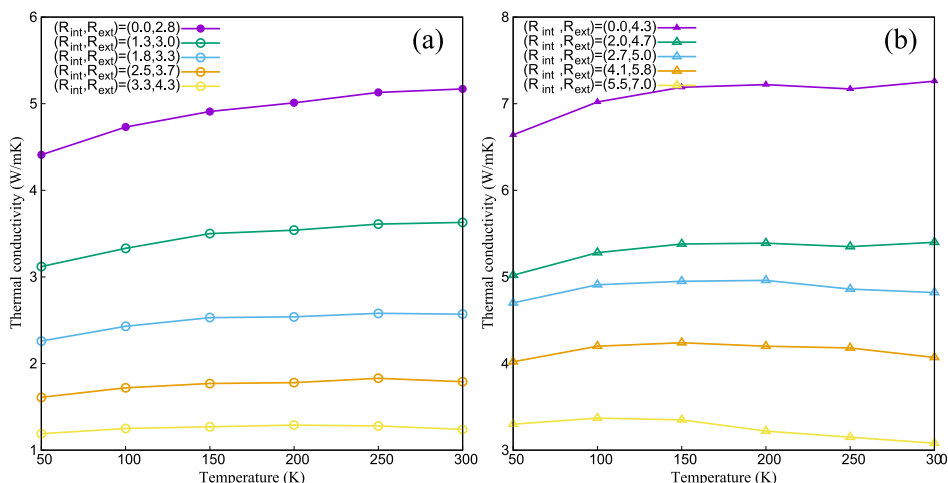


Fig. 5. The thermal conductivity vs. temperature with increasing the hollow space inside the nanowires with (a) cylindrical and (b) triangular prismatic shapes. The shell area $\approx 24 \text{ nm}^2$ and the length $L = 30 \text{ nm}$ are same for all cases.

along the nanowire axis for triangular nanowires, both with compact and hollow geometry, at temperature 100 K. The averaged heat flux was obtained by averaging over both time and half length of nanowire i.e. where slope of the temperature profile does not change sign. The color bar indicates the heat flux in eV/atom.fs units. It can be seen that there is no obvious heat channel and the distribution of heat flux fluctuate around a uniform value, within the nanowire cross section, for both geometries. Strictly speaking, however, it seems larger flux passes through the nanowire core in the absence of the hollow space. So with the empty space in the center of the nanowires we omit the main heat flux through its core, which leads to a lower thermal conductivity.

4.4. Core/shell nanowires

Core/shell nanoscale structures allow additional possibilities to engineer the thermal transport, via phonon scattering mechanisms. The control of phonon interference at the interface between the core and the

shell, and the phonon scattering in different geometries, makes core/shell nanowires a promising candidate for heat transport at nanoscale. In principle, the thermal conductivity of independent parallel nanowires should always be larger than the conductivity of each individual nanowire (as in the case of electrical conductivity). But for a core/shell nanowire, with two different materials in contact, it is more difficult to calculate the thermal conductivity, in order to incorporate the effects of the stress along the common interface, and the different phonon group velocities in each material.

In order to relate the cross section shape with the variation of the thermal conductivity, we performed three series of simulations. First the thermal conductivities for Si/Ge core/shell nanowires, between temperatures 50–300 K, were calculated for all cross sectional shapes. And then, the thermal conductivities for hollow and uniform nanowires, corresponding to the shell and core separated from each other, but using the same cross sectional area, number of atoms, and length, as for the core/shell structures. The lengths of all nanowires are 30 nm and the

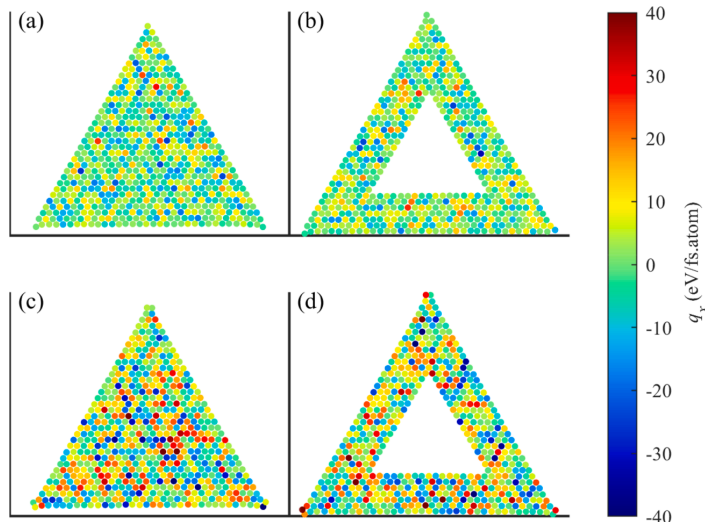


Fig. 6. Distribution of longitudinal heat flux (q_x) within nanowire cross-section. Snapshots of (a–b) q_x at a specific t and x , (c–d) the average of q_x over time and nanowire length i.e. $\langle q_x \rangle_{t,x}$.

cross sectional area is 24.5 nm^2 for both core and shell nanowires, respectively Si/Ge core/shell total cross sectional area is 49 nm^2 .

For understanding the thermal conductivity variation for each shape, we calculate the average thermal conductivity of the core (κ_c) and shell (κ_s) nanowires, $\kappa_{ave} = (\kappa_c + \kappa_s)/2$, for each specific shape, and we compare it with the true thermal conductivity of the Si/Ge core/shell nanowire of that shape (κ). The meaning of κ_{ave} is the thermal conductivity of the core/shell nanowire if the core and the shell would behave like independent heat transport channels (both core and shell have the same cross-sectional area). The thermal conductivities for the core, shell, and core/shell cases, and the corresponding deviation $(\kappa_{ave} - \kappa)/\kappa$ are reported in Table 1, for temperature 100 K. In all cases the true core/shell value κ is smaller than the average value, indicating that the interface between the core and the shell reduces the heat transport. We see that for the square and circular cross sections these differences are the smallest, less than 2%. The largest difference is again for the triangle, and then for the diamond.

A significant reduction of the thermal conductivity of a Si nanowire with square cross section, if coated with a Ge thin layer, was already reported in the literature [19]. This effect can be explained by the strong reduction of phonon group velocities in core/shell nanowires due to the redistribution of phonon energy spectra and mixing of high-velocity phonons from silicon with low-velocity phonons from germanium [70]. Here we find out that the reduction can be larger for other geometries, especially for those with large surface-to-volume ratio, like in the triangular case. The high deviation from average thermal conductivity κ_{ave} values for triangle shape can be created by phonon

Table 1

Thermal conductivity of Si core, Ge shell and Si-Ge core/shell nanowires with different cross sectional shapes. The temperature is 100 K. The length of all nanowires is 30 nm.

Cross section shape	Si core κ_c	Ge Shell κ_s	Si/Ge core/shell κ	Deviation of κ_{ave}
Circle	4.89	3.46	4.10	1.8%
Hexagon	5.76	3.04	4.14	6.3%
Diamond	6.11	5.27	5.28	7.7%
Square	4.87	3.49	4.11	1.7%
Triangle	7.09	5.30	5.33	16%

confinement effects imposed by the geometry. Due to this reason we chose the triangle shape for performing further simulations.

In the next phase of simulations for the Si/Ge case, the Si core cross-sectional area is 5.2 nm^2 and the Ge shell is 23.5 nm^2 , and lengths of both core and shell are 120 nm. In the Ge/Si case we use the same numbers of atoms for the core and shell, with the two materials exchanged. Note that due to the different lattice constant of Si and Ge, reaching exactly same area for two shapes is impossible but the total difference in whole volumetric size is near 2%. This difference had been included in calculation of thermal conductivity.

In Fig. 7 (a) we show the thermal conductivity vs. temperature of the Si/Ge example. Despite having less atoms in the Si core than in the Ge shell, the isolated Si core shows higher thermal conductivity than the isolated Ge shell, as can also be seen in Table 1. This is because of two main reasons. First, the hole inside the tubular Ge nanowire lead to a large reduction of the thermal conductivity, because of the large surface to volume ratio and consequently intense phonons scattering. Second, in general Si nanowires have higher thermal conductivity than Ge nanowires with similar geometric parameters [70,71]. The depression of the vibrational density of states of Si atoms on the surface with the addition of Ge shell atom leads to the reduction of the thermal conductivity of Si/Ge nanowire with respect to the Si core alone, as already shown by Hu et al. [19]. However, now we observe that the difference between the average conductivity (κ_{ave}) and the true value for the core/shell structure become smaller with increasing the temperature, and reverse order for temperatures about 170 K.

In Fig. 7 (b) we show the Ge/Si core/shell case, where the thermal conductivity of this structure is larger than for the Ge and Si separated components. Despite the hole in the Si shell, which reduces the thermal conductivity if we compare it to the solid one, it still remains larger than the thermal conductivity of the Ge core. Because of this, Ge/Si core/shell nanowires shows higher thermal conductivity than Si/Ge in all temperature regime. This inequality has been obtained before for the square geometry [14,70]. This difference is not huge because despite carrying large amount of heat through both core and shell in Ge/Si core/shell nanowires, we still have shell atoms depressing over core atoms from vibrational states.

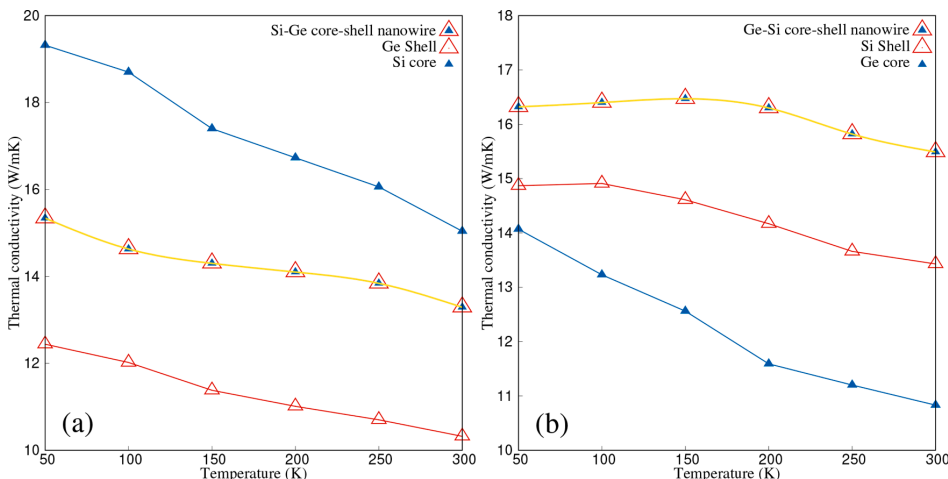


Fig. 7. Thermal conductivity variation with temperature for core/shell nanowires and separated solid nanowire and tubular nanowires. (a) Si/Ge core/shell nanowire and Si solid nanowire and tubular Ge nanowire. (b) Ge/Si core/shell nanowire and Ge solid nanowire and tubular Si nanowire.

5. Conclusions

We have studied the thermal conductivity of solid and tubular silicon nanowires with different cross-sectional area, lengths and geometries. For silicon nanowires the thermal conductivity increases linearly by increasing the cross sectional area, and increases with a power law in the length of nanowires. By considering the same length and cross sectional area for all silicon nanowires with different cross sectional geometries, the square shape shows the lowest thermal conductivity value and the triangular shape shows the highest value. Due to the increased surface to volume ratio, making an empty space inside nanowire, i.e. making a tubular nanowire, always leads to a decrease of the thermal conductivity. Tubular nanowires with thinner walls show less thermal conductivity and for the triangular shape the thermal conductivity decreases much more than for other geometries when the nanowires become thinner.

We also calculated the thermal conductivity of core/shell Si/Ge and Ge/Si nanowires. In this case, due to phonon scattering at the interface between the two materials, the thermal conductivity of the nanowire is different from a simple combination of the core and shell thermal conductivity values calculated separately.

By considering the same geometry parameters, but exchanging the materials order in core and shell (Ge/Si instead of Si/Ge), we can see a different thermal conductivity. Using nanowires of a specific geometry, and combining different materials, may be a promising way to engineer the heat transport at nanoscale.

Declaration of Competing Interest

The authors declare that they have no known competing financial interests or personal relationships that could have appeared to influence the work reported in this paper.

Acknowledgements

This work was supported by the Icelandic Research Fund, Grant 195943.

Supplementary material

Supplementary material associated with this article can be found, in the online version, at doi:10.1016/j.surfin.2022.101834

References

- [1] X. Duan, Y. Huang, Y. Cui, J. Wang, C.M. Lieber, Indium phosphide nanowires as building blocks for nanoscale electronic and optoelectronic devices, *Nature* 409 (6816) (2001) 66–69.
- [2] Z.L. Wang, J. Song, Piezoelectric nanogenerators based on zinc oxide nanowire arrays, *Science* 312 (5771) (2006) 242–246.
- [3] X. Zhao, C.M. Wei, L. Yang, M.Y. Chou, Quantum confinement and electronic properties of silicon nanowires, *Phys. Rev. Lett.* 92 (23) (2004) 236805.
- [4] S. Xu, Y. Qin, C. Xu, Y. Wei, R. Yang, Z.L. Wang, Self-powered nanowire devices, *Nat Nanotechnol* 5 (5) (2010) 366–373.
- [5] X. Duan, Y. Huang, R. Agarwal, C.M. Lieber, Single-nanowire electrically driven lasers, *Nature* 421 (6920) (2003) 241–245.
- [6] B. Tian, X. Zheng, T.J. Kempa, Y. Fang, N. Yu, G. Yu, J. Huang, C.M. Lieber, Coaxial silicon nanowires as solar cells and nanoelectronic power sources, *Nature* 449 (7164) (2007) 885–889.
- [7] A.I. Boukai, Y. Bunimovich, J. Tahir-Kheli, J.-K. Yu, W.A. Goddard III, J.R. Heath, Silicon nanowires as efficient thermoelectric materials, *Nature* 451 (7175) (2008) 168–171.
- [8] P.K. Schelling, L. Shi, K.E. Goodson, Managing heat for electronics, *Mater. Today* 8 (6) (2005) 30–35.
- [9] L.-D. Zhao, S.-H. Lo, Y. Zhang, H. Sun, G. Tan, C. Uher, C. Wolverton, V.P. Dravid, M.G. Kanatzidis, Ultralow thermal conductivity and high thermoelectric figure of merit in snc crystals, *Nature* 508 (7496) (2014) 373–377.
- [10] G.J. Snyder, E.S. Toberer, Complex thermoelectric materials, *Materials for sustainable energy: a collection of peer-reviewed research and review articles from Nature Publishing Group* (2011) 101–110.
- [11] A. Balandin, K.L. Wang, Significant decrease of the lattice thermal conductivity due to phonon confinement in a free-standing semiconductor quantum well, *Physical Review B* 58 (3) (1998) 1544.
- [12] A. Khitun, A. Balandin, K.L. Wang, Modification of the lattice thermal conductivity in silicon quantum wires due to spatial confinement of acoustic phonons, *Superlattices Microstruct* 26 (3) (1999) 181–193.
- [13] D. Li, Y. Wu, P. Kim, L. Shi, P. Yang, A. Majumdar, Thermal conductivity of individual silicon nanowires, *Appl Phys Lett* 83 (14) (2003) 2934–2936.
- [14] D.L. Nika, A.I. Cocemasov, D.V. Crismari, A.A. Balandin, Thermal conductivity inhibition in phonon engineered core-shell cross-section modulated Si/Ge nanowires, *Appl Phys Lett* 102 (21) (2013) 213109.
- [15] A.I. Cocemasov, D.L. Nika, V.M. Fomin, D. Grimm, O.G. Schmidt, Phonon-engineered thermal transport in si wires with constant and periodically modulated cross-sections: a crossover between nano-and microscale regimes, *Appl Phys Lett* 107 (1) (2015) 011904.
- [16] M. Hu, K.P. Giapis, J.V. Goicochea, X. Zhang, D. Poulikakos, Significant reduction of thermal conductivity in Si/Ge core-shell nanowires, *Nano Lett.* 11 (2) (2011) 618–623.
- [17] V.I. Brinzari, A.I. Cocemasov, D.L. Nika, G.S. Korotcenkov, Ultra-low thermal conductivity of nanogranular indium tin oxide films deposited by spray pyrolysis, *Appl Phys Lett* 110 (7) (2017) 071904.
- [18] L.J. Lauhon, M.S. Gudiksen, D. Wang, C.M. Lieber, Epitaxial core-shell and core-multishell nanowire heterostructures, *Nature* 420 (6911) (2002) 57–61.
- [19] M. Hu, K.P. Giapis, J.V. Goicochea, X. Zhang, D. Poulikakos, Significant reduction of thermal conductivity in Si/Ge coreshell nanowires, *Nano Lett.* 11 (2) (2011) 618–623, <https://doi.org/10.1021/nl103718a>.

- [20] M.U. Torres, A. Sitek, S.I. Erlingsson, G. Thorgilsson, V. Gudmundsson, A. Manolescu, Conductance features of core-shell nanowires determined by their internal geometry, *Physical Review B* 98 (8) (2018) 085419.
- [21] H.R. Heris, M. Kateb, S.I. Erlingsson, A. Manolescu, Thermoelectric properties of tubular nanowires in the presence of a transverse magnetic field, *Nanotechnology* 31 (42) (2020) 424006.
- [22] J. Xiang, W. Lu, Y. Hu, Y. Wu, H. Yan, C.M. Lieber, Ge/Si nanowire heterostructures as high-performance field-effect transistors, *Nature* 441 (7092) (2006) 489–493.
- [23] M.-F. Ng, L. Shen, L. Zhou, S.-W. Yang, V.B.C. Tan, Geometry dependent I-V characteristics of silicon nanowires, *Nano Lett.* 8 (11) (2008) 3662–3667.
- [24] A. Tessema, D. Zhao, J. Moll, S. Xu, R. Yang, C. Li, S.K. Kumar, A. Kidane, Effect of filler loading, geometry, dispersion and temperature on thermal conductivity of polymer nanocomposites, *Polym Test* 57 (2017) 101–106.
- [25] C. Ji, H.S. Park, The coupled effects of geometry and surface orientation on the mechanical properties of metal nanowires, *Nanotechnology* 18 (30) (2007) 305704.
- [26] G. Liang, W. Huang, C.S. Koong, J.-S. Wang, J. Lan, Geometry effects on thermoelectric properties of silicon nanowires based on electronic band structures, *J Appl Phys* 107 (1) (2010) 014317.
- [27] P. Yang, The chemistry and physics of semiconductor nanowires, *MRS Bull.* 30 (2) (2005) 85–91.
- [28] J. Zou, M. Paladugu, H. Wang, G.J. Auchterlonie, Y.-N. Guo, Y. Kim, Q. Gao, H. J. Joyce, H.H. Tan, C. Jagadish, Growth mechanism of truncated triangular III-V nanowires, *Small* 3 (3) (2007) 389–393.
- [29] L. Ren, H. Zhang, P. Tan, Y. Chen, Z. Zhang, Y. Chang, J. Xu, F. Yang, D. Yu, Hexagonal selenium nanowires synthesized via vapor-phase growth, *The Journal of Physical Chemistry B* 108 (15) (2004) 4627–4630.
- [30] J. Noborisaka, J. Motohisa, T. Fukui, Catalyst-free growth of GaAs nanowires by selective-area metalorganic vapor-phase epitaxy, *Appl Phys Lett* 86 (21) (2005) 213102.
- [31] X. Yuan, P. Caroff, F. Wang, Y. Guo, Y. Wang, H.E. Jackson, L.M. Smith, H.H. Tan, C. Jagadish, Antimony induced $\{112\}$ A faceted triangular GaAs $_{1-x}$ Sb $_x$ /InP core/shell nanowires and their enhanced optical quality, *Adv Funct Mater* 25 (33) (2015) 5300–5308.
- [32] L. Qin, J. Xu, X. Dong, Q. Pan, Z. Cheng, Q. Xiang, F. Li, The template-free synthesis of square-shaped SnO $_2$ nanowires: the temperature effect and acetone gas sensors, *Nanotechnology* 19 (18) (2008) 185705.
- [33] X. He, G. Shen, R. Xu, W. Yang, C. Zhang, Z. Liu, B. Chen, J. Liu, M. Song, Hexagonal and square patterned silver nanowires/PEDOT: PSS composite grids by screen printing for uniformly transparent heaters, *Polymers (Basel)* 11 (3) (2019) 468.
- [34] G. Pennelli, M. Pioletto, Fabrication and characterization of silicon nanowires with triangular cross section, *J Appl Phys* 100 (5) (2006) 054507.
- [35] R. Prasher, Thermal conductivity of tubular and core/shell nanowires, *Appl Phys Lett* 89 (6) (2006) 063121.
- [36] J. Chen, G. Zhang, B. Li, Impacts of atomistic coating on thermal conductivity of germanium nanowires, *Nano Lett.* 12 (6) (2012) 2826–2832.
- [37] J. Chen, G. Zhang, B. Li, Phonon coherent resonance and its effect on thermal transport in core-shell nanowires, *J Chem Phys* 135 (10) (2011) 104508.
- [38] S.-c. Wang, X.-g. Liang, X.-h. Xu, T. Ohara, Thermal conductivity of silicon nanowire by nonequilibrium molecular dynamics simulations, *J Appl Phys* 105 (1) (2009) 014316.
- [39] M.S. Green, Markoff random processes and the statistical mechanics of time-dependent phenomena. II. irreversible processes in fluids, *J Chem Phys* 22 (3) (1954) 398–413.
- [40] R. Kubo, Statistical-mechanical theory of irreversible processes. I. general theory and simple applications to magnetic and conduction problems, *J. Phys. Soc. Jpn.* 12 (6) (1957) 570–586.
- [41] S.G. Volz, G. Chen, Molecular dynamics simulation of thermal conductivity of silicon nanowires, *Appl Phys Lett* 75 (14) (1999) 2056–2058, <https://doi.org/10.1063/1.124914>.
- [42] D. Ma, H. Ding, H. Meng, L. Feng, Y. Wu, J. Shiomi, N. Yang, et al., Nano-cross-junction effect on phonon transport in silicon nanowire cages, *Physical Review B* 94 (16) (2016) 165434.
- [43] A. Soleimani, H. Araghi, Z. Zabih, A. Alibakhshi, A comparative study of molecular dynamics simulation methods for evaluation of the thermal conductivity and phonon transport in Si nanowires, *Comput. Mater. Sci* 142 (2018) 346–354.
- [44] I. Ponomareva, D. Srivastava, M. Menon, Thermal conductivity in thin silicon nanowires: phonon confinement effect, *Nano Lett.* 7 (5) (2007) 1155–1159.
- [45] H. Dong, Z. Fan, L. Shi, A. Harju, T. Ala-Nissila, Equivalence of the equilibrium and the nonequilibrium molecular dynamics methods for thermal conductivity calculations: from bulk to nanowire silicon, *Physical Review B* 97 (9) (2018) 094305.
- [46] M.H. Khadem, A.P. Wemhoff, Comparison of Green-Kubo and NEMD heat flux formulations for thermal conductivity prediction using the Tersoff potential, *Comput. Mater. Sci* 69 (2013) 428–434, <https://doi.org/10.1016/j.commatsci.2012.12.016>.
- [47] P.K. Schelling, S.R. Phillpot, P. Keblinski, Comparison of atomic-level simulation methods for computing thermal conductivity, *Physical Review B* 65 (14) (2002) 144306, <https://doi.org/10.1103/PhysRevB.65.144306>.
- [48] Z. Li, S. Xiong, C. Sievers, Y. Hu, Z. Fan, N. Wei, H. Bao, S. Chen, D. Donadio, T. Ala-Nissila, Influence of thermostatting on nonequilibrium molecular dynamics simulations of heat conduction in solids, *J Chem Phys* 151 (23) (2019) 234105, <https://doi.org/10.1063/1.5132543>.
- [49] F. Müller-Plathe, A simple nonequilibrium molecular dynamics method for calculating the thermal conductivity, *J Chem Phys* 106 (14) (1997) 6082–6085, <https://doi.org/10.1063/1.473271>.
- [50] D. Surblyis, H. Matsuura, G. Kikugawa, T. Ohara, Application of atomic stress to compute heat flux via molecular dynamics for systems with many-body interactions, *Physical Review E* 99 (5) (2019) 051301, <https://doi.org/10.1103/PhysRevE.99.051301>.
- [51] S. Plimpton, Fast parallel algorithms for short-range molecular dynamics, *J Comput Phys* 117 (1) (1995) 1–19, <https://doi.org/10.1006/jcph.1995.1039>.
- [52] A. Rohskopf, H.R. Seyf, K. Gordiz, T. Tadano, A. Henry, Empirical interatomic potentials optimized for phonon properties, *npj Comput. Mater.* 3 (1) (2017) 1–7.
- [53] Y. Zhou, X. Zhang, M. Hu, Nonmonotonic diameter dependence of thermal conductivity of extremely thin Si nanowires: competition between hydrodynamic phonon flow and boundary scattering, *Nano Lett.* 17 (2) (2017) 1269–1276.
- [54] Z. Fan, Y. Wang, X. Gu, P. Qian, Y. Su, T. Ala-Nissila, A minimal Tersoff potential for diamond silicon with improved descriptions of elastic and phonon transport properties, *J. Phys.: Condens. Matter* 32 (13) (2019) 135901.
- [55] J. Tersoff, New empirical approach for the structure and energy of covalent systems, *Physical review B* 37 (12) (1988) 6991.
- [56] J. Tersoff, Modeling solid-state chemistry: interatomic potentials for multicomponent systems, *Physical review B* 39 (8) (1989) 5566.
- [57] L. Verlet, Computer “experiments” on classical fluids. I. thermodynamical properties of Lennard-Jones molecules, *Physical Review* 159 (1) (1967) 98.
- [58] M. Kateb, K. Dehghani, Comparison of fracture behavior of sharp with blunt crack tip in nanocrystalline materials by molecular dynamics simulation, *International Journal of Modern Physics: Conference Series* 5 (2012) 410–417.
- [59] D.E. Angelescu, M.C. Cross, M.L. Roukes, Heat transport in mesoscopic systems, *Superlattices Microstruct* 23 (3–4) (1998) 673–689.
- [60] L.G.C. Rego, G. Kirczenow, Rego and Kirczenow reply, *Phys. Rev. Lett.* 81 (22) (1998) 5038.
- [61] M.G. Holland, Analysis of lattice thermal conductivity, *Physical review* 132 (6) (1963) 2461.
- [62] J.R. Lukes, H. Zhong, Thermal conductivity of individual single-wall carbon nanotubes, *J Heat Transfer* 129 (6) (2006) 705–716.
- [63] M. Alaghemandi, E. Algaer, M.C. Böhm, F. Müller-Plathe, The thermal conductivity and thermal rectification of carbon nanotubes studied using reverse nonequilibrium molecular dynamics simulations, *Nanotechnology* 20 (11) (2009) 115704.
- [64] C. Yu, L. Shi, Z. Yao, D. Li, A. Majumdar, Thermal conductance and thermopower of an individual single-wall carbon nanotube, *Nano Lett.* 5 (9) (2005) 1842–1846.
- [65] T. Yamamoto, S. Watanabe, K. Watanabe, Universal features of quantized thermal conductance of carbon nanotubes, *Phys. Rev. Lett.* 92 (7) (2004) 075502.
- [66] T. Yamamoto, K. Watanabe, Nonequilibrium greens function approach to phonon transport in defective carbon nanotubes, *Phys. Rev. Lett.* 96 (25) (2006) 255503.
- [67] M. Hu, X. Zhang, K.P. Giapis, D. Poulikakos, Thermal conductivity reduction in core-shell nanowires, *Physical Review B* 84 (8) (2011) 085442.
- [68] K.-H. Lin, A. Strachan, Thermal transport in sige superlattice thin films and nanowires: effects of specimen and periodic lengths, *Physical Review B* 87 (11) (2013) 115302.
- [69] X. Lü, J. Chu, Lattice thermal conductivity in a silicon nanowire with square cross section, *J Appl Phys* 100 (1) (2006) 014305.
- [70] D.V. Crismari, D.L. Nika, Thermal conductivity reduction in Si/Ge core/shell nanowires, *J. Nanoelectron. Optoelectron.* 7 (7) (2012) 701–705.
- [71] N. Mingo, L. Yang, D. Li, A. Majumdar, Predicting the thermal conductivity of Si and Ge nanowires, *Nano Lett.* 3 (12) (2003) 1713–1716.

Paper III

Charge and heat currents in prismatic tubular nanowires

H. R. Heris* , K.O. Klausen* , Anna Sitek[†] , S. I. Erlingsson* , A. Manolescu*

*Department of Engineering, Reykjavik University, Menntavegur 1, IS-102 Reykjavik, Iceland

[†]Department of Theoretical Physics, Wrocław University of Science and Technology, Wybrzeże Wyspińskiego 27, 50-370 Wrocław, Poland

2022 International Semiconductor Conference (CAS)

DOI: 10.1109/CAS56377.2022.9934669

Charge and heat currents in prismatic tubular nanowires

H. R. Heris^{*}, K.O. Klausen^{*}, Anna Sitek[†], S. I. Erlingsson^{*}, A. Manolescu^{*}

^{*}Department of Engineering, Reykjavik University, Menntavegur 1, IS-102 Reykjavik, Iceland

[†]Department of Theoretical Physics, Wrocław University of Science and Technology,

Wybrzeże Wyspiańskiego 27, 50-370 Wrocław, Poland

Email: hadi19@ru.is

Abstract—We calculate electronic charge and heat transport in tubular nanowires generated by a temperature gradient or a chemical potential bias. These nanowires correspond to semiconductor core-shell nanowires with insulating (undoped) core and conductive (doped) shell, such that the conduction takes place only in the shell. The cross section of such nanowires is typically polygonal. We study the influence of the cross section shape and shell thickness on the electric and heat conduction of the shell. We use the Landauer-Büttiker approach to calculate the electric and heat currents as a non-linear function of temperature and chemical potential bias beyond the linear regime.

Index Terms—Thermoelectric current, heat transport, tubular nanowires, polygonal cross section

I. INTRODUCTION

Nanowires made of different materials allow several controllable properties of the electronic states within channels of widths from tens to hundreds of nanometers. Such structures can be built as radial heterojunctions of two different semiconductor materials, and are known as core-shell nanowires [1], [2]. Such nanostructures have a variety of electronic properties, determined by the band alignment between the two materials, by the size of the core, or by the shell thickness or shape, which make them attractive for a variety of applications of quantum devices such as nanosensors, solar cells, optical detectors or thermoelectric convertors [3]–[6].

Core-shell nanowire based on III-V semiconductors are almost always prismatic, with a polygonal profile. The typical cross section shape is hexagonal [7], although other prismatic geometries such as square and triangular have also been fabricated [8], [9]. Interestingly, it is also possible to remove the core, and to obtain hollow nanowires, with vacuum inside [7]. Because of these many possibilities, understanding the implications of the geometry on electronic properties such as electric and heat conductance is important.

In the present work we consider models of shells with several geometries: cylindrical, hexagonal, square, and triangular, with lateral thickness of up to 40% of the overall diameter of the nanowire, and we calculate the electric and heat current of electrons in the presence of a temperature gradient and chemical potential bias. A temperature gradient across a conducting material induces an energy gradient which leads to charge or energy transport. The particles on the hotter side have larger kinetic energy than those at the colder side,

and therefore the net particle flow is expected to be from the hotter to the colder side. However, the thermoelectric current can be positive or negative, depending on the type of carriers, i.e. electrons or holes, or more generally, depending on the occupation fraction of the transverse modes contributing to the transport [10].

For a tubular nanowire with circular symmetry the electrons have uniform angular distribution within the shell. In the case of polygonal shells the localization pattern, especially for low-energy states, is much more complicated [11], [12]. Consequently, the properties of polygonal nanowires may differ considerably from their circular counterparts. In general, the lateral confinement of electrons in the tubular shell leads to an increase in thermoelectric current compared to the values in the bulk materials [13]. At the same time the thermal conductivity due to phonons can be strongly suppressed in nanowires with a diameter below the phonon mean free path [6], [14]. Therefore semiconductor core-shell nanowires provide a unique opportunity to design desired nanoscale devices by engineering the charge and heat transport related only to electrons, through the cross section area configuration. Depending on the purpose, suppressing heat and increasing charge current, or vice versa, can be achieved via geometric elements [15], [16]. By considering electronic conductance features and variations as function of transverse geometry and shell thickness, and the transported heat through the core, one can calculate the figure of merit or the thermoelectric efficiency, and find optimal situations. Note that for this purpose the heat transported by phonons and electron-phonon interaction must also be considered [17], [18].

II. MODEL AND METHODS

Our model is a systems of electrons confined in prismatic shell with cylindrical, hexagonal, square or triangular cross section. In all cases we consider an external radius of the polygonal shell of 50 nm (i. e. the radius of the circle encompassing the entire cross section), and initially the side thickness will be 20 nm. The Hamiltonian can be decomposed into a transverse term and a longitudinal term. The transverse Hamiltonian is defined on a lattice of points that cover the cross section of shell. For this purpose first we define a radial lattice within a circular disk on which we integrate the desired polygonal shell and exclude from the Hamiltonian the lattice

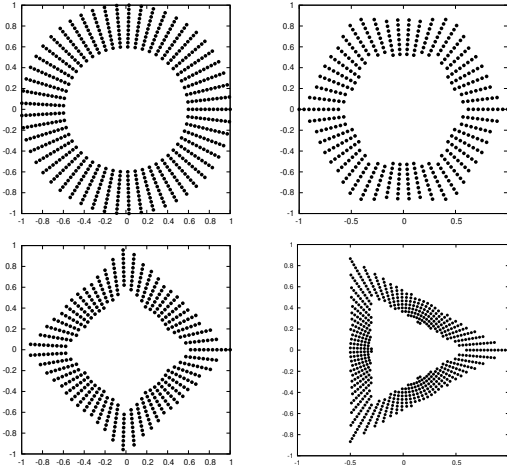


Fig. 1. The discretized polygon with external radius of 50 nm and thickness of 20 nm. The cross section of the prismatic shells are defined by applying boundaries on a circular ring discretized in polar coordinates—points indicate the shell thickness.

points which are outside of the shell [19]. The transverse geometry of our nanowire models is presented in Figure 1. The discretized ring was represented by 10-15 radial \times 40-54 angular sites, depending on the polygon shape and shell thickness. The electron effective mass is as for bulk InAs, $m_{\text{eff}} = 0.023 m_e$.

We calculate the charge current, I_c , and heat current, I_q , through the nanowire using Landauer-Büttiker approach, based on the transmission function $\mathcal{T}(E)$:

$$I_c = \frac{e}{h} \int \mathcal{T}(E) [f_L(E) - f_R(E)] dE, \quad (1)$$

$$I_q = \frac{1}{h} \int \mathcal{T}(E) [E - \mu] [f_L(E) - f_R(E)] dE, \quad (2)$$

where

$$f_{L,R}(E) = \frac{1}{1 - e^{(E - \mu_{L,R})/k_B T_{L,R}}} \quad (3)$$

is the Fermi function for the left (L) or right (R) reservoirs with the chemical potential $\mu_{L,R}$ and temperature $T_{L,R}$.

We consider a fixed chemical potential bias $\Delta\mu = \mu_L - \mu_R$ and change the values of the chemical potentials simultaneously, at each end of nanowire, in each step. For studying the effect of the cross section shape, the values of the chemical potential at the left reservoir start from 45 meV, which is the minimum value corresponding to the circular cross section, and goes up to 225 meV, which is the highest energy level considered in the triangular cross section. For studying thickness effects, the left reservoir chemical potential range will be 140-850 meV, for nanowires with thicknesses of 20 nm and 5 nm. Because of the different geometries, the energy spectra are different. In each case we shall consider the first ten transverse modes to be inspected with the chemical potential window.

We consider a fixed temperature gradient $\Delta T = T_L - T_R = 35$ K (which is very close $k_B T$ value) and we change both ends temperatures at the same time in each step. In the first step, $T_L = 36$ K and $T_R = 1$ K and simultaneously we increase each reservoir temperature by 35 K in each step. There are 12 steps for each of the charge and heat currents in both cases of cross section and thickness calculations. The energy integral is calculated numerically using the trapezoidal method.

We calculate the charge and heat currents I_c and I_q by varying one parameter at a time. Note that we neglect carriers interaction and scattering with impurities, and consider only ballistic transport of electrons in the nanowires. In this case the transmission function \mathcal{T} is a multistep function of energy. The presence of disorder indeed changes the transmission function, but in the present work we neglect disorder, or assume it is sufficiently weak such that disorder effects are dominated by the thermal effects.

III. RESULTS AND DISCUSSION

A. Effect of transverse geometry

In shells with polygonal cross section area, the lowest energy states are localized along the corners, and there is a considerable energy gap between the states localized at corners and the next group of states localized on polygon sides. This gap increases with decreasing the shell thickness and with decreasing the number of corners [11]. However, experimentally, this localization effect has not been thoroughly investigated. Whereas for the electrical conductance without a temperature bias, i. e. when $T_L = T_R$, the conductance is expected to have steps corresponding to the transverse modes [19], the thermoelectric and heat transport are different. Figure 2 presents electrical and heat currents as function of left reservoir chemical potential and temperature for different cross sectional shapes of our tubular nanowires. In Figure 2(a) we can see that the electrical current increases with increasing the chemical potential for all shapes, and that it reaches larger values for the polygonal geometry than for the circular case. Although for each cross section the energy states are different, the charge current in all cases simply follow the transmission function and the energy window associated with the chemical potentials. By increasing the chemical potentials more states will participate in transmission which lead to a higher charge current flow. The largest electric current corresponds to the triangular cross section. These values for electrical conductance are obtained for all shapes without a temperature bias, $T_L = T_R = 200$ K, and as a function of chemical potential bias. Another interesting issue about electrical current variation with the chemical potential for different cross sectional shapes is that in all cases electrical current will be saturated at high values of chemical potentials.

The heat current variation with increasing the chemical potential shows a peak for all shapes but we can also see a rapid decrease after that peak, Figure 2(b). The position of the peaks is related to the fixed temperatures of both ends, i.e. if we choose both temperatures 300 K instead of 200 K these peak shift a little to the right side. The reason for this shift

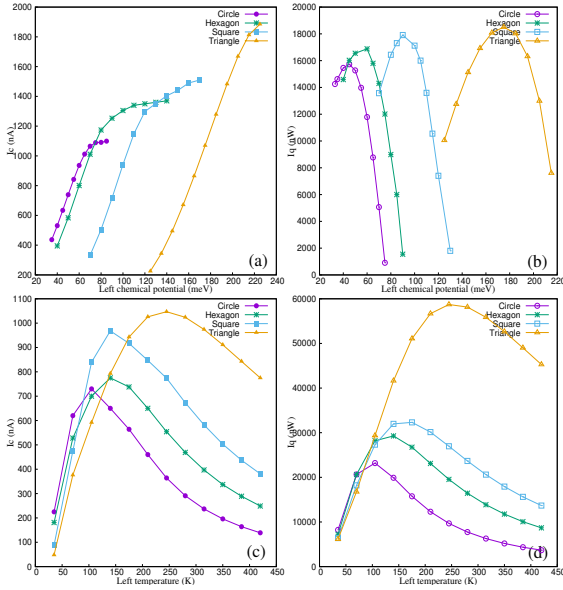


Fig. 2. Cross section shape effect on electrical current and heat current as function of left reservoir chemical potential (a) and (b) and temperature (c) and (d). (a) and (c) are representative of electrical current and (b) and (d) are for heat current. In case of chemical potential bias, $T_L = T_R = 200$ K and in presence of temperature gradient chemical potentials values calculated as mentioned in text.

is that when we increase the temperature, $k_B T$ will increase and the system needs a higher chemical potential to activate the higher number of carriers.

For calculating the temperature effect on the electrical conduction we change left and right reservoir temperatures as mentioned in Section II. Now there is no chemical potential bias in the system, and for each geometry the chemical potentials of the left and right reservoirs are considered equal, $\mu_L = \mu_R = (\mu_{max} - \mu_{min})/2$. For the circular cross section $\mu_{max} = 88$ meV and $\mu_{min} = 46$ meV, so we put both chemical potentials at 67 meV. The same had been applied to the other shapes and chemical potential values are 80 meV, 130 meV and 183 meV, for the hexagon, square, and triangle, respectively. In Figure 2(c), by increasing the temperature of the left lead, the electric current initially increases, but after reaching a maximum it decays slowly. The maximum values of the charge current for each shape occur at different temperature. The lowest peak occurs in the circular case, and the highest peak for the triangular geometry. The highest value of the charge current for triangle shape occurs at 250 K, which is a quite high temperature regime with respect to the other geometries. Also, the charge current values at high temperature are nearly two or three times larger than for other shapes. At low temperatures the charge current for polygonal shapes with fewer corners is lower, while by increasing the temperature we see the reverse situation, i. e. polygonal shapes with fewer corners show higher charge current. The heat current variation with

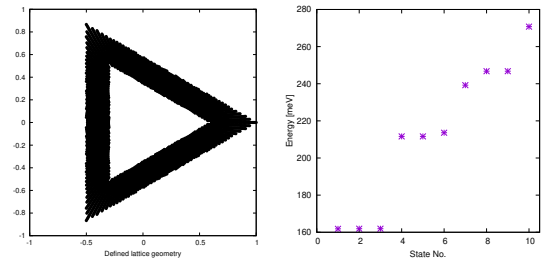


Fig. 3. The energies of the transverse modes for a triangular shell of 20 nm thickness and 50 nm external radius, are shown in the right figure. There are three states at ≈ 160 meV (spin degenerated), localized in the corners, and six states at $\approx 212 - 215$ meV localized on the sides. The energy gap between these states increases when the shell thickness decreases.

the left temperature shows the same behavior up to 100 K for all shapes, but above that temperature again the triangular case has the highest current and the circular the lowest values for the transported heat. Just like the electric current, heat current has a peak occurring different temperatures for different cross sectional shapes, and after that it decreases smoothly to a saturated value.

B. Effect of thickness

Next we shall consider the triangular cross sectional shape for studying the thickness effect on the electronic charge and heat transport. The working samples will have a fixed external radius and variable side thickness. The energy levels strongly depend on the aspect of ratio of the polygonal cross section, i. e. the ratio of thickness to diameter, in a way that the energy differences increase when this ratio is small. In particular, for the triangular case the energy gap between states localized at corners and states localized on sides strongly increases with decreasing the side thickness and keeping the total thickness fixed [12]. An example is shown in Figure 3. In the next calculations we shall use four shell thicknesses, 5, 10, 15, and 20 nm and constant external radii 50 nm. Similar to the calculations for variable geometry, in this part we consider $T_L = T_R = 200$ K in case of a chemical potential bias. And for a temperature bias we consider left and right chemical potentials as average of minimum and maximum of chemical potentials for that specific thickness.

In Figure 4 we present values of the charge and heat currents for different thickness of the equilateral triangular shell while increasing the left chemical potential and temperature. The higher chemical potential leads more states to participate in transmission and the electric current increase, and this is clearly observable in Figure 4(a) regardless of thickness of sample. But this increase is different for each thickness, and from a step like behavior for the 5 nm shell it evolves to an almost linear function. An equation to describe analytically this I-V characteristics is however beyond the intention of our present study. For thinner shells with respect to the diameter of nanowires, corner localization cause more effect on electrons distribution. And for thin shells the energy gap between the

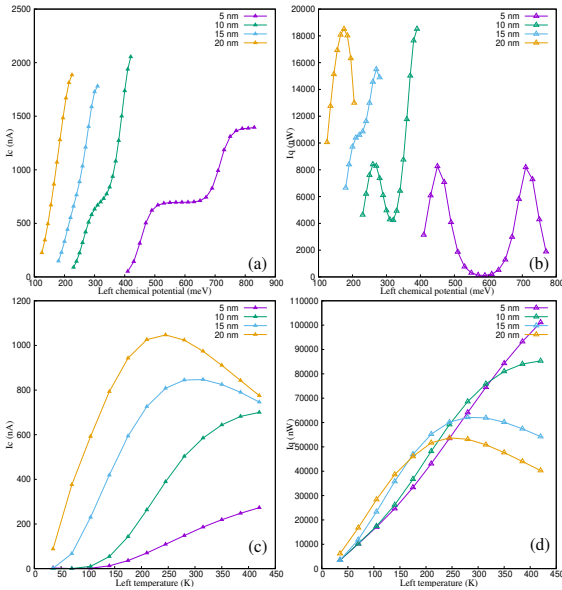


Fig. 4. Shell thickness effect on electrical and heat currents as function of left chemical potential (a) and (b) and temperature (c) and (d). (a) and (c) are representative of electrical current and (b) and (d) are for heat current.

corner and side states are higher. Due to this reason step like behavior was expected from thinner shell and by increasing shell thickness this step like behavior vanish gradually. We can expect these step like behavior for other geometries if we decrease the thickness of shell below 10 nm.

Fig. 4(b) shows the variation of the heat current with increasing the left chemical potential, with one or two maxima for each thickness. The energy interval between maxima is related to the energy gap between corner and side states. Fig. 4(c) shows that the thermoelectric current increases with increasing the shell thickness, with an almost linear variation with the temperature bias for the smallest thicknesses, and with a maximum point for the largest thickness. Finally, in Fig. 4(d) we can also see a linear behavior of the heat current for 5 nm thickness, and a non-linear characteristic with a maximum current developing for the other cases. Interestingly, the relative magnitude of these heat currents reverses between low and high temperatures.

IV. CONCLUSIONS

In this paper we reported computed features of charge and heat transport in core-shell nanowires when the electronic transport occurs within the shell. These features were studied for different cross sectional geometries of the shell. The charge and heat conductivity, as functions with respect to the chemical potential and temperature biases, depend significantly on the geometry. Shells with triangular cross section lead to larger charge and heat currents in the presence of a temperature gradient, but not in the case of a chemical potential bias. Also, the

charge and heat currents were found to change substantially with decreasing shell thickness, due to the increasing of the gap between corner and side states.

ACKNOWLEDGMENT

This work was supported by funding from the Icelandic Research Fund Grant Nos. 195943-051 and 229078-051.

REFERENCES

- [1] C. Blömers, T. Rieger, P. Zellekens, F. Haas, M. Lepsa, H. Hardtdegen, Ö. Gül, N. Demarina, D. Grützmacher, H. Lüth, et al., "Realization of nanoscaled tubular conductors by means of gaas/inas core/shell nanowires," *Nanotechnology*, vol. 24, no. 3, p. 035203, 2013.
- [2] T. Shi, H. E. Jackson, L. M. Smith, N. Jiang, Q. Gao, H. H. Tan, C. Jagadish, C. Zheng, and J. Etheridge, "Emergence of localized states in narrow gaas/algaas nanowire quantum well tubes," *Nano Letters*, vol. 15, no. 3, pp. 1876–1882, 2015.
- [3] M.-E. Pistol and C. Pryor, "Band structure of core-shell semiconductor nanowires," *Physical Review B*, vol. 78, no. 11, p. 115319, 2008.
- [4] J. Tang, Z. Huo, S. Brittman, H. Gao, and P. Yang, "Solution-processed core-shell nanowires for efficient photovoltaic cells," *Nature nanotechnology*, vol. 6, no. 9, pp. 568–572, 2011.
- [5] K. Peng, P. Parkinson, L. Fu, Q. Gao, N. Jiang, Y.-N. Guo, F. Wang, H. J. Joyce, J. L. Boland, H. H. Tan, et al., "Single nanowire photoconductive terahertz detectors," *Nano letters*, vol. 15, no. 1, pp. 206–210, 2015.
- [6] F. Dominguez-Adame, M. Martin-Gonzalez, D. Sanchez, and A. Cantarero, "Nanowires: A route to efficient thermoelectric devices," *Physica E: Low-dimensional Systems and Nanostructures*, vol. 113, pp. 213–225, 2019.
- [7] T. Rieger, M. Luysberg, T. Schäpers, D. Grützmacher, and M. I. Lepsa, "Molecular beam epitaxy growth of gaas/inas core-shell nanowires and fabrication of inas nanotubes," *Nano letters*, vol. 12, no. 11, pp. 5559–5564, 2012.
- [8] F. Qian, S. Gradecak, Y. Li, C.-Y. Wen, and C. M. Lieber, "Core/multishell nanowire heterostructures as multicolor, high-efficiency light-emitting diodes," *Nano letters*, vol. 5, no. 11, pp. 2287–2291, 2005.
- [9] D. J. O. Göransson, M. Heurlin, B. Dalelkhan, S. Abay, M. E. Messing, V. F. Maisi, M. T. Borgström, and H. Q. Xu, "Coulomb blockade from the shell of an inp-inas core-shell nanowire with a triangular cross section," *Applied Physics Letters*, vol. 114, no. 5, p. 053108, 2019.
- [10] S. I. Erlingsson, A. Manolescu, G. A. Nemnes, J. H. Bardarson, and D. Sanchez, "Reversal of thermoelectric current in tubular nanowires," *Physical review letters*, vol. 119, no. 3, p. 036804, 2017.
- [11] A. Sitek, L. Serra, V. Gudmundsson, and A. Manolescu, "Electron localization and optical absorption of polygonal quantum rings," *Phys. Rev. B*, vol. 91, p. 235429, Jun 2015.
- [12] A. Sitek, G. Thorgilsson, V. Gudmundsson, and A. Manolescu, "Multi-domain electromagnetic absorption of triangular quantum rings," *Nanotechnology*, vol. 27, no. 22, p. 225202, 2016.
- [13] H. R. Heris, M. Kateb, S. I. Erlingsson, and A. Manolescu, "Thermoelectric properties of tubular nanowires in the presence of a transverse magnetic field," *Nanotechnology*, vol. 31, no. 42, p. 424006, 2020.
- [14] A. I. Boukai, Y. Bunimovich, J. Tahir-Kheli, J.-K. Yu, W. A. Goddard III, and J. R. Heath, "Silicon nanowires as efficient thermoelectric materials," *nature*, vol. 451, no. 7175, pp. 168–171, 2008.
- [15] P. K. Schelling, L. Shi, and K. E. Goodson, "Managing heat for electronics," *Materials Today*, vol. 8, no. 6, pp. 30–35, 2005.
- [16] L.-D. Zhao, S.-H. Lo, Y. Zhang, H. Sun, G. Tan, C. Uher, C. Wolverton, V. P. Dravid, and M. G. Kanatzidis, "Ultralow thermal conductivity and high thermoelectric figure of merit in snse crystals," *nature*, vol. 508, no. 7496, pp. 373–377, 2014.
- [17] H. R. Heris, M. Kateb, S. I. Erlingsson, and A. Manolescu, "Effects of transverse geometry on the thermal conductivity of si and ge nanowires," *Surfaces and Interfaces*, vol. 30, p. 101834, 2022.
- [18] M. Tsaousidou, "Energy relaxation of hot electrons in semiconducting carbon nanotubes," *Physica E: Low-dimensional Systems and Nanostructures*, vol. 40, no. 5, pp. 1127–1129, 2008.
- [19] M. U. Torres, A. Sitek, S. I. Erlingsson, G. Thorgilsson, V. Gudmundsson, and A. Manolescu, "Conductance features of core-shell nanowires determined by their internal geometry," *Physical Review B*, vol. 98, no. 8, p. 085419, 2018.

Paper IV

Effect of Impurities on Charge and Heat Transport in Tubular Nanowires

Hadi Rezaie Heris¹, Kristjan Ottar Klausen¹, Anna Sitek², Sigurdur Ingi Erlingsson¹, and Andrei Manolescu¹

¹Department of Engineering, Reykjavik University, Menntavegur 1, IS-102 Reykjavik, Iceland

²Department of Theoretical Physics, Wroclaw University of Science and Technology, Wybrzeże Wyspiańskiego 27, 50-370 Wroclaw, Poland

arXiv:2302.02164

doi.org/10.48550/arXiv.2302.02164

Effect of Impurities on Charge and Heat Transport in Tubular Nanowires

Hadi Rezaie Heris,¹ Kristjan Ottar Klausen,¹ Anna Sitek,² Sigurdur Ingi Erlingsson,¹ and Andrei Manolescu¹

¹*Department of Engineering, Reykjavik University, Menntavegur 1, IS-102 Reykjavik, Iceland*

²*Department of Theoretical Physics, Wrocław University of Science and Technology, Wybrzeże Wyspiańskiego 27, 50-370 Wrocław, Poland*

We calculate charge and heat current of charge carriers (electrons or holes), originating from a temperature gradient and a chemical potential difference between two ends of a tubular nanowire with different cross-sectional areas. We consider a nanowire based on a semiconductor material, and use the Landauer-Büttiker approach to calculate the transport quantities. Values of the heat and charge current are calculated in the presence of different variations of impurities, with respect to the left temperature and left side chemical potential. Results are obtained for a temperature regime from 1 to 420 K and chemical potential 35 to 225 meV. The temperature difference between two sides is 35 K for all cases with a chemical potential difference of 5 meV. Electronic transmission is compared for the main prismatic cross-section geometries, in the presence of impurities of varying densities and strengths.

I. INTRODUCTION

Semiconductor nanowires are potential candidates for several fields of technology such as nanoelectronics [1–5], quantum information processing [6], solar cells [7, 8], biological sensors [9], thermoelectrics and energy conversion devices [10–12], and integrated circuits [13]. In many of these applications understanding the charge and heat current is crucial. Thermoelectric devices demand a high charge current associated with low heat transport to reach high efficiency [14, 15], while nanoelectronic devices necessitate high heat transport and sinks to take heat out from nano chips [16]. In particular, core-shell nanowires, which are radial heterojunctions of two or more different semiconductor materials, enable the control of charge and heat transfer through specific geometry. In such structures, electronic properties can be determined by the band alignment between materials, core size, and shell thickness. Similarly, heat transport can be guided or trapped through core-shell nanowires [17].

Core-shell nanowires with a doped shell and an undoped core are tubular conductors, such that conduction takes place only in the shell [18]. It is also possible to achieve tubular nanowires by etching the core part [19]. Semiconductor core-shell nanowires based on III-V materials are most commonly prismatic. The typical shape of the cross-section is hexagonal [20–22], but other prismatic shapes can also be fabricated, like square [23] or triangular [24, 25]. The prismatic geometry of core-shell nanowires, especially tubular nanowires, presents a unique window to important features. These include conductance and electron localization [26, 27], quantum confinement effect over charge carriers [28], interacting several Majorana states with each other [29] and inducing the sign reversal of the electric current generated by the temperature gradient in presence of a transversal magnetic field [30].

In tubular nanowires apart of the geometry mainly three factors lead to changes in charge and heat current: surface roughness, impurities and phonons. Surface

roughness leads to a reduction in charge current but practically it is easy to estimate the range of this deviation for different materials [31]. Electron-phonon interaction can be neglected in thin shells. Impurities play a significant role in the conduction feature of tubular nanowires, and it is different for transported charge and heat current for each cross-section with respect to chemical potential bias or temperature gradient. Different numbers of impurities or varying intensities show distinct behavior in each case of cross-section geometry. Understanding the combination of heat and charge current is essential in many cases of nanoscale studies, and the purpose of this work is to provide a comprehensive view of impurities' effect on electronic conduction of tubular nanowires. We study the effect of the density of the impurities, and of the strength of the associated potential, on the charge and heat currents, in prismatic shells. Due to the fact that nowadays it is feasible to fabricate tubular nanowires with the desired cross-section and different doping variations, our study can be useful to establish a direct relation between different cross-sections and transport properties of core-shell nanowires.

The paper is structured in the following sections: Section 2 contains our model and methodology. In Section 3 we present the results, in particular we show how the presence of impurities affects conductance through wires of different cross sections. Further, we focus on wires having hexagonal and triangular cross sections and we study the impact of the number and intensity of impurities on the conductance. Finally, Section 4 contains the conclusions.

II. MODEL AND METHODS

Our model is a single-wire system of a tubular nanowire, with a finite length, and with different cross-sectional geometries. We implement a temperature gradient and different chemical potentials between two ends in the longitudinal direction of the wire. We assume the charge carriers are electrons, i. e. the shell material is

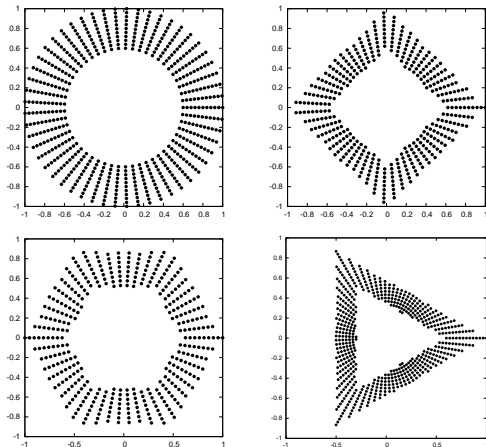


FIG. 1. The discretized polygon with external radius of 50 nm and thickness of 20 nm. The cross-section of the prismatic shells are defined by applying boundaries on a circular ring discretized in polar coordinates—points indicate the shell thickness. Note that for calculations all shells consist of a high number of radial and angular sites in comparison to the above shapes. Due to better illustration we use a small number of points here.

n-doped. Then for each example, we consider a particular number of impurities whose strength varies within a certain range. We calculate the electronic charge and heat currents for four cross section shapes: cylindrical, hexagonal, square and triangular. In all cases the external radius of the nanowire is 50 nm (i.e. the radius of the circle encompassing the entire cross section) and the shell thickness is 20 nm, so that conduction takes place in the narrow shell cross-sectional area. All nanowire's length are 500 nm.

The Hamiltonian of the nanowire consists of a longitudinal and a transverse term. The transverse Hamiltonian is discretized in polar coordinates [32, 33]. A specific cross-section of the polygonal shell, defined on a set of lattice of points, is obtained from a circular disk, after excluding every point from the lattice which stands outside the shell boundaries [26]. The electron effective mass is $m_{\text{eff}} = 0.023 m_e$, as for bulk InAs. We calculate heat current I_q and electrical current I_c driven by the temperature gradient and chemical potential bias applied between two ends of nanowire using the Landauer-Buttiker approach:

$$I_c = \frac{e}{h} \int \mathcal{T}(E) [f_R(E) - f_L(E)] dE, \quad (1)$$

$$I_q = \frac{1}{h} \int \mathcal{T}(E) [E - \mu] [f_R(E) - f_L(E)] dE, \quad (2)$$

where \mathcal{T} is the transmission function, and

$$f_{L,R}(E) = \frac{1}{1 + e^{(E - \mu_{L,R})/kT_{L,R}}}$$

is the Fermi function for the left (L) or right (R) reservoir with chemical potential $\mu_{L,R}$ and temperature $T_{L,R}$ (and k denoting Boltzmann's constant).

For clarity reasons we study the conduction under the temperature gradient case and chemical potential bias case separately. So in each case one type of bias is constant and the other one is variable. The chemical potential bias $\Delta\mu = \mu_L - \mu_R$ is always present at the two ends of the nanowire, and in each step of the calculation we change the left and the right reservoir values simultaneously, but keeping $\Delta\mu = 3 \text{ meV}$ fixed. In all cases, we consider the first 10 transverse modes in our numerical calculation regardless of geometries or impurities variation.

Different cross-sectional areas lead to different energy spectra for each shape and consequently different chemical potential windows appear. Due to this reason, first we need to find the maximum and minimum possible values of the chemical potentials, corresponding to each specific cross-section. Then, the entire energy interval between the lowest and highest energy states (corresponding to the first 10 transverse modes) is explored stepwise. During this series of calculations, i. e. in the presence of a chemical potential bias, we consider no temperature gradient, and $T_R = T_L = 200 \text{ K}$. To compute the currents, the energy limits are considered between the ground state and the highest available state for each cross-section. For instance, this range for circular cross section is 35-85 meV, and for triangle cross section is 120-220 meV.

In the case of a temperature gradient, we fix $\Delta T = T_L - T_R = 35 \text{ K}$. In the first step, we set $T_L = 36 \text{ K}$ and $T_R = 1 \text{ K}$ and then we increase the temperature of both sides simultaneously. This process is repeated several times, while the left temperature varies between 36 - 420 K. The temperature gradient effect on the conductance is calculated using the same chemical potentials at the left and right end of the nanowire. For each geometry these values are calculated as $\mu_L = \mu_R = (\mu_{\text{max}} + \mu_{\text{min}})/2$, where the minimum and maximum values are equal to the minimum and maximum energy in the computed electronic spectra, respectively. For example, in the case of the circular cross section $\mu_{\text{max}} = 85 \text{ meV}$ and $\mu_{\text{min}} = 35 \text{ meV}$, and we set both chemical potentials at 60 meV. By applying the same rule to the other geometries, chemical potential values are 75 meV, 110 meV, and 170 meV, for the hexagon, square and triangle, respectively.

III. RESULTS AND DISCUSSION

A. Impurities in different cross section geometries

Tubular nanowires increase thermoelectric current due to the lateral electron confinement [34, 35] and decrease heat transport due to the strong suppression of phonons with a diameter below the phonon mean free path [17, 36]. Core-shell nanowires with polygonal cross-sections show a stronger electron localization at the corners than on the sides of the polygon. The energy structure of shells with polygonal cross-sections has a strong dependence on the number of corners [27, 37]. There is a remarkable energy gap between the states localized at corners and the next states which stand on polygon's sides. This gap increases with decreasing the shell thickness or the number of corners [38]. The lowest energy states are always localized in the corners. The polygonal shell properties differ considerably from each other because of the complexity of the localization of low energy states.

Implementing disorder in the shell such as impurities makes these properties even more complex, but at the same time with some promising results. Figure 2 presents charge and heat current versus the left chemical potential and temperature for tubular nanowires with different cross-sections in the presence of 10^4 impurities. All implemented impurities are repulsive with the strength of 10 meV. Despite different energy states for each cross-section, the charge current for all geometries follows the transmission function and the energy window associated with the chemical potential. So increasing the chemical potential allows a larger number of states to participate in the transmission, which leads to a higher charge current. This occurs for pure wires, and for those with impurities as well.

It is clear from all curves in Figure 2 that the presence of impurities leads to a reduction in charge and heat current values with respect to temperature or chemical potential. These reductions can be seen easily as difference between the magnitude of currents with no impurities (dashed lines curves) and the magnitude with impurities (solid lines curves) with the same color. In Figure 2(a) we can see that despite having the same area and number of impurities (10000 impurities with a magnitude of 10 meV) for all polygonal shapes, the triangular shell can carry charge way better than others. The cross-sections with fewer corners have higher values of thermoelectric current. This can be explained by the fewer transverse modes, but with steeper energy dispersion at the energy reached by higher values of the variable chemical potential.

While in the case of heat current, the variation with the nanowire shape is smaller. We can see an order between different cross sections in charge and heat transported by electrons as a function of both left chemical potential and left temperature. Also, the reduction of currents due to impurities is different for each geometry. By using the

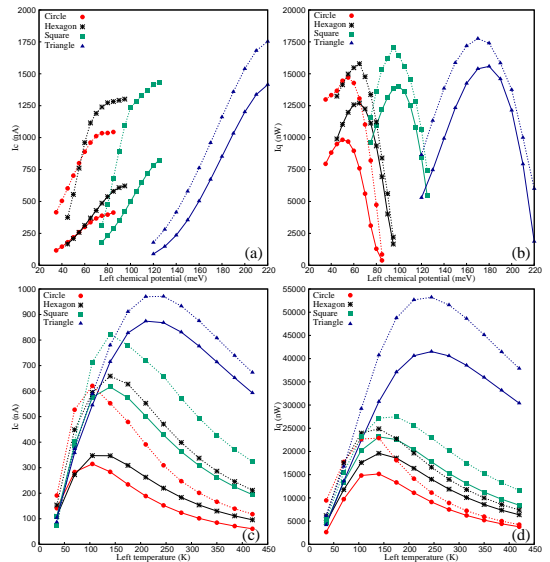


FIG. 2. High number of impurities effect in different geometries of shell over charge and heat current. (a) and (c) figures present electrical current and (b) and (d) present heat current. Conduction features are studied as a function of left chemical potential in (a) and (b) and as a function of left temperature in (c) and (d). The lines with dash represent tubular nanowires with no impurity and solid lines are representative of nanowires with 10000 impurities each one 10 meV.

same number of impurities in different cross-sections, we can see that in the case of the circular cross-section the charge and heat transport decrease dramatically in comparison to other geometries. On the average the circular cross-section shows 65% reduction of the charge current values and 30% reduction of the heat current values in the presence of impurities. The corresponding values for the triangular cross-section are 10% and 15%, respectively (see Figure 2(a) and (b)). Figure 2(c) and (d) also present the values of charge and heat current for pure shells and their reduction in the presence of impurities with respect to the left side temperature. These reductions are smaller than in the case of a chemical potential bias. Despite the presence of the 10^4 impurities, with the magnitude of 10 meV, the triangular shell still shows the highest values of both electrical and thermal currents.

Considering impurities in a system as a disorder, one should take into account both the number and strength of implemented impurities. Therefore, in the next series of calculations instead of the high number of impurities we consider a small amount of them but with strong intensity to see the variation of thermoelectric properties again as a function of chemical potential and temperature for different shell cross sections. In all cases, we implement 300 impurities with a strength of 200 meV. According to Figure 3(a) we can see a again significant reduction in

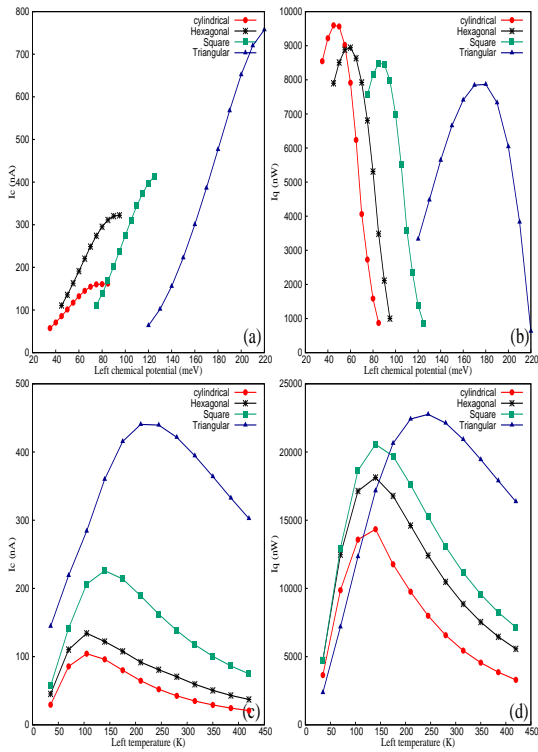


FIG. 3. Effect of impurities intensity in conduction of different cross sections of shells. Conduction features are studied as a function of left chemical potential in (a) and (b) and as a function of left temperature in (c) and (d). (a) and (c) figures present electrical current and (b) and (d) present heat current.

the magnitude of both electrical and heat current for all geometries. But interestingly, implementing impurities with strong potentials leads to a reduction of near 70% for the circular cross-section and 48% in the case of the triangular cross-section. The reduction of the heat transport for the circular cross section is much weaker than for triangular one, which results in the reversed order of the curves. Compare Figure 2(a) and Figure 3(a) for I_c values, and compare Figure 2(b) and Figure 3(b) for I_q values. This noticeable shift in I_c and I_q magnitudes and sequence order is not limited to chemical potential bias and we can see the same behavior also in the case of the temperature gradient.

B. Effect of the number of impurities

Considering both Figure 2 and Figure 3, one can think of a way to engineer thermoelectric properties in shells of different cross sectional geometries by controlling the

number and strength of impurities. The thermoelectric efficiency of the device can be increased by increasing the charge current and reducing both electronic and phononic heat currents [39]. Due to these reasons, and based on the fact that the typical shape of the cross section for III-V materials is hexagonal, we choose the triangular and hexagonal shells to explore further the effects of impurities in these cases. We consider in our systems impurities with different numbers for each case (0, 100, 1000, 5000, 10000) with a fixed magnitude of 10 meV. Increasing the number of impurities always leads to a reduction in values of both electrical current and heat current regardless of chemical potential or temperature gradient variation.

A small number of impurities will not play a noticeable role in the reduction of conduction. As can be seen in Figure 4 (a) and (c) the presence of up to 1000 impurities does not affect much the charge current, but further increase of the number of impurities results in the reduction of 15-25% in the current for the triangular shell. The current reduction due to impurities is much larger for hexagonal shells, where the percentage drop may be twice larger than in the case of triangular wire, Figure 5. The process that causes the current reduction here is scattering, each impurity acts as a scattering center, and thus the effect increases with the number of impurities in the wire. However, the stronger localization of electrons at corners in the triangular geometry, where the corners are sharper than in the hexagonal case, leads to a more robust electronic states in the triangular case, and thus to currents less sensitive to impurities.

C. Effect of the strength of impurities

In this section we consider a small number of impurities (300) with the magnitudes of their associated potential varying from zero (pure, or clean shell) to 200 meV. Such systems, i.e. with a low number of high strength impurities, are particularly interesting because they can model different physical situations. For instance, these impurities can be considered as small, but heavy ionized doping concentrations [40]. And in some cases, the scattering of free carriers by phonons can be modelled with such strong potentials [41, 42].

Contrary to the case of large number of low strength impurities, in the case of the small number of impurities with high strength there is a large deviation from the clean shell for all studied cases (Figure 6 and Figure 7). The reduction of the currents becomes 50% for triangle shell and 85% in some cases for hexagonal shells. In Figure 6(a) we show the variation of the currents with the increasing the left chemical potential. By shifting the left chemical potential values we increase the transmission window, and thus allow, more states to participate to the transport, which leads to a higher electrical current. This increase in values of the electrical current of triangle shells with no impurities reaches almost ninefold of the initial value, while in shells with impurities this increase

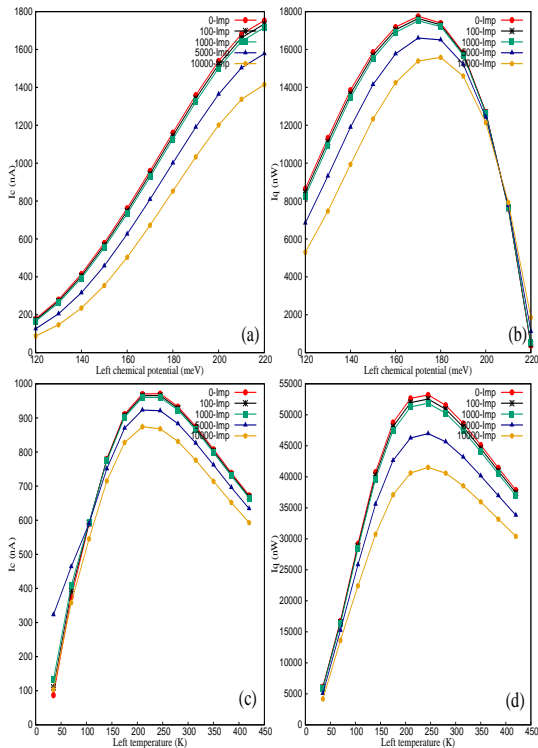


FIG. 4. Electronic conduction variation in triangle shell in presence of different number of impurities. (a) present electrical current as a function of left chemical potential, and (b) shows heat current as a function of left chemical potential. (c) shows electrical current with left temperature and (d) shows heat current with left temperature.

is strongly suppressed.

In Figure 6 (b) we show the heat current as a function of the left chemical potential for a few values of impurity strength. The current decrease is significant and reaches 12-40% in the peaks for stronger impurities. Both electrical and heat currents, as functions of left temperature, also decrease in presence of stronger impurities, Figure 6 (c) and (d). A close look at the values of I_c and I_q in Figure 6 (c) and (d), with respect to the shell with no impurity indicates interesting features. Both the charge and the heat currents show peaks between 200-250K. And in this temperature range, with strong impurities in the system, we obtain 50% reduction of I_c , while for the same temperature range the reduction of I_q reaches 65-70%. So in the presence of a temperature gradient, in the triangular shells, with strong impurities, we can reach a system that suppresses electrical current less than heat current. This feature is very desirable in thermoelectric applications.

In hexagonal shells, the charge current in the pres-

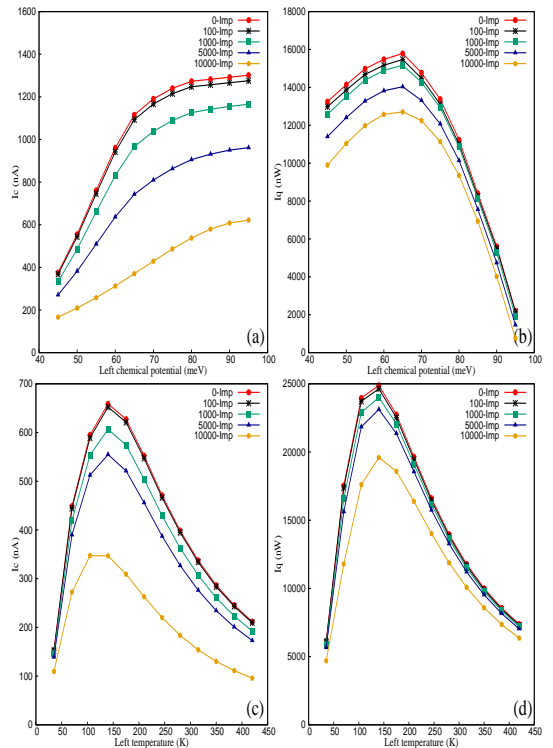


FIG. 5. Number of impurities effect in the hexagonal shell over charge and heat current. (a) and (c) figures present electrical current and (b) and (d) present heat current. Conduction features are studied as a function of left chemical potential in (a) and (b) and as a function of left temperature in (c) and (d).

ence of intense impurities shows a significant reduction, of $\approx 75-85\%$ on the average, when the chemical potential and temperature are varied. In all cases the charge current in the hexagonal shell is much stronger suppressed than in the triangular shell. While heat current in hexagonal shells shows a smaller reduction in comparison to triangle shells. By comparing Figure 6 and Figure 7 one can see that strong impurities lead to different behavior of the charge and heat current of hexagonal and triangular shells. For the triangular shell, the heat current is more suppressed in presence of intense impurities than the charge current, while the opposite occurs in the case of a hexagonal shell. By considering values of charge and heat current in hexagonal shells (Figure 7) in the presence of intense impurities, this shell is a good candidate for removing and expunging heat.

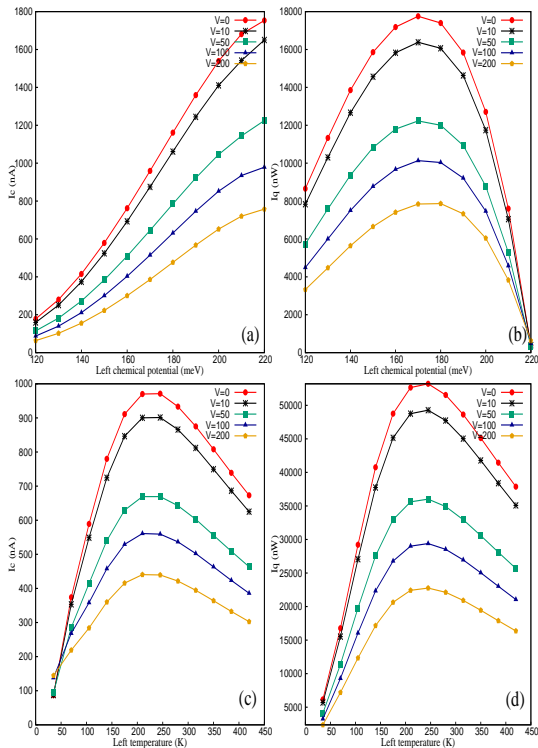


FIG. 6. Effect of different impurities intensity in conduction of triangle shells. (a) present electrical current as a function of left chemical potential, and (b) shows heat current as a function of left chemical potential. (c) shows electrical current with left temperature and (d) shows heat current with left temperature.

IV. CONCLUSIONS

We studied the number and intensity of impurities effect in different cross-sections of tubular nanowires. We began with a clean shell (or pure, i. e. without impurities) in each case and increased gradually the number of impurities. As expected these impurities lead to an increase of the scattering of electrons, and due to this reason the charge and heat current transported by carriers always decrease. We could obtain a further reduction of the currents by using a smaller number of impurities, but with a stronger associated potential. This effect may be also expected, since in general the impurity effects scale linearly with the impurity density, but quadratically with their strength. However, we show that the charge and heat current, and the effect of impurities on them, depend on the shell geometry. In the presence of impurities

the triangular shell carries a charge current almost four times more than the hexagonal shell, for the same temperature gradient (35 K). While the heat current for the

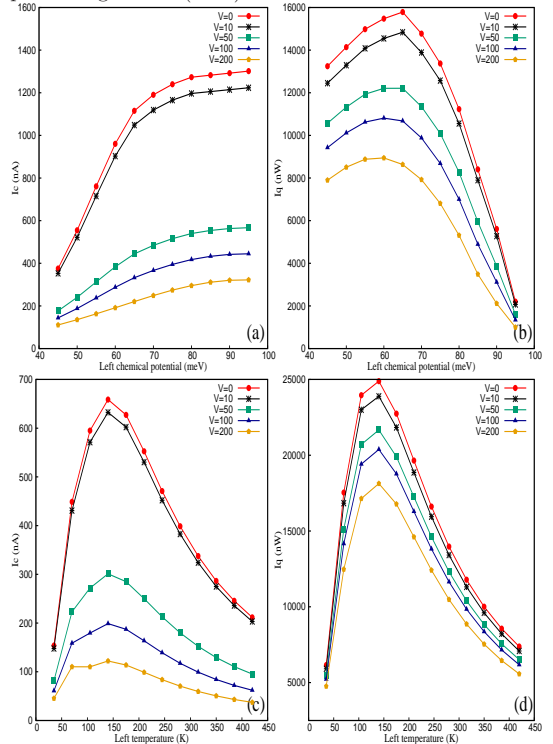


FIG. 7. Effect of different impurities intensity in conduction of hexagonal shells. (a) and (c) figures present electrical current and (b) and (d) present heat current. Conduction features are studied as a function of left chemical potential in (a) and (b) and as a function of left temperature in (c) and (d).

triangular shell is only 15% higher than hexagonal shells. An interesting result is that the effect of impurities on the charge and heat transport is smaller in the triangular shell than in the hexagonal shell. The reason is that the localization of the electrons on the corner and on the sides of the polygonal shell is more pronounced in the triangular case, which leads to higher energy intervals between different transverse states and consequently to a reduced scattering, compared to the hexagonal case.

ACKNOWLEDGMENT

This work was supported by the Icelandic Research Fund, Grant 195943-051 and 229078-051.

-
- [1] S. Xu, Y. Qin, C. Xu, Y. Wei, R. Yang, and Z. L. Wang, *Nature nanotechnology* **5**, 366 (2010).
- [2] W. Lu and C. M. Lieber, *Nature Materials* **6**, 841 (2007).
- [3] R. Chau, S. Datta, and A. Majumdar, in *IEEE Compound Semiconductor Integrated Circuit Symposium* (IEEE, 2005) p. 4.
- [4] E. Alexandro dos Santos, M. V. P. dos Santos, R. B. Campanelli, P. G. Pagliuso, J. Bettini, K. R. Pirota, and F. Béron, *Nanoscale Advances* **3**, 3251 (2021).
- [5] W. Yuan, G. Tutuncuoglu, A. T. Mohabir, R. Thorpe, L. C. Feldman, M. A. Filler, and J. W. Shan, *ACS Applied Nano Materials* **4**, 3852 (2021).
- [6] Y. Hu, H. O. Churchill, D. J. Reilly, J. Xiang, C. M. Lieber, and C. M. Marcus, *Nature nanotechnology* **2**, 622 (2007).
- [7] T. J. Kempa, B. Tian, D. R. Kim, J. Hu, X. Zheng, and C. M. Lieber, *Nano letters* **8**, 3456 (2008).
- [8] S. Gao, X. Zhao, Q. Fu, T. Zhang, J. Zhu, F. Hou, J. Ni, C. Zhu, T. Li, Y. Wang, *et al.*, *Journal of Materials Science & Technology* **126**, 152 (2022).
- [9] Y. Cui, Q. Wei, H. Park, and C. M. Lieber, *science* **293**, 1289 (2001).
- [10] A. I. Boukai, Y. Bunimovich, J. Tahir-Kheli, J.-K. Yu, W. A. Goddard Iii, and J. R. Heath, *Nature* **451**, 168 (2008).
- [11] A. I. Hochbaum, R. Chen, R. D. Delgado, W. Liang, E. C. Garnett, M. Najarian, A. Majumdar, and P. Yang, *Nature* **451**, 163 (2008).
- [12] Y. Li, G. Wang, M. Akbari-Saatlu, M. Procek, and H. H. Radamson, *Frontiers in Materials* **8**, 611078 (2021).
- [13] S. Nam, X. Jiang, Q. Xiong, D. Ham, and C. M. Lieber, *Proceedings of the National Academy of Sciences* **106**, 21035 (2009).
- [14] G. J. Snyder and E. S. Toberer, *Nature Materials* **7**, 105 (2008).
- [15] L. Peri, D. Prete, V. Demontis, V. Zannier, F. Rossi, L. Sorba, F. Beltram, and F. Rossella, *Nano Energy* **103**, 107700 (2022).
- [16] P. K. Schelling, L. Shi, and K. E. Goodson, *Materials Today* **8**, 30 (2005).
- [17] H. R. Heris, M. Kateb, S. I. Erlingsson, and A. Manolescu, *Surfaces and Interfaces* **30**, 101834 (2022).
- [18] Ö. Gül, N. Demarina, C. Blömers, T. Rieger, H. Lüth, M. Lepsa, D. Grützmacher, and T. Schäpers, *Physical Review B* **89**, 045417 (2014).
- [19] F. Haas, K. Sladek, A. Winden, M. Von der Ahe, T. Weirich, T. Rieger, H. Lüth, D. Grützmacher, T. Schäpers, and H. Hardtdegen, *Nanotechnology* **24**, 085603 (2013).
- [20] C. Blömers, T. Rieger, P. Zellekens, F. Haas, M. Lepsa, H. Hardtdegen, Ö. Gül, N. Demarina, D. Grützmacher, H. Lüth, *et al.*, *Nanotechnology* **24**, 035203 (2012).
- [21] E. Petronijevic, M. Centini, A. Belardini, G. Leahu, T. Hakkarainen, and C. Sibilta, *Optics Express* **25**, 14148 (2017).
- [22] Y. Chen, D. A. Ohlberg, and R. S. Williams, *Journal of Applied Physics* **91**, 3213 (2002).
- [23] H. Fan, M. Knez, R. Scholz, K. Nielsch, E. Pippel, D. Hesse, U. Gösele, and M. Zacharias, *Nanotechnology* **17**, 5157 (2006).
- [24] M. Heurlin, T. Stankevicius, S. Mickevicius, S. Yngman, D. Lindgren, A. Mikkelsen, R. Feidenhans'l, M. T. Borgstrom, and L. Samuelson, *Nano Letters* **15**, 2462 (2015).
- [25] F. Khosravi, S. A. Hosseini, and B. A. Hamidi, *Thin-Walled Structures* **148**, 106591 (2020).
- [26] M. U. Torres, A. Sitek, S. I. Erlingsson, G. Thorgilsson, V. Gudmundsson, and A. Manolescu, *Physical Review B* **98**, 085419 (2018).
- [27] A. Sitek, L. Serra, V. Gudmundsson, and A. Manolescu, *Physical Review B* **91**, 235429 (2015).
- [28] Y. Tian, M. R. Sakr, J. M. Kinder, D. Liang, M. J. MacDonald, R. L. Qiu, H.-J. Gao, and X. P. Gao, *Nano letters* **12**, 6492 (2012).
- [29] A. Manolescu, A. Sitek, J. Osca, L. Serra, V. Gudmundsson, and T. D. Stanescu, *Physical Review B* **96**, 125435 (2017).
- [30] S. I. Erlingsson, A. Manolescu, G. A. Nemnes, J. H. Bardarson, and D. Sanchez, *Physical review letters* **119**, 036804 (2017).
- [31] J. M. Ziman, *Electrons and phonons: the theory of transport phenomena in solids* (Oxford university press, 2001).
- [32] C. Daday, A. Manolescu, D. Marinescu, and V. Gudmundsson, *Physical Review B* **84**, 115311 (2011).
- [33] A. Sitek, G. Thorgilsson, V. Gudmundsson, and A. Manolescu, *Nanotechnology* **27**, 225202 (2016).
- [34] L. Balaghi, S. Shan, I. Fotev, F. Moebus, R. Rana, T. Venanzi, R. Hübner, T. Mikolajick, H. Schneider, M. Helm, *et al.*, *Nature communications* **12**, 1 (2021).
- [35] E. B. Ramayya, D. Vasileska, S. M. Goodnick, and I. Knezevic, *IEEE transactions on nanotechnology* **6**, 113 (2007).
- [36] T. Juntunen, T. Koskinen, V. Khayrudinov, T. Haggren, H. Jiang, H. Lipsanen, and I. Tittonen, *Nanoscale* **11**, 20507 (2019).
- [37] C. Estarellas and L. Serra, *Superlattices and Microstructures* **83**, 184 (2015).
- [38] H. Heris, K. Klausen, A. Sitek, S. Erlingsson, and A. Manolescu, in *2022 International Semiconductor Conference (CAS)* (IEEE, 2022) pp. 177–180.
- [39] G. J. Snyder and T. S. Ursell, *Physical review letters* **91**, 148301 (2003).
- [40] T. Sadi, C. Medina-Bailon, M. Nedjalkov, J. Lee, O. Badami, S. Berrada, H. Carrillo-Nunez, V. Georgiev, S. Selberherr, and A. Asenov, *Materials* **12**, 124 (2019).
- [41] T. Markussen, R. Rurali, A.-P. Jauho, and M. Brandbyge, *Physical review letters* **99**, 076803 (2007).
- [42] V. A. Fonoberov and A. A. Balandin, *Nano Letters* **6**, 2442 (2006).

Bibliography

- [1] R. Chau, S. Datta, and A. Majumdar, “Opportunities and challenges of iii-v nanoelectronics for future high-speed, low-power logic applications,” in *IEEE Compound Semiconductor Integrated Circuit Symposium, 2005. CSIC’05.*, IEEE, 2005, 4–pp.
- [2] W. Lu and C. M. Lieber, “Nanoelectronics from the bottom up,” *Nature materials*, vol. 6, no. 11, pp. 841–850, 2007.
- [3] S. Xu, Y. Qin, C. Xu, Y. Wei, R. Yang, and Z. L. Wang, “Self-powered nanowire devices,” *Nature nanotechnology*, vol. 5, no. 5, pp. 366–373, 2010.
- [4] E. Alexandro dos Santos, M. V. P. Dos Santos, R. B. Campanelli, *et al.*, “Low-temperature electronic transport of manganese silicide shell-protected single crystal nanowires for nanoelectronics applications,” *Nanoscale Advances*, vol. 3, no. 11, pp. 3251–3259, 2021.
- [5] Y. Hu, H. O. Churchill, D. J. Reilly, J. Xiang, C. M. Lieber, and C. M. Marcus, “A ge/si heterostructure nanowire-based double quantum dot with integrated charge sensor,” *Nature nanotechnology*, vol. 2, no. 10, pp. 622–625, 2007.

- [6] S. Nadj-Perge, S. Frolov, E. Bakkers, and L. P. Kouwenhoven, "Spin-orbit qubit in a semiconductor nanowire," *Nature*, vol. 468, no. 7327, pp. 1084–1087, 2010.
- [7] G. J. Snyder and E. S. Toberer, "Complex thermoelectric materials," *Nature materials*, vol. 7, no. 2, pp. 105–114, 2008.
- [8] G. Nolas, D. Morelli, and T. M. Tritt, "Skutterudites: A phonon-glass-electron crystal approach to advanced thermoelectric energy conversion applications," *Annual Review of Materials Science*, vol. 29, no. 1, pp. 89–116, 1999.
- [9] C. Wood, "Materials for thermoelectric energy conversion," *Reports on progress in physics*, vol. 51, no. 4, p. 459, 1988.
- [10] A. I. Boukai, Y. Bunimovich, J. Tahir-Kheli, J.-K. Yu, W. A. Goddard Iii, and J. R. Heath, "Silicon nanowires as efficient thermoelectric materials," *nature*, vol. 451, no. 7175, pp. 168–171, 2008.
- [11] Y. Li, G. Wang, M. Akbari-Saatlu, M. Procek, and H. H. Radamson, "Si and sige nanowire for micro-thermoelectric generator: A review of the current state of the art," *Frontiers in Materials*, vol. 8, p. 611 078, 2021.
- [12] J. Gangwar, B. K. Gupta, P. Kumar, S. K. Tripathi, and A. K. Srivastava, "Time-resolved and photoluminescence spectroscopy of al₂o₃ nanowires for promising fast optical sensor applications," *Dalton transactions*, vol. 43, no. 45, pp. 17 034–17 043, 2014.
- [13] A. Galdámez-Martinez, G. Santana, F. Güell, P. R. Martinez-Alanis, and A. Dutt, "Photoluminescence of zno nanowires: A review," *Nanomaterials*, vol. 10, no. 5, p. 857, 2020.

- [14] E. Fakhri, M. Sultan, A. Manolescu, *et al.*, “Synthesis and photoluminescence study of silicon nanowires obtained by metal assisted chemical etching,” in *2021 International Semiconductor Conference (CAS)*, IEEE, 2021, pp. 147–150.
- [15] S. Nam, X. Jiang, Q. Xiong, D. Ham, and C. M. Lieber, “Vertically integrated, three-dimensional nanowire complementary metal-oxide-semiconductor circuits,” *Proceedings of the National Academy of Sciences*, vol. 106, no. 50, pp. 21 035–21 038, 2009.
- [16] K. Zekentes, J. Choi, V. Stambouli, E. Bano, O. Karker, and K. Rogdakis, “Progress in sic nanowire field-effect-transistors for integrated circuits and sensing applications,” *Microelectronic Engineering*, p. 111 704, 2022.
- [17] E. Fakhri, R. Plugaru, M. T. Sultan, *et al.*, “Piezoresistance characterization of silicon nanowires in uniaxial and isostatic pressure variation,” *Sensors*, vol. 22, no. 17, p. 6340, 2022.
- [18] E. Fakhri, M. Sultan, A. Manolescu, S. Ingvarsson, and H. Svavarsson, “Germanium coated silicon nanowires as human respiratory sensing device,” in *2022 International Semiconductor Conference (CAS)*, IEEE, 2022, pp. 163–166.
- [19] N. P. Dasgupta, J. Sun, C. Liu, *et al.*, “25th anniversary article: Semiconductor nanowires—synthesis, characterization, and applications,” *Advanced materials*, vol. 26, no. 14, pp. 2137–2184, 2014.
- [20] R. Plugaru, E. Fakhri, C. Romanitan, *et al.*, “Structure and electrical behavior of silicon nanowires prepared by mace process,” *Surfaces and Interfaces*, vol. 33, p. 102 167, 2022.
- [21] J. Zou and A. Balandin, “Phonon heat conduction in a semiconductor nanowire,” *Journal of Applied Physics*, vol. 89, no. 5, pp. 2932–2938, 2001.

- [22] A. Buin, A. Verma, and M. Anantram, "Carrier-phonon interaction in small cross-sectional silicon nanowires," *Journal of Applied Physics*, vol. 104, no. 5, p. 053 716, 2008.
- [23] Y. Wu, R. Fan, and P. Yang, "Block-by-block growth of single-crystalline si/sige superlattice nanowires," *Nano letters*, vol. 2, no. 2, pp. 83–86, 2002.
- [24] A. Fuhrer, L. E. Fröberg, J. N. Pedersen, *et al.*, "Few electron double quantum dots in inas/inp nanowire heterostructures," *Nano letters*, vol. 7, no. 2, pp. 243–246, 2007.
- [25] L. J. Lauhon, M. S. Gudiksen, D. Wang, and C. M. Lieber, "Epitaxial core-shell and core-multishell nanowire heterostructures," *nature*, vol. 420, no. 6911, pp. 57–61, 2002.
- [26] W. Lu, J. Xiang, B. P. Timko, Y. Wu, and C. M. Lieber, "One-dimensional hole gas in germanium/silicon nanowire heterostructures," *Proceedings of the National Academy of Sciences*, vol. 102, no. 29, pp. 10 046–10 051, 2005.
- [27] X. Jiang, Q. Xiong, S. Nam, F. Qian, Y. Li, and C. M. Lieber, "Inas/inp radial nanowire heterostructures as high electron mobility devices," *Nano letters*, vol. 7, no. 10, pp. 3214–3218, 2007.
- [28] J. Nah, D. C. Dillen, K. M. Varahramyan, S. K. Banerjee, and E. Tutuc, "Role of confinement on carrier transport in ge-si x ge1-x core-shell nanowires," *Nano letters*, vol. 12, no. 1, pp. 108–112, 2012.
- [29] H. Heris, K. Klausen, A. Sitek, S. Erlingsson, and A. Manolescu, "Charge and heat currents in prismatic tubular nanowires," in *2022 International Semiconductor Conference (CAS)*, IEEE, 2022, pp. 177–180.

- [30] H. R. Heris, M. Kateb, S. I. Erlingsson, and A. Manolescu, "Effects of transverse geometry on the thermal conductivity of si and ge nanowires," *Surfaces and Interfaces*, vol. 30, p. 101 834, 2022.
- [31] S.-H. Tsai, H.-C. Chang, H.-H. Wang, *et al.*, "Significant efficiency enhancement of hybrid solar cells using core-shell nanowire geometry for energy harvesting," *ACS nano*, vol. 5, no. 12, pp. 9501–9510, 2011.
- [32] G. Ferrari, G. Goldoni, A. Bertoni, G. Cuoghi, and E. Molinari, "Magnetic states in prismatic core multishell nanowires," *Nano Letters*, vol. 9, no. 4, pp. 1631–1635, 2009.
- [33] M. U. Torres, A. Sitek, S. I. Erlingsson, G. Thorgilsson, V. Gudmundsson, and A. Manolescu, "Conductance features of core-shell nanowires determined by their internal geometry," *Physical Review B*, vol. 98, no. 8, p. 085 419, 2018.
- [34] S. Fust, A. Faustmann, D. J. Carrad, *et al.*, "Quantum-confinement-enhanced thermoelectric properties in modulation-doped gaas-algaas core-shell nanowires," *Advanced Materials*, vol. 32, no. 4, p. 1 905 458, 2020.
- [35] F. Qian, S. Gradecak, Y. Li, C.-Y. Wen, and C. M. Lieber, "Core/multishell nanowire heterostructures as multicolor, high-efficiency light-emitting diodes," *Nano letters*, vol. 5, no. 11, pp. 2287–2291, 2005.
- [36] D. Göransson, M. Heurlin, B. Dalekhan, *et al.*, "Coulomb blockade from the shell of an inp-inas core-shell nanowire with a triangular cross section," *Applied Physics Letters*, vol. 114, no. 5, p. 053 108, 2019.
- [37] Ö. Gül, N. Demarina, C. Blömers, *et al.*, "Flux periodic magnetoconductance oscillations in gaas/inas core/shell nanowires," *Physical Review B*, vol. 89, no. 4, p. 045 417, 2014.

- [38] T. Rieger, M. Luysberg, T. Schäpers, D. Grützmacher, and M. I. Lepsa, "Molecular beam epitaxy growth of GaAs/InAs core-shell nanowires and fabrication of InAs nanotubes," *Nano letters*, vol. 12, no. 11, pp. 5559–5564, 2012.
- [39] W. Yan, J. Y. Kim, W. Xing, K. C. Donovan, T. Ayzvazian, and R. M. Penner, "Lithographically patterned gold/manganese dioxide core/shell nanowires for high capacity, high rate, and high cyclability hybrid electrical energy storage," *Chemistry of Materials*, vol. 24, no. 12, pp. 2382–2390, 2012.
- [40] O. Hayden, A. B. Greytak, and D. C. Bell, "Core-shell nanowire light-emitting diodes," *Advanced Materials*, vol. 17, no. 6, pp. 701–704, 2005.
- [41] J. Yi, H. Pan, J. Lin, *et al.*, "Ferromagnetism in ZnO nanowires derived from electro-deposition on Al₂O₃ template and subsequent oxidation," *Advanced Materials*, vol. 20, no. 6, pp. 1170–1174, 2008.
- [42] S. Mathur, H. Shen, V. Sivakov, and U. Werner, "Germanium nanowires and core-shell nanostructures by chemical vapor deposition of [Ge(C₂H₅)₂]," *Chemistry of materials*, vol. 16, no. 12, pp. 2449–2456, 2004.
- [43] Y. Zhao, Y. Zhang, Y. Li, and Z. Yan, "A flexible chemical vapor deposition method to synthesize copper@carbon core-shell structured nanowires and the study of their structural electrical properties," *New Journal of Chemistry*, vol. 36, no. 5, pp. 1161–1169, 2012.
- [44] P. Mohan, J. Motohisa, and T. Fukui, "Fabrication of InP/InAs/InP core-multishell heterostructure nanowires by selective area metalorganic vapor phase epitaxy," *Applied Physics Letters*, vol. 88, no. 13, p. 133105, 2006.
- [45] G. MAHAN, "Good thermoelectrics," in *Solid State Physics*, ser. Solid State Physics, H. Ehrenreich and F. Spaepen, Eds., vol. 51, Academic Press, 1998,

- pp. 81–157. DOI: [https://doi.org/10.1016/S0081-1947\(08\)60190-3](https://doi.org/10.1016/S0081-1947(08)60190-3). [Online]. Available: <https://www.sciencedirect.com/science/article/pii/S0081194708601903>.
- [46] A. Majumdar, “Thermoelectricity in semiconductor nanostructures,” *Science*, vol. 303, no. 5659, pp. 777–778, 2004.
- [47] A. Bejan and A. D. Kraus, *Heat transfer handbook*. John Wiley & Sons, 2003, vol. 1.
- [48] L. D. Hicks and M. S. Dresselhaus, “Thermoelectric figure of merit of a one-dimensional conductor,” *Physical review B*, vol. 47, no. 24, p. 16 631, 1993.
- [49] P. Pichanusakorn and P. Bandaru, “Minimum length scales for enhancement of the power factor in thermoelectric nanostructures,” *Journal of Applied Physics*, vol. 107, no. 7, p. 074 304, 2010.
- [50] P. Pichanusakorn and P. Bandaru, “Nanostructured thermoelectrics,” *Materials Science and Engineering: R: Reports*, vol. 67, no. 2-4, pp. 19–63, 2010.
- [51] K. Lee, T. Choi, S. Lee, and D. Poulikakos, “Focused ion beam-assisted manipulation of single and double β -sic nanowires and their thermal conductivity measurements by the four-point-probe $3-\omega$ method,” *Nanotechnology*, vol. 21, no. 12, p. 125 301, 2010.
- [52] D. M. Rowe, *CRC handbook of thermoelectrics*. CRC press, 2018.
- [53] D. M. Rowe, *Thermoelectrics handbook: macro to nano*. CRC press, 2018.
- [54] G. Gadea, A. Morata, and A. Tarancon, “Semiconductor nanowires for thermoelectric generation,” in *Semiconductors and Semimetals*, vol. 98, Elsevier, 2018, pp. 321–407.

- [55] A. Boukai, K. Xu, and J. R. Heath, "Size-dependent transport and thermoelectric properties of individual polycrystalline bismuth nanowires," *Advanced Materials*, vol. 18, no. 7, pp. 864–869, 2006.
- [56] Y.-M. Lin, O. Rabin, S. Cronin, J. Y. Ying, and M. Dresselhaus, "Semimetal–semiconductor transition in $\text{Bi}_{1-x}\text{Sb}_x$ alloy nanowires and their thermoelectric properties," *Applied Physics Letters*, vol. 81, no. 13, pp. 2403–2405, 2002.
- [57] D. Rowe and G. Min, "An α -in σ plot as a thermoelectric material performance indicator," *Journal of materials science letters*, vol. 14, no. 9, pp. 617–619, 1995.
- [58] S. Siouane, S. Jovanović, and P. Poure, "A novel identification method of thermal resistances of thermoelectric modules combining electrical characterization under constant temperature and heat flow conditions," *Transactions on Environment and Electrical Engineering*, vol. 1, 2016.
- [59] O. Kwon, L. Shi, and A. Majumdar, "Scanning thermal wave microscopy (stwm)," *J. Heat Transfer*, vol. 125, no. 1, pp. 156–163, 2003.
- [60] M. S. Dresselhaus, G. Chen, M. Y. Tang, *et al.*, "New directions for low-dimensional thermoelectric materials," *Advanced materials*, vol. 19, no. 8, pp. 1043–1053, 2007.
- [61] N. Mingo, "Calculation of si nanowire thermal conductivity using complete phonon dispersion relations," *Physical Review B*, vol. 68, no. 11, p. 113 308, 2003.
- [62] M. Cutler and N. F. Mott, "Observation of anderson localization in an electron gas," *Physical Review*, vol. 181, no. 3, p. 1336, 1969.

- [63] C. Kittel and P. McEuen, *Introduction to solid state physics*. John Wiley & Sons, 2018.
- [64] G. Pennelli, M. Totaro, M. Piotto, and P. Bruschi, “Seebeck coefficient of nanowires interconnected into large area networks,” *Nano letters*, vol. 13, no. 6, pp. 2592–2597, 2013.
- [65] S. K. Bux, R. G. Blair, P. K. Gogna, *et al.*, “Nanostructured bulk silicon as an effective thermoelectric material,” *Advanced Functional Materials*, vol. 19, no. 15, pp. 2445–2452, 2009.
- [66] D. Angelescu, M. Cross, and M. Roukes, “Heat transport in mesoscopic systems,” *Superlattices and Microstructures*, vol. 23, no. 3-4, pp. 673–689, 1998.
- [67] M. Blencowe, “Quantum energy flow in mesoscopic dielectric structures,” *Physical Review B*, vol. 59, no. 7, p. 4992, 1999.
- [68] L. G. Rego and G. Kirczenow, “Quantized thermal conductance of dielectric quantum wires,” *Physical Review Letters*, vol. 81, no. 1, p. 232, 1998.
- [69] T. Yamamoto, K. Watanabe, and S. Watanabe, “Thermal transport of small systems,” 2010.
- [70] H.-Y. Chiu, V. Deshpande, H. C. Postma, *et al.*, “Ballistic phonon thermal transport in multiwalled carbon nanotubes,” *Physical review letters*, vol. 95, no. 22, p. 226 101, 2005.
- [71] T. Yamamoto, S. Watanabe, and K. Watanabe, “Universal features of quantized thermal conductance of carbon nanotubes,” *Physical review letters*, vol. 92, no. 7, p. 075 502, 2004.

- [72] R. Wolfe and G. Smith, "Effects of a magnetic field on the thermoelectric properties of a bismuth-antimony alloy," *Applied Physics Letters*, vol. 1, no. 1, pp. 5–7, 1962.
- [73] N. Cooper, B. Halperin, and I. Ruzin, "Thermoelectric response of an interacting two-dimensional electron gas in a quantizing magnetic field," *Physical Review B*, vol. 55, no. 4, p. 2344, 1997.
- [74] E. Mun, S. L. Bud'ko, M. S. Torikachvili, and P. C. Canfield, "Experimental setup for the measurement of the thermoelectric power in zero and applied magnetic field," *Measurement Science and Technology*, vol. 21, no. 5, p. 055 104, 2010.
- [75] S. I. Erlingsson, A. Manolescu, G. A. Nemnes, J. H. Bardarson, and D. Sanchez, "Reversal of thermoelectric current in tubular nanowires," *Physical review letters*, vol. 119, no. 3, p. 036 804, 2017.
- [76] B. D. Chandran and S. C. Cowley, "Thermal conduction in a tangled magnetic field," *Physical Review Letters*, vol. 80, no. 14, p. 3077, 1998.
- [77] T. Biewer, C. Forest, J. Anderson, *et al.*, "Electron heat transport measured in a stochastic magnetic field," *Physical review letters*, vol. 91, no. 4, p. 045 004, 2003.
- [78] Y. Hasegawa, Y. Ishikawa, T. Komine, *et al.*, "Magneto-seebeck coefficient of a bismuth microwire array in a magnetic field," *Applied physics letters*, vol. 85, no. 6, pp. 917–919, 2004.
- [79] W. Liang, A. I. Hochbaum, M. Fardy, O. Rabin, M. Zhang, and P. Yang, "Field-effect modulation of seebeck coefficient in single pbse nanowires," *Nano letters*, vol. 9, no. 4, pp. 1689–1693, 2009.

- [80] R. Rurali, “Colloquium: Structural, electronic, and transport properties of silicon nanowires,” *Reviews of Modern Physics*, vol. 82, no. 1, p. 427, 2010.
- [81] Y. Gao and S. Okada, “Electronic properties of diamond nanowires under an external electric field,” *Diamond and Related Materials*, vol. 125, p. 109 029, 2022.
- [82] J.-A. Yan, L. Yang, and M. Chou, “Size and orientation dependence in the electronic properties of silicon nanowires,” *Physical Review B*, vol. 76, no. 11, p. 115 319, 2007.
- [83] X. Yuan, P. Caroff, F. Wang, *et al.*, “Antimony induced {112} a faceted triangular gaas1- xsbx/inp core/shell nanowires and their enhanced optical quality,” *Advanced Functional Materials*, vol. 25, no. 33, pp. 5300–5308, 2015.
- [84] F. Boxberg, N. Søndergaard, and H. Xu, “Photovoltaics with piezoelectric core-shell nanowires,” *Nano letters*, vol. 10, no. 4, pp. 1108–1112, 2010.
- [85] B. Tian, X. Zheng, T. J. Kempa, *et al.*, “Coaxial silicon nanowires as solar cells and nanoelectronic power sources,” *nature*, vol. 449, no. 7164, pp. 885–889, 2007.
- [86] M. Hu, X. Zhang, K. P. Giapis, and D. Poulidakos, “Thermal conductivity reduction in core-shell nanowires,” *Physical Review B*, vol. 84, no. 8, p. 085 442, 2011.
- [87] M. Hu, K. P. Giapis, J. V. Goicochea, X. Zhang, and D. Poulidakos, “Significant reduction of thermal conductivity in si/ge core- shell nanowires,” *Nano letters*, vol. 11, no. 2, pp. 618–623, 2011.

- [88] J. Chen, G. Zhang, and B. Li, "A universal gauge for thermal conductivity of silicon nanowires with different cross sectional geometries," *The Journal of chemical physics*, vol. 135, no. 20, p. 204 705, 2011.
- [89] L.-D. Zhao, S.-H. Lo, Y. Zhang, *et al.*, "Ultralow thermal conductivity and high thermoelectric figure of merit in sntse crystals," *nature*, vol. 508, no. 7496, pp. 373–377, 2014.
- [90] P. Graziosi, C. Kumarasinghe, and N. Neophytou, "Impact of the scattering physics on the power factor of complex thermoelectric materials," *Journal of Applied Physics*, vol. 126, no. 15, p. 155 701, 2019.
- [91] N. Jia, J. Cao, X. Y. Tan, *et al.*, "Thermoelectric materials and transport physics," *Materials Today Physics*, vol. 21, p. 100 519, 2021.
- [92] P. K. Schelling, L. Shi, and K. E. Goodson, "Managing heat for electronics," *Materials Today*, vol. 8, no. 6, pp. 30–35, 2005.
- [93] D. Li, G. Wu, W. Wang, *et al.*, "Enhancing flow boiling heat transfer in microchannels for thermal management with monolithically-integrated silicon nanowires," *Nano letters*, vol. 12, no. 7, pp. 3385–3390, 2012.
- [94] Q. Xiong, J. Wang, O. Reese, L. Lew Yan Voon, and P. Eklund, "Raman scattering from surface phonons in rectangular cross-sectional w-zns nanowires," *Nano Letters*, vol. 4, no. 10, pp. 1991–1996, 2004.
- [95] Q. Xiong, G. Chen, J. Acord, *et al.*, "Optical properties of rectangular cross-sectional zns nanowires," *Nano Letters*, vol. 4, no. 9, pp. 1663–1668, 2004.
- [96] T. Kuykendall, P. Pauzauskie, S. Lee, Y. Zhang, J. Goldberger, and P. Yang, "Metalorganic chemical vapor deposition route to gan nanowires with triangular cross sections," *Nano Letters*, vol. 3, no. 8, pp. 1063–1066, 2003.

- [97] G. Pennelli and M. Piotto, "Fabrication and characterization of silicon nanowires with triangular cross section," *Journal of applied physics*, vol. 100, no. 5, p. 054 507, 2006.
- [98] J. Zou, M. Paladugu, H. Wang, *et al.*, "Growth mechanism of truncated triangular iii-v nanowires," *Small*, vol. 3, no. 3, pp. 389–393, 2007.
- [99] P. Mohanty, T. Kang, B. Kim, and J. Park, "Synthesis of single crystalline tellurium nanotubes with triangular and hexagonal cross sections," *The Journal of Physical Chemistry B*, vol. 110, no. 2, pp. 791–795, 2006.
- [100] A. Sitek, L. Serra, V. Gudmundsson, and A. Manolescu, "Electron localization and optical absorption of polygonal quantum rings," *Physical Review B*, vol. 91, no. 23, p. 235 429, 2015.
- [101] A. Sitek, G. Thorgilsson, V. Gudmundsson, and A. Manolescu, "Multi-domain electromagnetic absorption of triangular quantum rings," *Nanotechnology*, vol. 27, no. 22, p. 225 202, 2016.
- [102] C. Daday, A. Manolescu, D. Marinescu, and V. Gudmundsson, "Electronic charge and spin density distribution in a quantum ring with spin-orbit and coulomb interactions," *Physical Review B*, vol. 84, no. 11, p. 115 311, 2011.
- [103] C. Dames and G. Chen, "Theoretical phonon thermal conductivity of si/ge superlattice nanowires," *Journal of Applied Physics*, vol. 95, no. 2, pp. 682–693, 2004.
- [104] X. Lü, W. Shen, and J. Chu, "Size effect on the thermal conductivity of nanowires," *Journal of applied physics*, vol. 91, no. 3, pp. 1542–1552, 2002.

- [105] W. Li, L. Lindsay, D. A. Broido, D. A. Stewart, and N. Mingo, "Thermal conductivity of bulk and nanowire $\text{mg}_2\text{si}_{1-x}\text{sn}_x$ alloys from first principles," *Physical Review B*, vol. 86, no. 17, p. 174 307, 2012.
- [106] A. Balandin and K. L. Wang, "Significant decrease of the lattice thermal conductivity due to phonon confinement in a free-standing semiconductor quantum well," *Physical Review B*, vol. 58, no. 3, p. 1544, 1998.
- [107] A. Khitun, A. Balandin, and K. Wang, "Modification of the lattice thermal conductivity in silicon quantum wires due to spatial confinement of acoustic phonons," *Superlattices and microstructures*, vol. 26, no. 3, pp. 181–193, 1999.
- [108] D. Li, Y. Wu, P. Kim, L. Shi, P. Yang, and A. Majumdar, "Thermal conductivity of individual silicon nanowires," *Applied Physics Letters*, vol. 83, no. 14, pp. 2934–2936, 2003.
- [109] D. L. Nika, A. I. Cocemasov, D. V. Crismari, and A. A. Balandin, "Thermal conductivity inhibition in phonon engineered core-shell cross-section modulated si/ge nanowires," *Applied physics letters*, vol. 102, no. 21, p. 213 109, 2013.
- [110] A. Cocemasov, D. Nika, V. Fomin, D. Grimm, and O. Schmidt, "Phonon-engineered thermal transport in si wires with constant and periodically modulated cross-sections: A crossover between nano-and microscale regimes," *Applied Physics Letters*, vol. 107, no. 1, p. 011 904, 2015.
- [111] A. Sellitto, F. X. Alvarez, and D. Jou, "Geometrical dependence of thermal conductivity in elliptical and rectangular nanowires," *International journal of heat and mass transfer*, vol. 55, no. 11-12, pp. 3114–3120, 2012.

- [112] V. I. Brinzari, A. I. Cocemasov, D. L. Nika, and G. S. Korotcenkov, "Ultra-low thermal conductivity of nanogranular indium tin oxide films deposited by spray pyrolysis," *Applied Physics Letters*, vol. 110, no. 7, p. 071 904, 2017.
- [113] S. Fan, C. Gao, C. Duan, *et al.*, "Geometry effect of copper nanoparticles and nanowires on polyetheretherketone-matrix nanocomposites: Thermal conductivity, dynamic mechanical properties and wear resistance," *Composites Science and Technology*, vol. 219, p. 109 224, 2022.
- [114] Z. Wei, G. Wehmeyer, C. Dames, and Y. Chen, "Geometric tuning of thermal conductivity in three-dimensional anisotropic phononic crystals," *Nanoscale*, vol. 8, no. 37, pp. 16 612–16 620, 2016.
- [115] R. Prasher, "Thermal conductivity of tubular and core/shell nanowires," *Applied physics letters*, vol. 89, no. 6, p. 063 121, 2006.
- [116] H. R. Heris, M. Kateb, S. I. Erlingsson, and A. Manolescu, "Thermoelectric properties of tubular nanowires in the presence of a transverse magnetic field," *Nanotechnology*, vol. 31, no. 42, p. 424 006, 2020.
- [117] J. Xiang, W. Lu, Y. Hu, Y. Wu, H. Yan, and C. M. Lieber, "Ge/si nanowire heterostructures as high-performance field-effect transistors," *nature*, vol. 441, no. 7092, pp. 489–493, 2006.
- [118] J. Chen, G. Zhang, and B. Li, "Impacts of atomistic coating on thermal conductivity of germanium nanowires," *Nano letters*, vol. 12, no. 6, pp. 2826–2832, 2012.
- [119] J. Chen, G. Zhang, and B. Li, "Phonon coherent resonance and its effect on thermal transport in core-shell nanowires," *The Journal of chemical physics*, vol. 135, no. 10, p. 104 508, 2011.

- [120] D. Ma, H. Ding, H. Meng, *et al.*, “Nano-cross-junction effect on phonon transport in silicon nanowire cages,” *Physical Review B*, vol. 94, no. 16, p. 165 434, 2016.
- [121] A. Soleimani, H. Araghi, Z. Zabihi, and A. Alibakhshi, “A comparative study of molecular dynamics simulation methods for evaluation of the thermal conductivity and phonon transport in si nanowires,” *Computational Materials Science*, vol. 142, pp. 346–354, 2018.
- [122] H. Dong, Z. Fan, L. Shi, A. Harju, and T. Ala-Nissila, “Equivalence of the equilibrium and the nonequilibrium molecular dynamics methods for thermal conductivity calculations: From bulk to nanowire silicon,” *Physical Review B*, vol. 97, no. 9, p. 094 305, 2018.
- [123] I. Ponomareva, D. Srivastava, and M. Menon, “Thermal conductivity in thin silicon nanowires: Phonon confinement effect,” *Nano letters*, vol. 7, no. 5, pp. 1155–1159, 2007.
- [124] M. H. Khadem and A. P. Wemhoff, “Comparison of green–kubo and nemd heat flux formulations for thermal conductivity prediction using the tersoff potential,” *Computational materials science*, vol. 69, pp. 428–434, 2013.
- [125] P. K. Schelling, S. R. Phillpot, and P. Keblinski, “Comparison of atomic-level simulation methods for computing thermal conductivity,” *Physical Review B*, vol. 65, no. 14, p. 144 306, 2002.
- [126] Z. Li, S. Xiong, C. Sievers, *et al.*, “Influence of thermostating on nonequilibrium molecular dynamics simulations of heat conduction in solids,” *The Journal of chemical physics*, vol. 151, no. 23, p. 234 105, 2019.

- [127] E. Bosoni, D. Campi, D. Donadio, G. Sosso, J. Behler, and M. Bernasconi, “Atomistic simulations of thermal conductivity in gete nanowires,” *Journal of Physics D: Applied Physics*, vol. 53, no. 5, p. 054001, 2019.
- [128] C. Huang, Q. Wang, and Z. Rao, “Thermal conductivity prediction of copper hollow nanowire,” *International Journal of Thermal Sciences*, vol. 94, pp. 90–95, 2015.
- [129] V. Kuryliuk, O. Tyvonovych, and S. Semchuk, “Impact of ge clustering on thermal conductivity of sige nanowires: Atomistic simulations study,” *Physical Chemistry Chemical Physics*, 2023.
- [130] X. Yang and A. C. To, “Thermal conductivity in thin silicon nanowires with rough surfaces by molecular dynamics simulations,” in *AIP Conference Proceedings*, American Institute of Physics, vol. 1233, 2010, pp. 806–811.
- [131] F. Müller-Plathe, “A simple nonequilibrium molecular dynamics method for calculating the thermal conductivity,” *The Journal of chemical physics*, vol. 106, no. 14, pp. 6082–6085, 1997.
- [132] S. Plimpton, “Fast parallel algorithms for short-range molecular dynamics,” *Journal of computational physics*, vol. 117, no. 1, pp. 1–19, 1995.
- [133] M. Alaghemandi, E. Algaer, M. C. Böhm, and F. Müller-Plathe, “The thermal conductivity and thermal rectification of carbon nanotubes studied using reverse non-equilibrium molecular dynamics simulations,” *Nanotechnology*, vol. 20, no. 11, p. 115704, 2009.
- [134] J. R. Lukes and H. Zhong, “Thermal conductivity of individual single-wall carbon nanotubes,” 2007.

- [135] C. Yu, L. Shi, Z. Yao, D. Li, and A. Majumdar, "Thermal conductance and thermopower of an individual single-wall carbon nanotube," *Nano letters*, vol. 5, no. 9, pp. 1842–1846, 2005.
- [136] S.-c. Wang, X.-g. Liang, X.-h. Xu, and T. Ohara, "Thermal conductivity of silicon nanowire by nonequilibrium molecular dynamics simulations," *Journal of Applied Physics*, vol. 105, no. 1, p. 014 316, 2009.
- [137] X. Lü and J. Chu, "Lattice thermal conductivity in a silicon nanowire with square cross section," *Journal of applied physics*, vol. 100, no. 1, p. 014 305, 2006.
- [138] K.-H. Lin and A. Strachan, "Thermal transport in sige superlattice thin films and nanowires: Effects of specimen and periodic lengths," *Physical Review B*, vol. 87, no. 11, p. 115 302, 2013.
- [139] K. Vuttivorakulchai, M. Luisier, and A. Schenk, "Effect of stacking faults and surface roughness on the thermal conductivity of inas nanowires," *Journal of Applied Physics*, vol. 124, no. 20, p. 205 101, 2018.
- [140] J. M. Ziman, *Electrons and phonons: the theory of transport phenomena in solids*. Oxford university press, 2001.
- [141] H. Rezaie Heris, K. Ó. Klausen, A. Sitek, S. I. Erlingsson, and A. Manolescu, "Effect of impurities on charge and heat transport in tubular nanowires," *Nanotechnology*, 2023.
- [142] D. Cantrell and P. Butcher, "A calculation of the phonon-drag contribution to the thermopower of quasi-2d electrons coupled to 3d phonons. ii. applications," *Journal of Physics C: Solid State Physics*, vol. 20, no. 13, p. 1993, 1987.

- [143] D. Cantrell and P. Butcher, "A calculation of the phonon drag contribution to thermopower in two dimensional systems," *Journal of Physics C: Solid State Physics*, vol. 19, no. 20, p. L429, 1986.
- [144] P. N. Butcher, N. H. March, and M. P. Tosi, *Physics of low-dimensional semiconductor structures*. Springer Science & Business Media, 2013.
- [145] N. Mott, "Conduction in non-crystalline materials," *Oxford University Press, Walton Street, Oxford OX 2 6 DP, UK, 1987.*, 1987.
- [146] V. Karavolas, M. Smith, T. Fromhold, *et al.*, "The effect of interface roughness scattering and background impurity scattering on the thermopower of a 2deg in a si mosfet," *Journal of Physics: Condensed Matter*, vol. 2, no. 51, p. 10 401, 1990.
- [147] V. Karavolas and P. Butcher, "Diffusion thermopower of a 2deg," *Journal of Physics: Condensed Matter*, vol. 3, no. 15, p. 2597, 1991.
- [148] O. Mironov, I. Gerleman, P. Phillips, *et al.*, "Thermoelectric power of the si/si_{0.8}ge_{0.2} two-dimensional hole gas," *Thin Solid Films*, vol. 294, no. 1-2, pp. 182-185, 1997.
- [149] X. Zianni and P. Butcher, "The effect of interface roughness on the transport properties of a two-dimensional electron gas in a si-mosfet," *Journal of Physics: Condensed Matter*, vol. 6, no. 14, p. 2713, 1994.
- [150] X. Zianni, P. Butcher, and M. Kearney, "Semiclassical magnetothermopower of a quasi-two-dimensional electron gas," *Physical Review B*, vol. 49, no. 11, p. 7520, 1994.

- [151] P. Butcher and M. Tsaousidou, “Effect of electron and phonon anisotropy on the phonon-drag thermopower of a classical two-dimensional electron gas in a magnetic field,” *Physical review letters*, vol. 80, no. 8, p. 1718, 1998.
- [152] S. Lyo, “Low-temperature phonon-drag thermoelectric power in heterojunctions,” *Physical Review B*, vol. 38, no. 9, p. 6345, 1988.
- [153] B. Tieke, R. Fletcher, U. Zeitler, M. Henini, and J. Maan, “Thermopower measurements of the coupling of phonons to electrons and composite fermions,” *Physical Review B*, vol. 58, no. 4, p. 2017, 1998.
- [154] R. Fletcher, V. Pudalov, Y. Feng, M. Tsaousidou, and P. Butcher, “Thermoelectric and hot-electron properties of a silicon inversion layer,” *Physical Review B*, vol. 56, no. 19, p. 12 422, 1997.